Title
Control Design and Implementation of Hard Disk Drive Servos

Author
Nie, Jianbin

Publication Date
2011

Peer reviewed|Thesis/dissertation

Control Design and Implementation of Hard Disk Drive Servos

by

Jianbin Nie

A dissertation submitted in partial satisfaction of the

requirements for the degree of

Doctor of Philosophy

in

Engineering-Mechanical Engineering

in the

Graduate Division

of the

University of California, Berkeley

Committee in charge:

Professor Roberto Horowitz, Chair
Professor Masayoshi Tomizuka
Professor David Brillinger

Spring 2011

Control Design and Implementation of Hard Disk Drive Servos

by

Jianbin Nie

Abstract

Control Design and Implementation of Hard Disk Drive Servos

by

Jianbin Nie

Doctor of Philosophy in Engineering-Mechanical Engineering

University of California, Berkeley

Professor Roberto Horowitz, Chair

In this dissertation, the design of servo control algorithms is investigated to produce high-density and cost-effective hard disk drives (HDDs). In order to sustain the continuing increase of HDD data storage density, dual-stage actuator servo systems using a secondary micro-actuator have been developed to improve the precision of read/write head positioning control by increasing their servo bandwidth. In this dissertation, the modeling and control design of dual-stage track-following servos are considered. Specifically, two track-following control algorithms for dual-stage HDDs are developed. The designed controllers were implemented and evaluated on a disk drive with a PZT-actuated suspension-based dual-stage servo system.

Usually, the feedback position error signal (PES) in HDDs is sampled on some specified servo sectors with an equidistant sampling interval, which implies that HDD servo systems with a regular sampling rate can be modeled as linear time-invariant (LTI) systems. However, sampling intervals for HDD servo systems are not always equidistant and, sometimes, an irregular sampling rate due to missing PES sampling data is unavoidable. With the natural periodicity of HDDs, which is related to the disk rotation, those HDD servo systems with missing PES samples can be modeled as linear periodically time-varying (LPTV) systems.

An explicit optimal H_∞ control synthesis algorithm for general LPTV systems is first obtained by solving discrete Riccati equations. Then, based on this result, the optimal H_∞ track-following control for irregular-sampling-rate servos is synthesized. Simulation and experiment studies, which have been carried out on a set of actual single-stage hard disk drives, demonstrate that the proposed control synthesis technique is able to handle irregular sampling rates and can be used to conveniently design a track-following servo that achieves the robust performance of a desired error

rejection function for disturbance attenuation. Moreover, experiment results show that compared to the currently-used methodology for irregular sampling rates, the proposed control algorithm has significantly improved servo performance.

The feedback signal in HDD servos is generated from servo patterns that must be pre-recorded using servo track writing process before the HDD can be used. Thus, the quality of the servo track writing process is also crucial to the accuracy of positioning read/write head. Recently, self-servo track writing has been developed in order to improve the quality of the written servo patterns and reduce the cost of servo track writing process. This dissertation considers two novel controller synthesis methodologies employing a feedforward control structure for performing concentric self-servo track writing in hard disk drives. Simulation results confirm that the two proposed control synthesis methodologies prevent error propagation from the previously written tracks and significantly improve servo track writing performance.

Contents

List of Figures

List of Tables

Acknowledgments

I would like to acknowledge many people who have helped me complete the research described in this dissertation. First and foremost, I express my sincere gratitude to Professor Roberto Horowitz for his enthusiastic support and guidance. When looking back over the past five years, I feel honored and lucky to have him as my research advisor. I am also grateful to have Professors Masayoshi Tomizuka, Karl Hedrick, Andrew Packard, David Brillinger and Ilan Adler on my qualification and dissertation committees.

I quite appreciate the help and advice I have received from my labmates. Especially, I would like to sincerely thank Richard Conway for his providing a great help and invaluable advice throughout my control theory study and reading this dissertation. I thank Sarah Felix and Stanley Kon for their great help in my experiment study. Also, I would like to thank my other labmates: Josiah Wernow, Claus Danielson and Edgar Ergueta.

I would like to extend my appreciation to our industrial collaborators. I am very grateful to the Servo Writing Group in Western Digital for providing a research grant for part of this dissertation. I particularly thank Edgar Sheh and Siri Weerasooriya for their invaluable support and advice for performing my research study. I also thank Jie Yu and Guoxiao Guo for donating us experimental hard disk drives and Hutchinson Technology Inc. for providing us experimental PZT-actuated suspensions. I thank the industrial partners of the Computer Mechanics Laboratory (CML) and the Information Storage Industry Consortium (INSIC) for their financial support.

Finally, I wish to express my deepest gratitude to my parents and my wife, Wen, for their constant love, encouragement, sacrifices, and support.

Chapter 1

Introduction

1.1 Hard Disk Drive Servo Systems

Since the first magnetic drive was invented in the 1950s by IBM, hard disk drives (HDDs) have been playing an increasingly important role in our life. Originally, they were developed for use with general purpose computers such as desktops, laptops and servers. During the 1990s, HDDs were introduced to embedded systems such as network attached storage (NAS) systems, redundant array of independent disks (RAID) systems, and storage area network (SAN) systems that are able to provide efficient and reliable access to large volumes of data. In the new century, the usage of HDDs has also been expanded into consumer applications such as digital video players, digital video recorders, video game consoles, and so on. In order to meet all of these increasing demands for hard disk drives, HDD companies are facing the following two critical questions: how to increase the areal density of HDDs and how to reduce the cost of HDDs. With higher areal densities, more data can be stored per square inch on the disk and then smaller dimension disk drives become feasible, which results in less materials required to produce a hard disk drive and thus the lower cost of HDDs.

Higher areal density requires more precise positioning of the read/write magnetic head in the presence of various disturbances that will be illustrated in detail in Chapter 2. The head positioning is accomplished by HDD servo systems. This dissertation focuses on the control design and implementation of HDD servo systems with the objective of increasing the areal density of hard disk drives.

1.1.1 Disk Drive Components

As shown in Fig. 1.1, a typical modern hard disk drive mainly consists of one or more disk platters, a spindle motor, an E-block, suspensions, sliders, magnetic read/write (R/W) heads, a voice coil motor (VCM), and a pivot. Data is recorded on the spinning disks, which are made of aluminum or glass with a thin layer of magnetic materials coated on their both sides. The spinning disks are driven by the spindle motor and the spinning speed could be distinct for HDDs within different product lines. When the disk is spinning, the sliders fly on a formed air-bearing surface (ABS) [31]. The magnetic heads are fabricated on the trailing edge of the slider [28]. The suspension, a thin flexible structure, carries the slider and read/write head and is also used to balance the uplifting aerodynamic force due to the spinning disk. In addition, the suspension is assembled onto the arms of the E-block that lies between the VCM and the suspension and contains the pivot point. The VCM, which is a rotary actuator, positions read/write heads on the disks by rotating the E-block about the pivot. Data

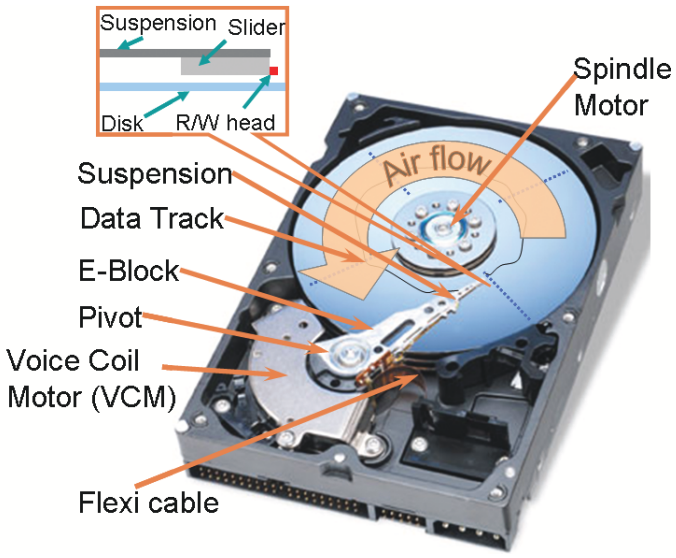

Figure 1.1: Schematic of a hard disk drive servo system

bits are stored in concentric circles called tracks on the disk surfaces. They can be read and written by read and write heads respectively as the heads move over them. Thus, by controlling the VCM to position the read/write heads, we can access desired data on different tracks.

1.1.2 Position Error Signal

In order to perform closed-loop feedback control for HDDs, the head position relative to the track must be provided to servo systems. Such a head position feedback signal

is referred as a position error signal. Modern hard disk drives utilize an embedded servo sector strategy [31] to generate the signal when read heads pass over special magnetic patterns called servo patterns. As shown in Fig. 1.2, servo patterns are written in designated areas on the disk surface known as servo sectors. Additionally, servo sectors are placed on all tracks interleaved with data sectors and patterned as radial spokes.

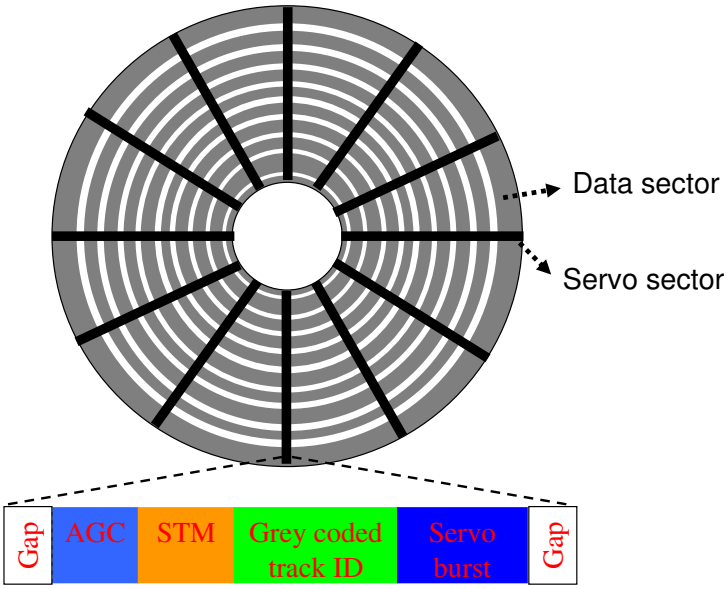

Figure 1.2: Embedded servo sectors and different fields in a servo sector

Different fields in a servo sector are also shown in Fig. 1.2 and each of them contains a specific pattern of magnetization. Usually, these fields [31] are DC-gap field, automatic gain control (AGC) field, servo timing mark (STM) field, grey coded track ID field and PES burst pattern field. Among these fields, only the grey coded track ID field and PES burst pattern field are directly utilized to generate PES. The grey coded track ID field contains the information about the track number, while the PES burst pattern is decoded to measure the off-track displacement of the read head from the track center, i.e, the fraction of track-pitch.

Here, a simple example for servo burst patterns is considered. A setting using A/B burst patterns [25] is illustrated in Fig. 1.3. When the read head passes over the bursts, a readback signal will be generated. The generated signal is proportional to the length of the part of the burst that is covered by the head as it flies over. Then, the fractional off-track error is generated from the difference between the signal amplitudes coming from A and B bursts. Modern disk drives utilize other more complicated burst patterns such as A/B/C/D four-burst patterns, null patterns, and phase patterns [63] to eliminate dead spots and increase resolution.

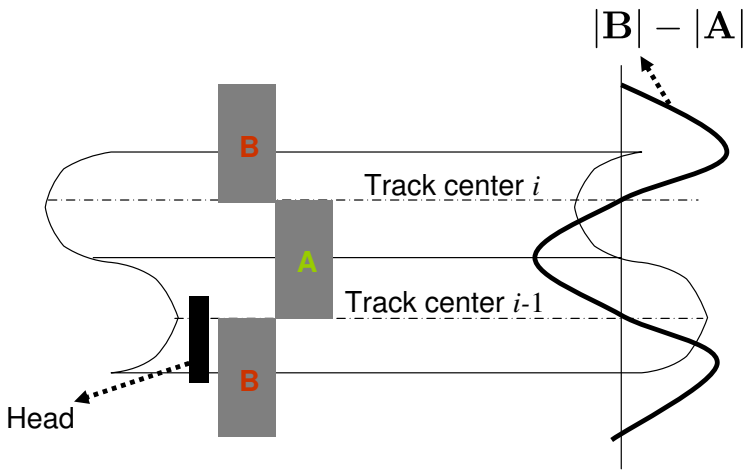

Figure 1.3: Servo patterns with A/B burst to generate fractional off-track error

Since the position feedback signal can only be obtained on the servo sectors that are located at discrete locations, the disk drive control system is a sampled digital control system. The sampling frequency is determined by the disk rotation speed and the number of servo sectors on a disk. For example, a disk drive with 7200 RPM and 220 servo sectors has a sampling frequency of 26.4 KHz ($= 7200 \times 220/60$). Although increasing the sampling frequency by increasing the number of servo sectors can improve servo positioning control, more servo sectors require more space to store servo patterns and thus reduce data storage efficiency.

The servo patterns used to generate position feedback signals must be pre-recorded before the HDD can be used. The process of writing servo patterns onto the disk surface at specific locations of servo sectors is known as servo track writing (STW). The accuracy and precision of the servo track writing process plays a crucial role in dictating the ultimate track density and areal storage density of HDDs. There are two critical control problems [31] associated with the STW process:

- The patterns used to define the tracks and sectors must be placed in a concentric fashion. Any radial misalignments and eccentricities that occur during the STW process will later appear as written-in repeatable runout, which degrades servo performance.

- The servo sectors in a given track must be precisely aligned with those of adjacent tracks. Misalignments along the tangential direction (i.e. along the disk's circumference) result in non-uniform PES sampling intervals.

In order to carry out a servo track writing process, a position reference signal must be provided by a servo system when the servo patterns of each concentric track are being recorded. There are several mechanisms for generating such a position reference signal, including conventional servo track writing [54], concentric based self-servo

track writing [59], and spiral self-servo track writing [4].

1.1.3 Track Mis-Registration

The main task of HDD servo systems is to precisely position the read/write head on the desired track. Tracking performance is typically characterized by track mis-registration (TMR). TMR is defined as the error from a nominal distance [58], as shown in Fig. 1.4. Two kinds of TMR concepts, write-to-read TMR and write-to-write TMR, are popularly considered in HDD servos. Write-to-read TMR is defined as the difference between the actual read track and the written servo track, while write-to-write TMR is defined as the difference between the nominal track pitch and the actual spacing between two adjacent written tracks. Write-to-read TMR, also referred as servo TMR, is characterized by the statistical distribution of the deviation of the head from the written servo track, which is measured by PES. Moreover, the PES is assumed to have a Gaussian distribution and its three-times the standard deviation $3\sigma_{PES}$ is often used to evaluate TMR.

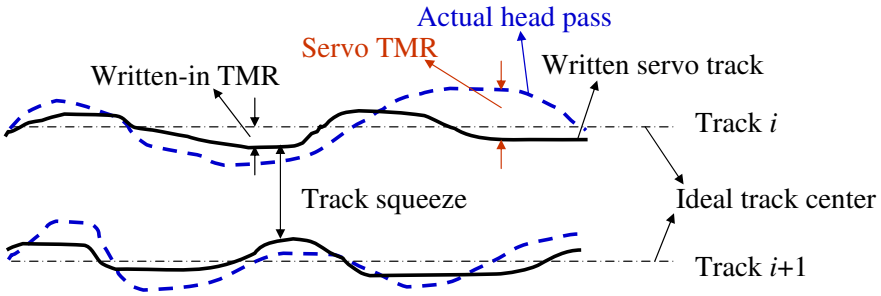

Figure 1.4: Illustration of track mis-registration

As discussed in the previous section, servo tracks are pre-written in a STW process during which an error called written-in TMR between the written servo track and ideal circle track may be introduced. Written-in TMR affects write-to-write TMR by squeezing adjacent tracks.

TMR can be broken down into a component due to repeatable runout (RRO) and a component due to non-repeatable runout (NRRO). RRO mainly results from disk eccentricity, non-ideal servo track writing (i.e. written-in TMR) [52], and spindle motor vibration and is hence synchronous with the disk rotation speed. All other runout other than RRO is referred to as NRRO. Furthermore, non-repeatable runout can be in turn categorized into torque disturbance, windage, non-repeatable disk motions and measurement noises. The torque disturbance—which is mainly caused by the bias force of the flexible cable, the pivot friction and the air-turbulence impinging on the voice coil motor—is typically a low frequency disturbance. Windage, which

is mainly due to air-turbulence directly exciting suspension resonance modes, is primarily a high frequency disturbance. Non-repeatable disk motions, which directly affect the position of R/W head relative to the servo track, result in additional track runout. Measurement noise, representing the effects of PES demodulation noise, includes electrical noise and A/D quantization noise.

1.2 Servo Control Architecture

HDD servo control systems [6] mainly involve three kinds of control tasks [1]: track-seeking control, settling control and track-following control. The head positioning servomechanism moves the read/write head as fast as possible from one track to another when commanded by the host system (track-seeking control). As the head approaches the desired track, a transitioning control servomechanism allows the smooth settling of the head within a small distance from the track while minimizing the excitation of mechanical vibration (settling control). Once the head is within a sufficiently small distance from the desired data track, its motion is regulated so that it can follow the center of the data track as precisely as possible during the operation of reading or writing data (track-following control). This dissertation will focus on the track-following control synthesis.

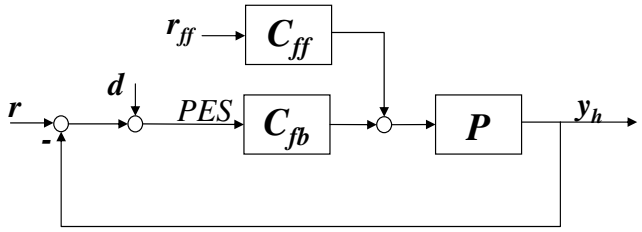

Figure 1.5: Hard disk drive servo control architecture

A typical hard disk drive servo control system can be represented by the block diagram shown in Fig 1.5. P is the disk drive actuator plant; C_{fb} and C_{ff} are the feedback and feedforward controllers respectively; r denotes the reference input, which is zero in a track-following control mode and a desired position trajectory in a track-seeking control mode; d represents all of disturbances including RRO and NRRO contributing to PES; r_{ff} is a reference input to the feedforward controller; y_h is the absolute position of the R/W head.

For a track-following control mode, the PES can be written as

$$PES(k) = S(q^{-1})d(k) - S(q^{-1})P(q^{-1})C_{ff}(q^{-1})r_{ff}(k) \tag{1.1}$$

where $S(q^{-1})$ is the sensitivity transfer function defined as

$$S(q^{-1}) = \frac{1}{1 + P(q^{-1})C_{fb}(q^{-1})} \ . \tag{1.2}$$

As illustrated by (1.1), the head position errors due to disturbances are characterized by the transfer sensitivity function $S(z)$ which is often called the error rejection function. Therefore, the sensitivity transfer function is a crucial index used to specify and evaluate the performance of HDD servo control systems. Since the major TMR sources are located in the low-frequency range, the most intuitive way to minimize the PES and increase the tracking accuracy is to increase the servo control bandwidth. However, traditional hard disk drives utilizing a single actuator VCM to move the head have two major limitations for their bandwidth increase: the VCM/E-block/suspension actuator assembly is large and massive; multiple mechanical resonance modes in the E-block arms and suspensions lie between the VCM and the heads. In order to overcome these two limitations, a smaller secondary micro-actuator (MA) is added to a traditional disk drive to form a dual-stage actuator servo system. Such a dual-stage assembly is able to increase the servo bandwidth by reducing the load to be moved by the secondary actuator and avoiding the excitation of some low-frequency resonance modes of the arm and the suspension.

As illustrated previously, a feedback PES sample is generated when the read head flies over each servo sector. Since the servo sectors are equally distributed on the disk, HDD servo systems possess a regular sampling rate whose sampling intervals are equidistant. Then, those servo systems can be modeled as linear time-invariant (LTI) systems. However, irregular sampling rates caused by non-equidistant sampling intervals may also occur in hard disk drives [39], for example in HDD servos with false PES demodulation and in some self-servo track writing (SSTW) servos with missing PES sampling data. Thus, the design of these servo systems with irregular sampling rates should also be considered.

In addition, since any written-in TMR introduced in servo track-writing process will later appear as written-in repeatable runout, the issue of improving the performance of servo track-writing process should also be addressed in order to further reduce the PES.

1.2.1 Dual-Stage Actuation Servo Systems

Dual-stage actuation (DSA), which combines the traditional VCM with an additional micro-actuator, has been proposed as a means of enhancing servo tracking performance by increasing the servo bandwidth. The configurations of dual-stage actuators

can be categorized into three groups according to the location of the secondary actuator: actuated suspension, actuated slider and actuated head. In this dissertation, we will focus on the control design of DSA servo systems with actuated suspensions.

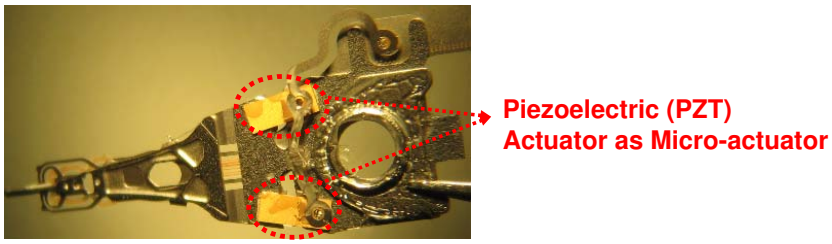

Figure 1.6: A picture of a PZT-actuated suspension (provided by Hutchinson Technology, Inc..)

Figure 1.6 shows the picture of a PZT-actuated suspension provided by Hutchinson Technology, Inc. (HTI). Two yellow PZT actuators are placed near the root of the suspension. They generate a push-pull action when driven by differential voltages. Meanwhile, a leverage mechanism is utilized to convert and amplify this small actuation displacements into large head motion.

Since dual-stage HDDs have two actuators, a DSA servo system can be represented by a dual-input-single-output (DISO) system as shown in Fig. 1.7 a). Since the PZT actuators may also excite some suspension resonances modes, the dual-stage actuators can be further represented as a DISO system with common suspension resonance modes as shown in Fig. 1.7 b).

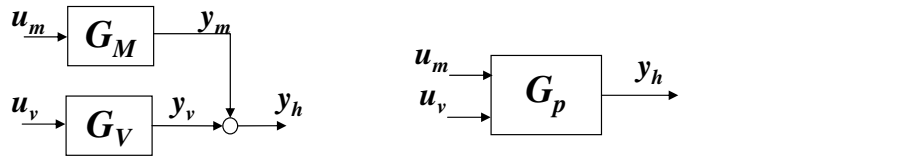

a) The dual-stage actuator b) Modeling with common resonance modes

Figure 1.7: The block diagram of the dual-stage actuators

For the DSA servo control design, we have to substitute the DISO plant G_p shown in Fig. 1.7 b) into the plant P in Fig. 1.5. As a result, the feedback controller in the servo architecture turns out to be a single-input-dual-output (SIDO) system.

1.2.2 Servo Systems with Irregular Sampling Rates

Although maintaining a regular sampling rate is quite attractive for HDD servos, sampling intervals for HDD servo systems are not always equidistant and sometimes, an irregular sampling rate due to missing PES sampling data is unavoidable. For example, false PES demodulation, due to incorrect servo address mark (SAM) detection [17] or damaged servo patterns in several servo sectors, makes the feedback PES unavailable in those servo sectors, resulting in an irregular sampling rate. In this dissertation, the unavailability of feedback signals at a given sampling instance is referred to as a "missing sample". In addition, irregular sampling rates also frequently occur during self-servo track writing process [4]. For example, during some SSTW processes, the time of writing final concentric servo patterns may coincide with the time of reading the feedback position error signal from previously written servo patterns. This conflict, caused by the fact that an HDD servo system can not read and write at the same time, is referred to as a "collision" of reading the PES with writing the final servo pattern. Such a collision makes the feedback signal unavailable resulting in an irregular sampling rate.

For the servo design of disk drives with these irregular sampling rates, we consider the block diagram of the actuator plant shown in Fig. 1.8. In the figure, $y(k)$ is a new feedback signal fed into the feedback controller C_{fb} in the servo control architecture illustrated in Fig. 1.5. Moreover, y is switched to PES when the PES is available, while y is switched to zero when the PES is unavailable [34].

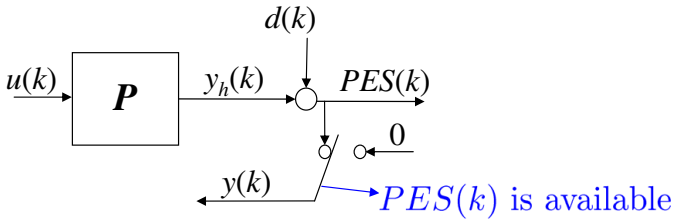

Figure 1.8: The block diagram of HDD servos with irregular sampling rates

Generally speaking, the location of damaged servo sectors and the collision in the self-servo track writing process is consistent on each single servo track. In other words, the unavailability of PES for HDD servo systems takes place at some fixed and predetermined positions for a given track. Furthermore, by considering that the natural periodicity of HDDs is related to the disk rotation, the servo system from the input $u(k)$ to the output $y(k)$ shown in Fig. 1.8 can be represented by a linear periodically time-varying system with period equal to the number of servo sectors.

1.2.3 Concentric Self-Servo Track Writing Servos

Self-servo track writing is an alternative method of writing servo patterns using the HDD's own reading and writing heads and servo system in order to decrease manufacturing cost and improve productivity as well as improve servowriting quality. The two most popular methodologies currently used by the HDD industry are the so-called concentric and spiral SSTWs. However, we will only focus on the servo design of concentric self-servo track writing in this dissertation.

In the concentric SSTW process, the timing and radial position reference information, which is used by the servo system to write the servo patterns for the current track using the write head, is read from the servo patterns that were written for the previous track using the read head. Because both timing information and radial position information are read by the read head from the previously written track, two separate feedback loops [31] are utilized in an SSTW control system. The radial position control loop controls the radial position of the write head relative to the radial position of the previous track, in order to record servo pattern tracks in a concentric fashion. Simultaneously, timing information is collected by the read head reading the servo patterns on the previous track for the timing control loop. With the aid of a phase lock loop (PLL), the timing control loop determines when to start recording the servo information of the current track so as to maintain a precise alignment of the servo sector information along the disk's circumference. Since the control design of these two control loops is similar, this dissertation will only focus on the servo control of the concentric SSTW radial position control loop.

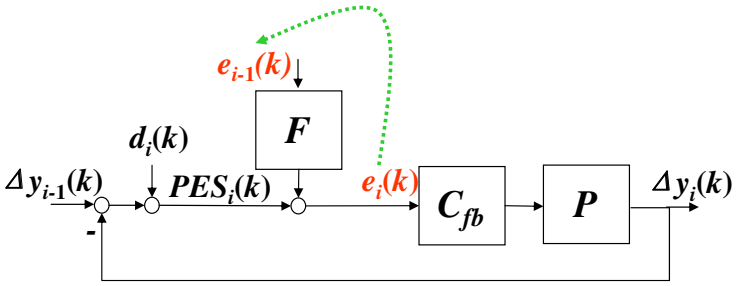

Figure 1.9: The control structure of SSTW servos with feedforward control

Figure 1.9 shows the block diagram of the concentric SSTW servo system. The system includes a feedback loop with the actuator plant P and the feedback controller C_{fb}. In the figure, i and k denote the track index and servo sector index respectively, while $\triangle y_i(k)$ and $d_i(k)$ respectively denote the track error and overall disturbances contributing to PES at the track position i and servo sector k. Since concentric self-servo track writing systems track-follow a previously written track using the read head, while writing the servo patterns for the current track using the write head, the

reference input becomes $\triangle y_{i-1}(k)$. As a result, track errors, which came into being when the previous track was written, can propagate into the currently written track.

As illustrated in Section 1.1.2, servo sectors on the current track must be aligned with the corresponding servo sectors on the previously written tracks. Therefore, by introducing a gap delay [50] between the read head and the write head, the "collision" of reading PES and writing servo patterns does not occur in concentric self-servo track writing process. Consequently, concentric SSTW servo systems can be treated as linear time-invariant systems [38].

An efficient and frequently used technique to prevent radial positioning error propagation in concentric SSTW servo systems is to incorporate a feedforward controller F, as depicted in Fig. 1.9. In this case, the control architecture includes a feedback compensator C_{fb} to attenuate disturbances and a feedforward compensator F to contain the error propagation from the previously written tracks. The feedforward control F generates an additional control action that is added to $PES_i(k)$ in order to generate the error signal $e_i(k)$ that is fed to the feedback compensator, by using the error signal, $e_{i-1}(k)$ that was generated when the previous track was written, as its input signal.

1.3 Research Objectives

This dissertation addresses the issue of disturbance attenuation to improve servo control performance in hard disk drives. The ultimate research objective is to develop control strategies in order to increase the storage density and reduce the manufacturing cost in HDDs. Recently, hard disk drives with the dual-stage actuator configuration have been deployed so as to increase their servo bandwidth. Accordingly, many dual-stage control design methodologies have been developed, including those based on single-input-single-output (SISO) design methods (such as sensitivity decoupling method [29], PQ method [43] and parallel design method [44]) and those based on modern optimal control design methods (such as LQG [10], H_∞ control [48], μ-synthesis [23], mixed H_2/H_∞ control [46], etc). In order to further improve HDDs' servo performance, the first objective of this dissertation is to develop new track-following controller design methodologies for dual-stage HDDs and evaluate them through experiment studies.

Since the control theory for linear time-invariant (LTI) systems has been well studied, most of HDD servos are designed based on a regular sampling rate, i.e. equidistant sampling intervals. However, sometime an irregular sampling rate caused by missing PES sampling data is unavoidable, for example, HDD servos with false PES demodulation and some self-servo track writing servos with missing PES sampling data. So far, not much attention has been paid to these irregular sampling rates in previous

work. The second objective of this dissertation is to develop control design methodologies to handle irregular sampling rates and thus to improve the servo performance for hard disk drives with missing PES sampling data.

As discussed in Section 1.1.2, position feedback signals for HDD servos are generated from the pre-written servo patterns on the disks and any written-in TMR introduced in servo track-writing process will later appear as written-in repeatable runout. Recently, concentric self-servo track writing techniques have been proposed to improve the servo track-writing quality and reduce its cost. The third objective of this dissertation is to investigate the novel control schemes of concentric SSTW servos in order to improve their servo track-writing performance.

1.4 Outline of the Dissertation

The dissertation is organized as follows. Chapter 2 discusses the design and implementation of track-following dual-stage servo systems. In this chapter, the experimental setup is described, an dual-stage servo system with an actuated-suspension assembly is modeled, and dual-stage track-following controllers are designed and implemented based on two proposed control design methodologies.

Chapters 3 and 4 present the optimal H_∞ control synthesis for HDDs with irregular sampling rates. In Chapter 3, optimal H_∞ control is extended to general linear periodically time-varying systems. Subsequently, a simulation study is conducted to evaluate the effectiveness of the H_∞ control design algorithm for LPTV systems derived in Chapter 3 on single-stage HDDs with both single-rate and multi-rate sampling and actuation. Finally, in Chapter 4, experimental studies are conducted on a set of single-stage HDDs with irregular sampling rates, which corroborates theoretical simulation results.

Chapter 5 discusses the servo design of concentric self-servo track writing. In this chapter, two novel control design methodologies are developed based on a feedforward control structure. In addition, a simulation study is provided to evaluate the proposed methodologies.

Chapter 6 concludes the dissertation by summarizing the results and major achievements. Future work is also discussed.

Chapter 2

Track-Following Control Design and Implementation of Dual-Stage HDDs

The continuously increasing storage capacity of hard disk drives poses a great challenge to precisely position the read/write head on the desired track. Typically, tracking performance is measured by track mis-registration (TMR). As discussed in the previous chapter, TMR can be broken down into a component due to repeatable runout (RRO) and a component due to non-repeatable runout (NRRO). RRO mainly results from disk eccentricity, non-ideal servo track writing [52], and spindle motor vibration and is hence synchronous with the disk rotation speed. NRRO can be categorized into torque disturbance, windage, non-repeatable disk motions and measurement noises. The torque disturbance, which is mainly caused by the bias force of the flexible cable, the pivot friction and the air-turbulence impinging on the VCM, is typically a low frequency disturbance. Windage, which is mainly due to air-turbulence directly exciting suspension resonance modes, is primarily a high frequency disturbance. Non-repeatable disk motions, which directly affect the position of R/W head relative to the servo track, result in additional track runout. Measurement noise, representing the effects of PES demodulation noise, includes electrical noise and A/D quantization noise. The goal of HDD servo systems is to reduce TMR as much as possible. A great deal of research effort has been focused on the development of disturbance rejection algorithms for canceling RRO, such as adaptive feedforward cancelation (AFC) [42, 62] and this topic will not be pursued in this dissertation.

In this chapter, we present two track-following control designs for dual-stage servo systems. The first controller was designed by combining an outer loop sensitivity-decoupling controller with an inner loop disturbance observer [55]. Two different Q filters were utilized in the inner-loop disturbance observer (DOB) to achieve both

good disturbance rejection and robust stability, by considering that the plant uncertainties for the VCM and the microactuator are quite different. The second track-following design technique is based on the idea of minimizing the H_2 norm of the nominal closed-loop system for a good performance as well as satisfying an H_∞ norm constraint for the robust stability. This idea turns out to be a mixed H_2/H_∞ control problem [37] that is usually transformed into a convex optimization with linear matrix inequalities (LMIs). However, the mixed H_2/H_∞ control synthesis through a convex optimization using LMIs may result in significant conservatism. A third controller design technique is discussed in this chapter, which consists in tuning a nominal H2 controller by adjusting control input frequency shaped weightings. It is shown that such a design achieves better robust performance than the mixed H_2/H_∞ control synthesis technique. In addition, an add-on integral action is incorporated so as to suppress constant and low-frequency disturbances. The designed controllers are implemented on a PZT-actuated suspension dual-stage servo system, which utilizes the micro-actuator to bend the suspension in order to generate a controlled fine radial head motion. The servo system's PES is obtained from the output of a laser Doppler vibrometer (LDV), which measures the absolute radial slider displacement. Since such a setup does not have track runout, a computer generated runout signal is injected into the control system to simulate track motion.

2.1 Test Setup and Modeling of the Dual-Stage Servo System

2.1.1 Experimental Setup

Figure 2.1 shows a picture of the experimental setup used in this research. A PZT-actuated suspension was assembled to an arm of the E-block of a commercial 3.5" 7200 RPM disk drive. A LDV was utilized to measure the absolute radial displacement of the slider. The resolution of the LDV is 2 nm for the measurement gain of 0.5 μ/V. The control circuits include a Texas Instrument TMS320C6713 DSP board and an in-house made analog board with a 12-bit ADC, a 12-bit DAC, a voltage amplifier to drive the MA, and a current amplifier to drive the voice coil motor (VCM). The DSP sampling frequency is 71.4 KHz in this chapter. And the input delay including ADC and DAC conversion delay and DSP computation delay is 6 μs. A hole was cut through the case of the drive to make laser shine into the drive. It should be noted that these modifications affected the response of the drive and may have detrimentally affected the attainable performance of the servo system, as will be discussed in Section 2.3.

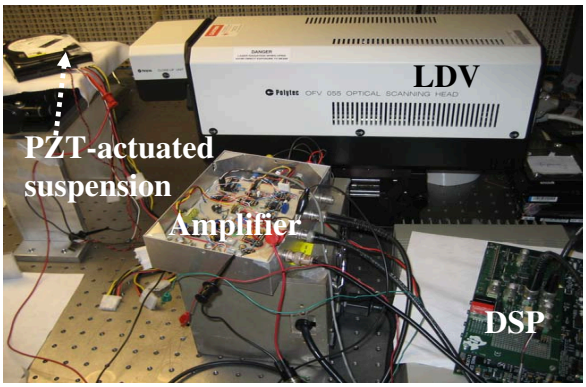

Figure 2.1: DSA experimental setup

2.1.2 Dual-Stage Actuator Modeling

The frequency response of the VCM shown in Fig. 2.2, was measured from the input of its current amplifier to the slider motion, while the frequency response of the microactuaor shown in Fig. 2.3, was measured from the input of its voltage amplifier to the slider motion. The experimentally-obtained frequency responses show that the flexi-cable mode is around 160 Hz and the microactuator resonance mode is around 18 KHz. Then, we did frequency response fitting for the experiment frequency responses by using Weighted Least Square (WLS) techniques. Consequently, the fitted VCM and micro-actuator transfer functions have 12 states and 10 states respectively.

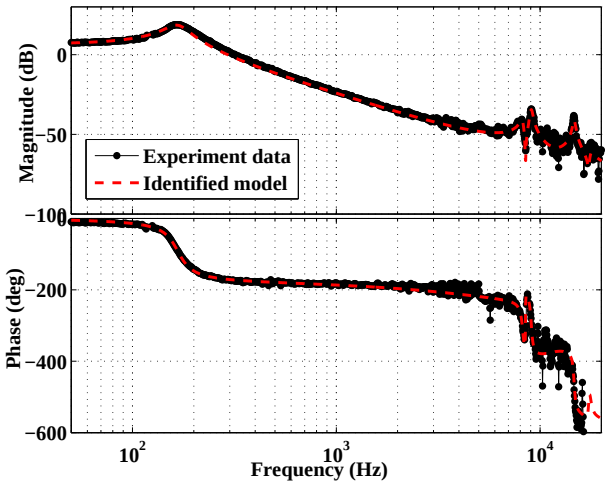

Figure 2.2: VCM frequency response

The experiment frequency responses show that the VCM and the micro-actuator have some common suspension resonance modes. In order to reduce the system order, all

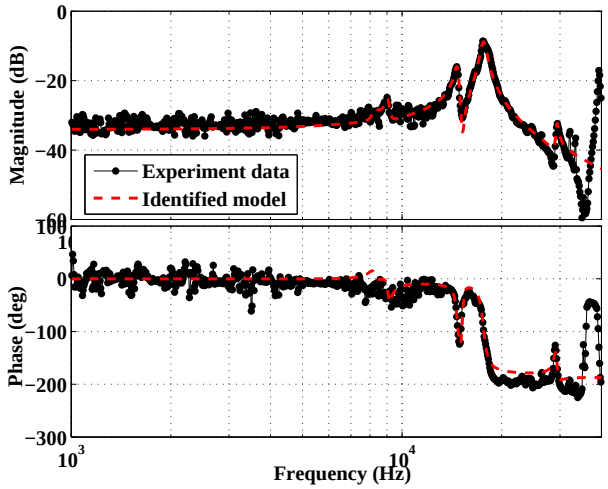

Figure 2.3: PZT micro-actuator frequency response

of the five suspension modes are treated as common modes. Then, the dual-stage actuator system was modeled as a double-input-single-output system with 12 states after the common mode identification. The simulated frequency responses for the identified VCM and MA models are shown in Fig. 2.2 and Fig. 2.3 respectively. With the identified disturbances presented in the following section, the complete dual-stage servo system is modeled as the block diagram illustrated in Fig. 2.4.

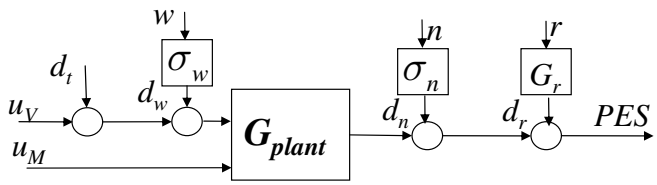

Figure 2.4: Modeling of complete DSA servo

2.1.3 Disturbance Identification

Measurement noise d_n

As the LDV integrates velocity signals to calculate displacement signals, its displacement measurement has a low frequency drift, which can be seen from the LDV measurement noise power spectrum density (PSD) shown in Fig. 2.5. The low frequency measurement noise can be considered as runout and is captured by a second order low-pass filter shown in Fig. 2.5. At high frequency, the LDV measurement noise was modeled as a white noise with $\sigma_n = 1.3$ nm.

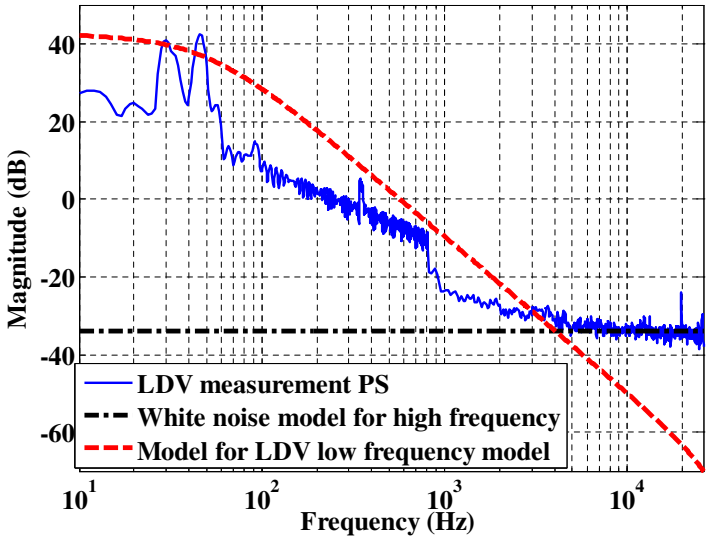

Figure 2.5: LDV measurement noise power spectrum density

Windage torque disturbance identification d_w

The windage torque disturbance—which is caused by the air-turbulence impinging on the VCM and directly exciting the suspension modes and is known to be a broad band excitation—is assumed to a white noise and denoted by the input signal d_w to VCM in Fig. 2.4. The amplitude σ_w was estimated by matching the power spectrum density of the absolute open-loop slider motion with the VCM plant.

Runout identification d_w

Although there is no track runout for our experimental setup, a runout model, characterized from the track runout data of a real drive, was included to make our control design more realistic. The real track runout caused by disk vibrations has several disk modes between 1 KHz and 3 KHz. In order to make the control synthesis simple, the disk mode peaks were characterized by a second order envelop shown in Fig. 2.6. Note that the LDV low frequency measurement noise was also treated as runout and the measurement noise is much higher than the real track runout at low frequency. Then, the LDV low frequency measurement noise and the second-order envelop for the disk modes were combined to construct the complete runout model shown in Fig. 2.6. The root-mean-square (RMS) value of this runout model is 118.12 nm.

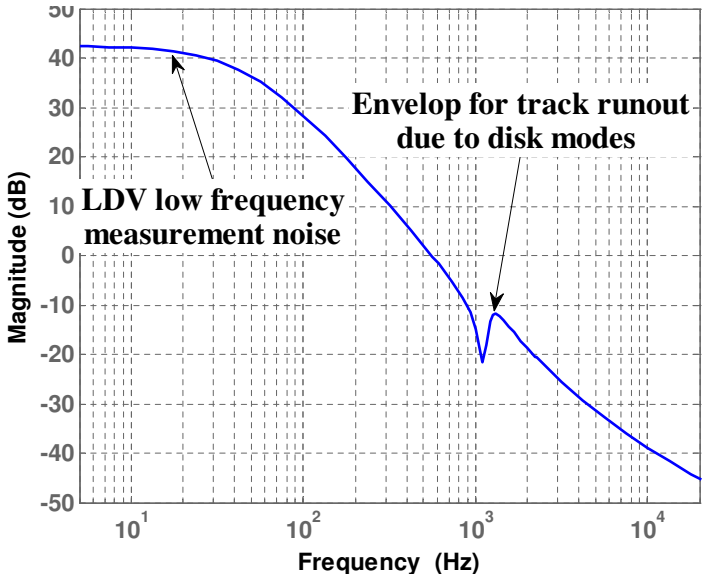

Figure 2.6: Complete runout model

Low frequency torque disturbance d_t

The torque disturbances due to the bias force of the flexible cable and the pivot friction have nonlinearities, which makes it difficult to model these disturbances. However, these torque disturbances are mainly at low frequency. Thus, to reject these torque disturbances, we just incorporated an integral action into the controllers instead of modeling these torque disturbances.

2.2 DSA Track-Following Control Design

2.2.1 Disturbance Observer Design

Design methodology

Disturbance observer control has been broadly used in mechatronic systems to do disturbance rejection with a proper Q filter selection [27]. In this chapter, we extended this technique to dual-stage actuation servo systems. By considering that the VCM and the micro-actuator have different plant uncertainties, two different Q filters were designed to achieve both good performance and robust stability. The sensitivity-decoupling dual-stage servo technique [29] was used to design the servo system's outer loop control. Figure 2.7 shows the block diagram of the disturbance observer, where G_V^n, G_M^n and d_{tot} represent the nominal VCM plant, the nominal MA plant and

the overall effect of all disturbances respectively. Note that here the nominal plants G_V^n and G_M^n are required to be minimum phase [51]. Their magnitude bode plots are shown in Fig. 2.8.

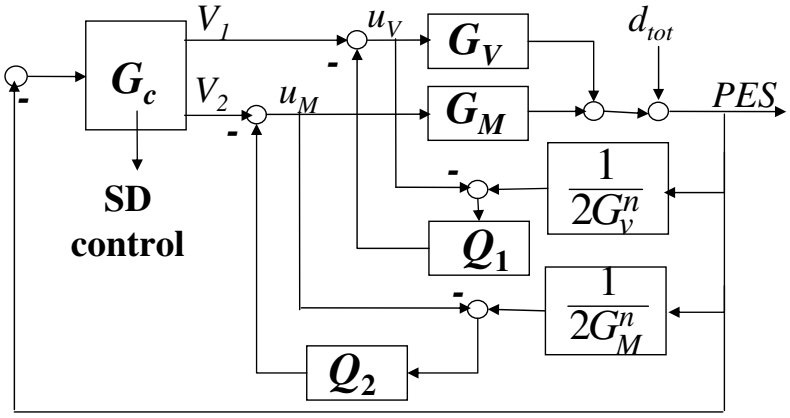

Figure 2.7: Dual-stage disturbance observer control design

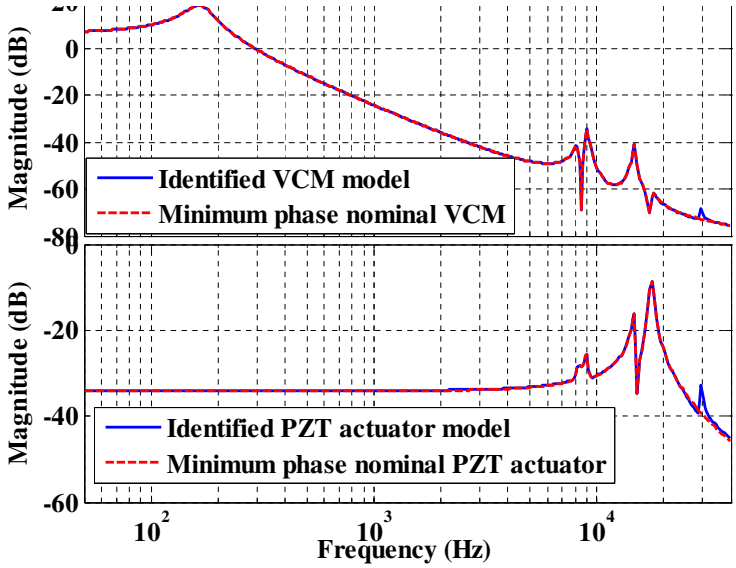

Figure 2.8: Nominal plants for VCM and MA

Then the PES can be written as:

$$PES(s) = \frac{\frac{1-Q_2(s)}{1-Q_1(s)}G_V(s)V_1(s) + G_M(s)V_2(s) + (1-Q_2(s))d_{tot}(s)}{\frac{1}{2}\left(1 + Q_2(s)\triangle_2(s) + \frac{1-Q_2}{1-Q_1}(1+Q_1(s)\triangle_1(s))\right)} \tag{2.1}$$

where $\triangle_1$ and $\triangle_2$ are respectively the VCM and MA model uncertainties, i.e. $G_V(s) = G_V^n(s)(1+\triangle_1(s))$ and $G_M(s) = G_M^n(s)(1+\triangle_2(s))$. For the robust stability, the Q_1

and Q_2 must satisfy the following constraint

$$\left\| \frac{(1-Q_1)Q_2\triangle_2 + (1-Q_2)Q_1\triangle_1}{1-Q_1+1-Q_2}(s) \right\|_\infty < 1 \ . \tag{2.2}$$

By considering the arbitrariness of $\triangle_1$ and $\triangle_2$, the robust stability constraint is transformed to the following constraint

$$\frac{|(1-Q_1)Q_2\triangle_2(j\omega)| + |(1-Q_2)Q_1\triangle_1(j\omega)|}{|(1-Q_1+1-Q_2)(j\omega)|} < 1, \text{ for } \forall\omega \ . \tag{2.3}$$

Selection of Q filters

Equation (2.1) shows that the disturbance error rejection transfer function of the servo system can be shaped by changing $Q_1(s)$ and $Q_2(s)$. In addition, the Q filters must be designed to satisfy the robust stability requirement in (2.3). Since many of the largest disturbances are at low frequency, the selection of high-pass filters of $1-Q_i\,(i=1,2)$ facilitates the low frequency disturbance rejection. Such a selection makes $Q_i\,(i=1,2)$ be low-pass filters and thus facilitates the attainment of the robust stability as well, since plant uncertainties are significant at high frequency. Moreover, in order to follow the track runout due to disk motions, Q_2 was designed to achieve good attenuation at the 1 KHz to 2 KHz frequency range for the overall sensitivity function from d_{tot} to PES shown in Fig. 2.7. In addition, by considering that the micro-actuator has less uncertainty than the VCM at high frequency, we designed the Q filters in such way that the DC gain of Q_2 for the MA is higher than that of Q_1 for the VCM and the corner frequency of Q_2 is also higher than that of Q_1. In order to minimize the order of the synthesized controller, the filters were chosen as first-order systems. Figure 2.9 shows the final selection of the Q filters. In order to verify the attainment of the robust stability constraint in (2.3), the magnitude of its left term, shown in Fig. 2.10, was calculated by replacing $\triangle_1$ and $\triangle_2$ with the differences between the nominal plants and the experiment frequency responses.

Outer loop control design

The outer loop controller was designed using the standard sensitivity-decoupling synthesis technique [29]. The VCM loop controller was designed to have a PI controller with a lead compensator and a notch filter to attenuate the biggest resonance peak at 9.06 KHz. The resulting gain crossover frequency for the VCM loop sensitivity function is 587 Hz. Since the microactuator has higher bandwidth than the VCM, the MA loop achieves a higher gain crossover frequency at 1.64 KHz, by designing the MA loop controller as a lag compensator with three notch filters to attenuate the three resonance peaks at 14.70 KHz, 17.71 KHz and 29.34 KHz. The corresponding

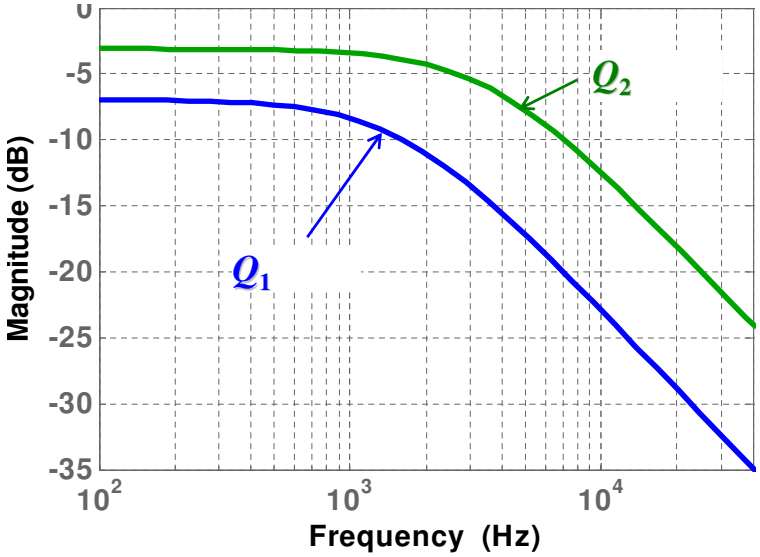

Figure 2.9: Selection of Q filters

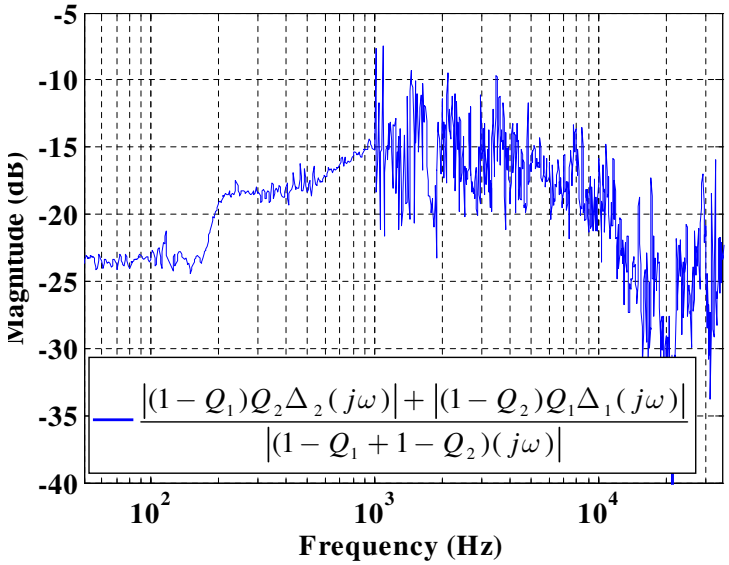

Figure 2.10: Robust stability verification

design results are shown in Fig. 2.11. The resulting gain margin, phase margin and gain crossover frequency for the overall outer loop are 6.72 dB, 28.8° and 1.34 KHz respectively.

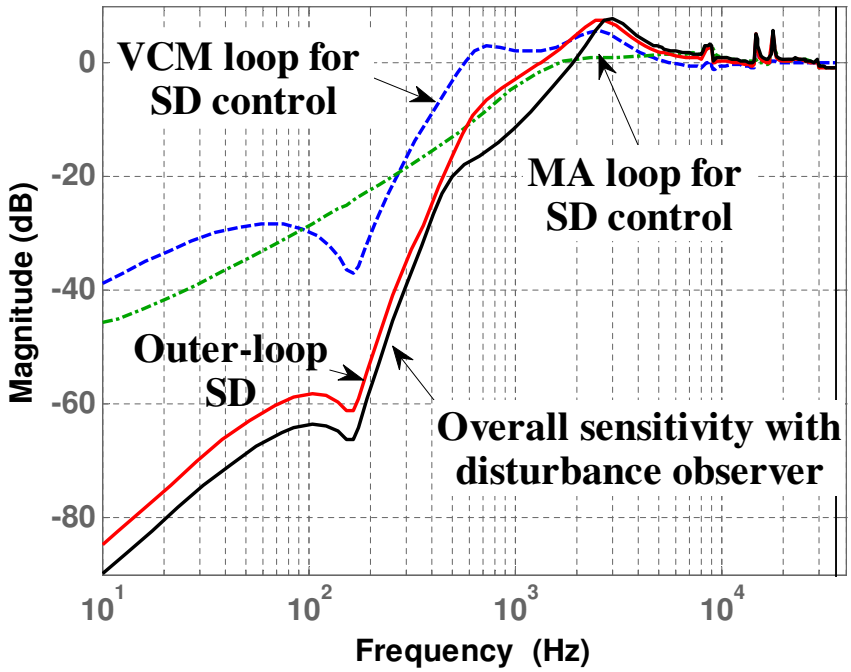

Figure 2.11: Sensitivity functions for DOB control design

As shown in Fig. 2.11, by using the disturbance observer outlined in this section, the overall gain margin, phase margin and gain crossover frequency can be improved to be 6.83 dB, 30.7° and 2.08 KHz respectively.

2.2.2 Mixed H_2/H_∞ Control Problem with Add-on Integral Action

Design methodology

In this section the dual-stage track-following servo synthesis problem is formulated by minimizing the variance of the PES while maintaining robust stability in the presence of plant input multiplicative unstructured uncertainties described as

$$P(s) = P_n(s)\left(I_2 + \begin{bmatrix} W_{\triangle V}(s) & 0 \\ 0 & W_{\triangle M}(s) \end{bmatrix}\right), \ \|\triangle(s)\|_\infty < 1\ . \tag{2.4}$$

$W_{\triangle V}$ and $W_{\triangle M}$ are respectively the VCM and MA uncertainty weighting functions, which must be selected by the designer. Based on the plant identification presented in Section 2.1, $W_{\triangle V}$ and $W_{\triangle M}$ were designed as first-order systems shown in Fig. 2.12.

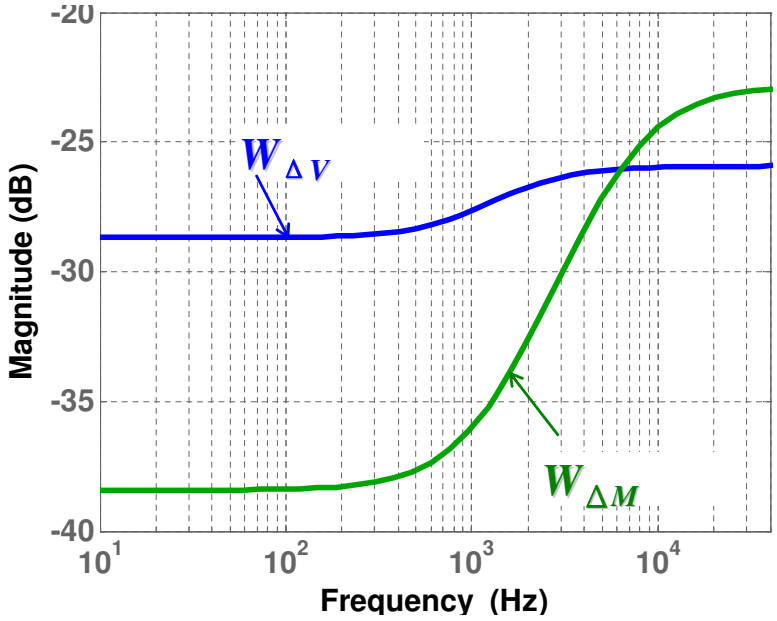

Figure 2.12: Uncertainty weighting functions

The linear fractional transformation (LFT) for the mixed H_2/H_∞ control design is shown in Fig. 2.13, in which the transfer function from d_∞ to z_∞ is used to measure the robust stability and W_u is a control input weight tuning value. In addition, the two tuning parameters γ_1 and γ_2 were introduced to analyze the conservatism in the control synthesis, which will be presented later. Then the optimal control synthesis can be written as the optimization problem in

$$\begin{aligned} \min_K \quad & \|T_{d_2 \leftarrow z_2}\|_2 \\ \text{s.t.} \quad & \|T_{d_\infty \leftarrow z_\infty}\|_\infty < 1 \end{aligned} \tag{2.5}$$

where "$T_{B \leftarrow A}$" means the closed-loop transfer function from input "A" to output "B" and "$\|T\|_2$" is the H_2 norm of the transfer function "T".

Mixed H_2/H_∞ control synthesis

To make the designed controller more implementable, mixed H_2/H_∞ controllers were synthesized in discrete-time domain. There are several control synthesis methods [7] to solve (2.5). In this chapter, a convex optimization approach via linear matrix

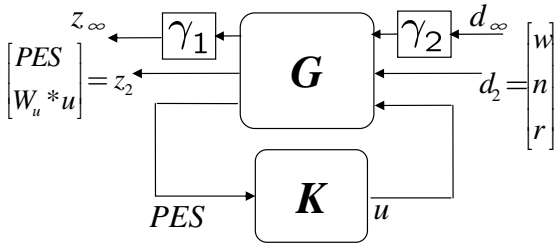

Figure 2.13: LFT for mixed H_2/H_∞ control synthesis

inequalities [22] was utilized for the control synthesis. The closed loop system with the output $\begin{bmatrix} z_\infty^T & z_2^T \end{bmatrix}^T$ from the input $\begin{bmatrix} d_\infty^T & d_2^T \end{bmatrix}^T$ can be written as:

$$G_{cl} = \left[\begin{array}{c|cc} A_{cl} & B_{cl\infty} & B_{cl2} \\ \hline C_{cl\infty} & D_{cl\infty\infty} & D_{cl\infty 2} \\ C_{cl2} & D_{cl2\infty} & D_{cl22} \end{array}\right] . \tag{2.6}$$

Then, by using the ideas of the congruent transformation, the optimization in (2.5) can be formulated as:

$$\begin{aligned} \min_{K,W,P_2,P_\infty} \ & \operatorname{trace}(W) \\ \text{s.t.} \ & \begin{bmatrix} W & \bar{C}_{cl2} P_2 & \bar{D}_{cl2} \\ * & P_2 & 0 \\ * & * & I \end{bmatrix} \succ 0 \\ & \begin{bmatrix} P_2 & \bar{A}_{cl} P_2 & \bar{B}_{cl2} \\ * & P_2 & 0 \\ * & * & I \end{bmatrix} \succ 0 \\ & \begin{bmatrix} P_\infty & A_{cl} P_\infty & B_{cl\infty} & 0 \\ * & P_\infty & 0 & P_\infty C_{cl\infty}^T \\ * & * & I & D_{cl\infty}^T \\ * & * & * & I \end{bmatrix} \succ 0 \end{aligned} \tag{2.7}$$

where the symbol "*" denotes the transpose of the corresponding element at its transposed position. The equivalence between the two optimizations does not require $P_2 = P_\infty$. However, it is necessary to impose the constraint

$$P_2 = P_\infty = P \tag{2.8}$$

to recover the convexity of the mixed H_2/H_∞ optimization [22]. The price of this restriction is that, as will be shown in the results that will be subsequently presented, a significant conservatism is thus brought into the design.

As the parameters γ_1 and γ_2 are reduced to 0, the solution of the mixed optimization H_2/H_∞ optimization given by (2.7) and (2.8) converges to the nominal H_2 design.

However, with $\gamma_1 = \gamma_2 = 1$ the solution of the mixed H_2/H_∞ optimization given by (2.7) and the imposition of the constraint by (2.8) results in a very conservative control design. As illustrated in Fig. 2.14, the mixed H_2/H_∞ control synthesis through the convex optimization approach attains a significantly worse performance than that attained by the nominal H_2 design which will be discussed in next section. Moreover, reducing the control input weighting function W_u to zero ("cheap" control), did not significantly alter the closed-loop sensitivity function from runout to PES of the mixed H_2/H_∞ design, as shown in Fig. 2.14.

Nominal H_2 control with robust stability

Since the mixed H_2/H_∞ control synthesis by using LMI optimization with (2.7) and (2.8) is too conservative to produce a good servo performance, another approach using the idea of the mixed H_2/H_∞ control problem is considered. Specifically, a controller was synthesized by the nominal H_2 control synthesis technique in which the input weighting value W_u was tuned to guarantee that the H_∞ norm constraint in (2.5) can be satisfied. In addition, the control actuation, by the designed nominal H_2 controller which resulted from the tuned control input weighting value, must be appropriate under the HDD hardware constraints such as the range limit for control actuation signals.

With the choice of $W_u = 0.1 * I_2$, the designed controller achieves the robust stability with $\|T_{z_\infty \leftarrow d_\infty}\|_\infty = 0.941 < 1$. The resulting sensitivity function from runout to PES for the nominal H_2 control is shown in Fig. 2.14. Obviously, the servo performance of the nominal H_2 control is much better than that of the mixed H_2/H_∞ control using the LMI optimization. As a result, we decided to implement the designed nominal H_2 controller so as to evaluate its performance on an actual hard disk drive.

In order to investigate the benefit of the micro-actuator, the sensitivity function from runout to PES was decomposed into a product of a VCM sensitivity function and a MA sensitivity function, following the procedure in the sensitivity-decoupling design technique [29]. As shown in Fig. 2.15, the gain crossover frequency of the MA sensitivity transfer function is 5.48 KHz, which means the microactuator has a significant impact in high frequency disturbance rejection.

Add-on integral action

An integral action was added onto the designed nominal H_2 controller to attenuate low frequency disturbances such as torque disturbances. Because of the small moving range of the PZT actuator, the integral action was only added onto the VCM controller

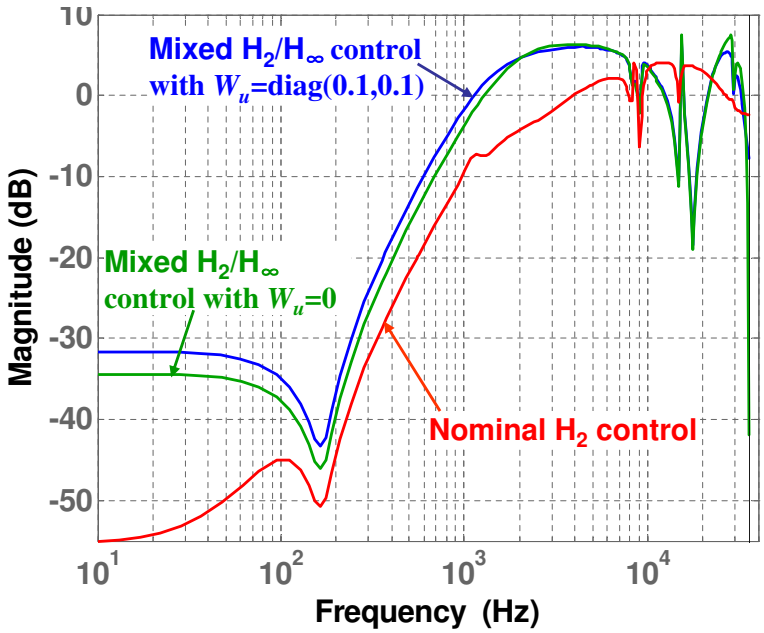

Figure 2.14: Sensitivity functions for the mixed H_2/H_∞ control synthesis by tuning W_u

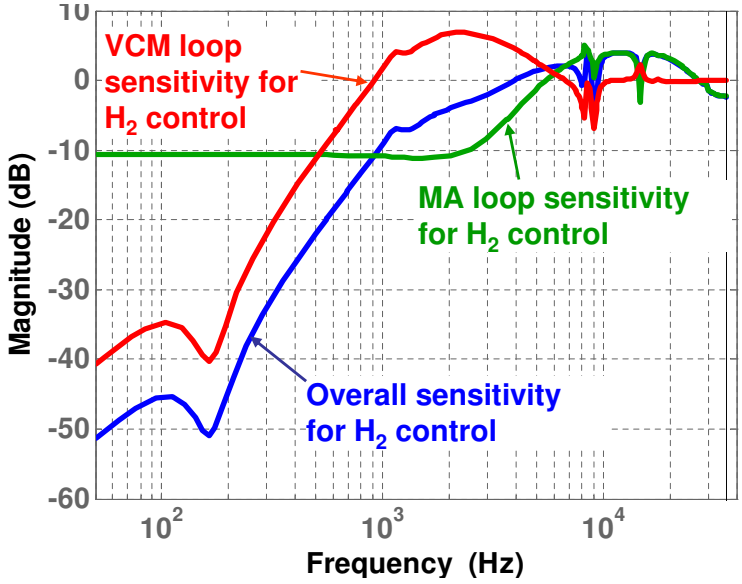

Figure 2.15: Sensitivity functions for nominal H_2 control

like

$$\tilde{K}(z) = \begin{bmatrix} g\frac{z-z_0}{z-1} & 0 \\ 0 & 1 \end{bmatrix} * K(z) \; . \tag{2.9}$$

In order to avoid degrading the performance of the original control, the parameters were chosen as $g = 1$, $z_0 = 0.9972$. With the add-on integral action, the constraint for the nominal H_2 control changes to $\|T_{d_\infty \to z_\infty}\|_\infty = 0.939 < 1$.

2.3 Implementation Results

2.3.1 Simulated Track Runout

In order to obtain a realistic evaluation of the dual-stage servo system performance, we used a computer generated runout signal to simulate track motions. The simulated track runout whose 3σ value is 11.4 nm, was generated from the power spectrum density of the real track runout data.

2.3.2 Experimental Results

In order to validate our system identification and control designs, the closed-loop sensitivity functions were first measured by using the sinusoidal sweeping signal. Because of the conservatism of the mixed H_2/H_∞ control, only the nominal H_2 control, which exhibited the better performance and the robust stability was implemented. The experimental results for the DOB baseline control (sensitivity-decoupling control) are shown in Fig. 2.16; the experimental results for the disturbance observer control with the base line control are shown in Fig. 2.17; the experimental results for the nominal H_2 control are shown in Fig. 2.18.

To analyze the closed-loop time-domain PES, 2048-point PES was recorded by the DSP. To highlight the advantage of the disturbance observer, the outer-loop sensitivity-decoupling controller was also implemented. The fast Fourier Transform (FFT) of the closed-loop PES without repeatable runout for the designed controllers is shown in Fig. 2.19.

The designed controllers in this chapter aim at rejecting non-repeatable runout, since repeatable runout can be canceled very well by using some specific compensators, such as adaptive feedforward cancelation [42, 62]. Therefore, it is helpful to take repeatable runout components out from the closed-loop PES to evaluate the designed controllers. Table 2.1 shows 3σ PES values for the designed controllers without repeatable runout components respectively.

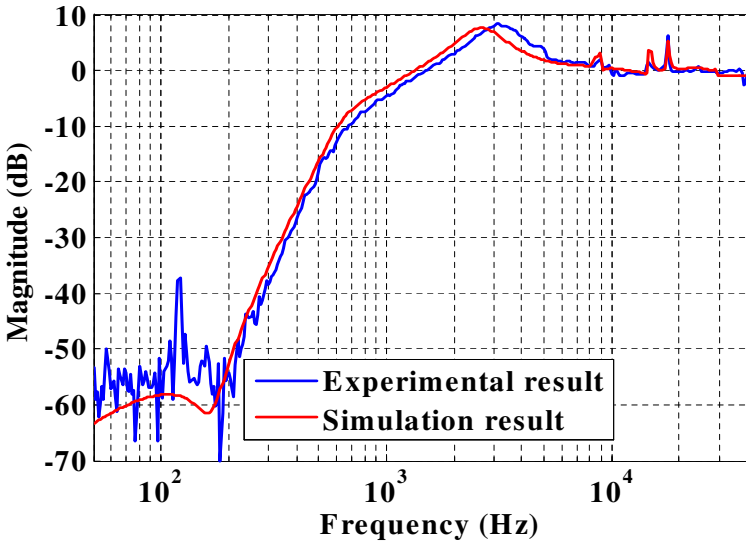

Figure 2.16: Sensitivity functions of sensitivity-decoupling control (the baseline control of the DOB design)

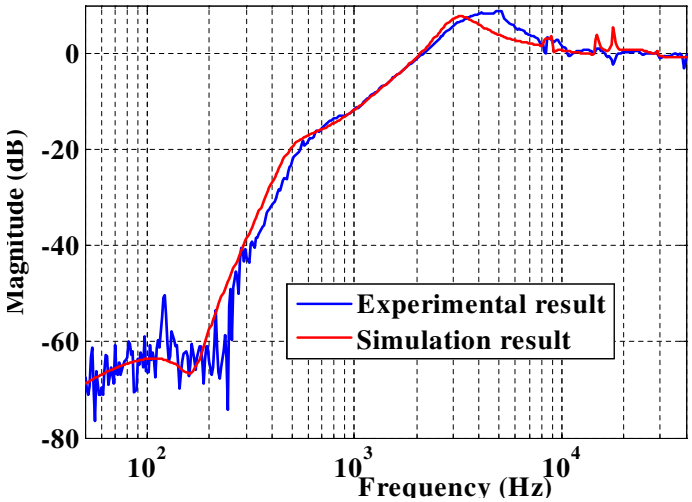

Figure 2.17: Sensitivity functions of DSA disturbance observer control

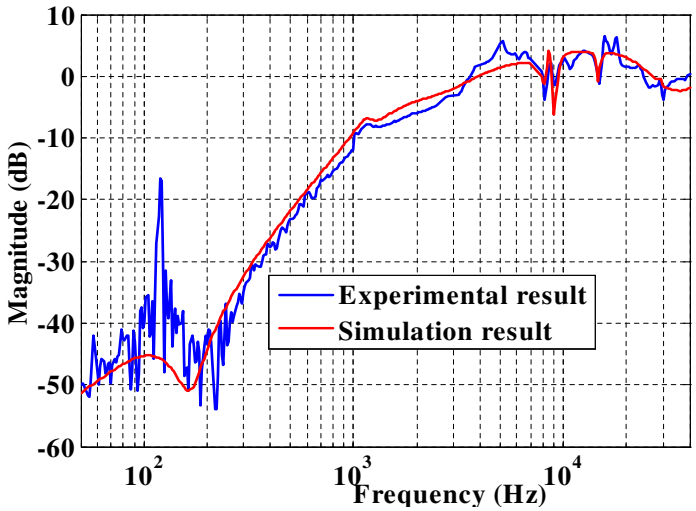

Figure 2.18: Sensitivity functions of nominal H_2 control

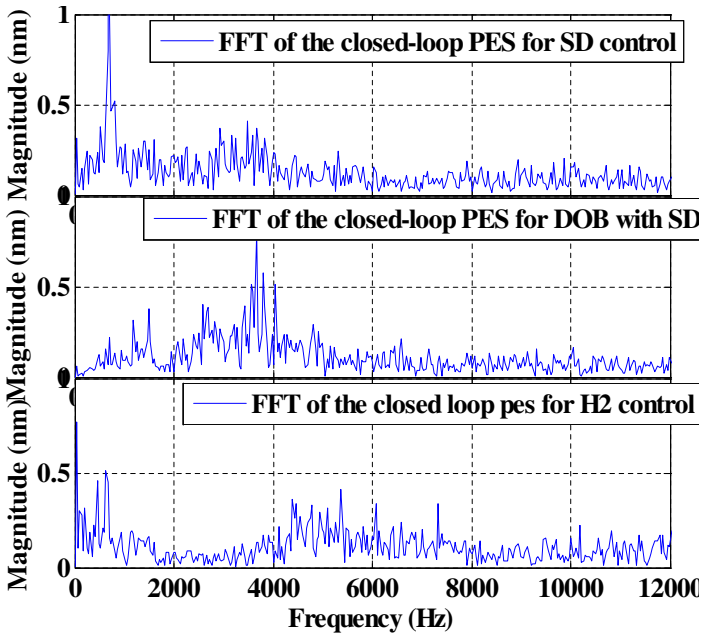

Figure 2.19: FFT of the closed-loop PES for DSA track-following servos

Table 2.1: Dual-stage track-following control implementation results

	3σ PES w/o RRO (nm)
SD control	17.0
Disturbance observer	13.1
Nominal H_2 control	9.4

2.3.3 Experimental Result Discussion

For the areal density of 1 Tb/in^2, the track pitch is approximately 50 nm, which requires that the 3σ TMR budget should be approximately 5 nm. In our experiments, the PZT-actuated suspension based dual-stage servo system achieved the best 3σ PES of 9.4 nm without repeatable runout. However, there are several factors that may detrimentally affect the servo performance in our experimental setup, making our results too pessimistic.

First, the LDV resolution is 2 nm, while the real PES resolution (8-bit PES) for the track pitch of 50 nm is around 0.2 nm. In addition, the LDV measurement noise at low frequency caused by the low frequency drift is quite high and the RMS value of the measurement noise is of the order of magnitude of 100 nm. Second, in our experiment one arm of the E-block was cut out, which may affect the original optimal structural dynamics of the E-block. Furthermore, we mounted the PZT-actuated suspension on the E-block by using a screw and E-POXY, which may introduce additional vibrations. Also, the disk drive we used in the experiment was modified from an off-the-shelf single stage commercial drive. Thus, the PZT-actuated suspension may not match the E-block very well and the slider flying height may not be set to its optimal value during the experiment.

2.4 Conclusion

In this chapter, two dual-stage track-following control design methodologies, the dual-stage disturbance observer with the sensitivity-decoupling control and the control using the idea of the mixed H_2/H_∞ problem, were developed. With the proposed dual-stage DOB technique, it is very convenient to make use of the loop-shaping scheme to design HDD servos by choosing two appropriate Q filters for VCM and MA respectively. Because of the conservatism of mixed H_2/H_∞ control synthesis using LMIs, a controller was alternatively designed using nominal H_2 control in which the control input weighting value was tuned to achieve robust stability. Consequently, the designed nominal H_2 control achieves not only good performances but also the robust stability. In addition, an integral action was incorporated into the designed nominal H_2 control in order to attenuate low frequency disturbances. The designs

were experimentally validated using a dual-stage servo system with a PZT-actuated suspension. The sensitivity-function crossover frequency of the disturbance observer design is 2.08 KHz and that of the H_2 design is 3.67 KHz. The 3σ PES without repeatable runout for the disturbance observer design is 13.1 nm, while the 3σ PES without repeatable runout for the H_2 design is 9.4 nm.

Chapter 3

Optimal H_∞ Control of Linear Periodically Time-Varying HDD Servos

As discussed in Chapter 1, an irregular sampling rate caused by missing PES sampling data sometime is unavoidable, and HDD servos with missing PES samples can be modeled as linear periodically time-varying (LPTV) systems. In fact, this class of systems is frequently encountered in mechatronic systems including hard disk drives in which the rotation of the disks induces periodic dynamic phenomena [42, 23, 39]. Moreover, as illustrated in this chapter, HDD servo systems with multi-rate sampling and actuation [12] can be easily represented as linear periodically time-varying systems for control synthesis purposes. Therefore, the control design of general linear periodically time-varying systems will be first considered.

H_∞ control is a popular control design methodology for synthesizing control systems that achieve robust stability or even robust performance. In addition, through the use of classical loop-shaping techniques, it is possible to design H_∞ controllers that that attain robust performance across an entire span of HDD units in a product line, by guaranteeing that each unit satisfy a minimum level of error rejection loop shaping. These techniques are potentially attractive in the design of mass-market mechatronic devices, such as HDDs, where consistent performance must be attained among tens of thousands of units in a given product line [21]. Furthermore, it is useful to extend these optimal H_∞ control design techniques to HDD servos with multi-rate sampling and actuation and missing PES sampling data. Since these servos are naturally modeled as linear periodically time-varying systems, the optimal H_∞ control synthesis for general LPTV systems will be addressed in this chapter.

Since the pioneering work of Zames in [61], significant progress has been made in the

design of optimal H_∞ control. In [15], a state-space solution to standard H_∞ control problems was given for continuous-time linear time-invariant (LTI) systems. As stated in [24], even though H_∞ control problems for discrete-time LTI systems can be solved by using the well-known bilinear transformation, it is more beneficial to solve the problems directly in the discrete-time domain. Peters and Iglesias [41] considered H_∞ control synthesis techniques for discrete-time linear time-varying (LTV) systems via the minimum-entropy control paradigm. The authors provided a procedure for solving output feedback H_∞ control synthesis problems for discrete-time LTV systems, by breaking the overall problem into a series of simpler control problems. The results and ideas presented in [41] are utilized here to derive explicit and implementable solutions for the minimum entropy H_∞ control of LPTV systems, using Riccati equations. Although it is possible to solve these types of problems as semi-definite programs (SDP) involving linear matrix inequality (LMI) constraints [8], we have found that the solutions via Riccati equations are often more computationally efficient and accurate than their corresponding SDP solutions [11].

The optimal H_∞ control synthesis techniques developed for LPTV systems in this chapter are used to design optimal H_∞ track-following controllers for single-stage HDD servo systems with both single-rate and multi-rate sampling and actuation [37], in order to evaluate their effectiveness. In next chapter, the control synthesis techniques will be applied to design HDD servos with missing position error signal samples.

3.1 Preliminaries

Here, we will consider general discrete-time linear periodically time-varying systems that admit a state-space realization with periodically time-varying entries like

$$G \sim \begin{bmatrix} x(k+1) \\ z(k) \\ y(k) \end{bmatrix} = \left[\begin{array}{c|cc} A(k) & B_1(k) & B_2(k) \\ \hline C_1(k) & D_{11}(k) & D_{12}(k) \\ C_2(k) & D_{21}(k) & 0 \end{array}\right] \begin{bmatrix} x(k) \\ w(k) \\ u(k) \end{bmatrix} \tag{3.1}$$

where $w(k)$ and $u(k)$ are respectively the disturbance and control inputs; $y(k)$ is the measurable output which is accessible to the control system; $z(k)$ is "performance monitoring" output, used in our optimization cost function. All time-varying matrix entries in G are assumed to be periodic with period N, for example, $A(k) = A(k+N)$.

Throughout this chapter, we will use the following notations, $B(k) = \begin{bmatrix} B_1(k) & B_2(k) \end{bmatrix}$, $D_{1\bullet}(k) = \begin{bmatrix} D_{11}(k) & D_{12}(k) \end{bmatrix}$, $C(k) = \begin{bmatrix} C_1(k) \\ C_2(k) \end{bmatrix}$, $D_{\bullet 1}(k) = \begin{bmatrix} D_{11}(k) \\ D_{21}(k) \end{bmatrix}$, and $D(k) = \begin{bmatrix} D_{11}(k) & D_{12}(k) \\ D_{21}(k) & 0 \end{bmatrix}$.

Before providing our developed control algorithm for the LPTV system in (3.1), we have the following notations and assumptions similar to the counterpart in [41]. The input disturbance $w(k)$ is assumed to belong to $\mathcal{L}_2$, the set of all square summable sequences. A bold operator will denote a linear operator corresponding to a time-varying system. Assume that every linear operator considered in this dissertation has a state-space realization and even a matrix representation under the usual basis. For example, let $\boldsymbol{G}$ be the linear operator of the time-varying system in (3.1) and $\boldsymbol{G}$ has a matrix representation $(\boldsymbol{G})_{i,j} = G_{i,j}$:

$$\boldsymbol{G} = \begin{bmatrix} \ddots & \vdots & \vdots & \iddots \\ \cdots & G_{0,0} & G_{0,1} & \cdots \\ \cdots & G_{1,0} & G_{1,1} & \cdots \\ \iddots & \vdots & \vdots & \ddots \end{bmatrix} .$$

Moreover, the system G could be denoted by the following state-space representation

$$G \sim \begin{cases} \boldsymbol{Z}\boldsymbol{x} = \boldsymbol{A}\boldsymbol{x} + \boldsymbol{B}\begin{bmatrix} \boldsymbol{w} \\ \boldsymbol{u} \end{bmatrix} \\ \begin{bmatrix} \boldsymbol{z} \\ \boldsymbol{y} \end{bmatrix} = \boldsymbol{C}\boldsymbol{x} + \boldsymbol{D}\begin{bmatrix} \boldsymbol{w} \\ \boldsymbol{u} \end{bmatrix} \end{cases} \sim \left[\begin{array}{c|c} \boldsymbol{A} & \boldsymbol{B} \\ \hline \boldsymbol{C} & \boldsymbol{D} \end{array}\right]$$

where $\boldsymbol{A} = \text{diag}\{A(k)\}_{k=0}^{\infty}$, $\boldsymbol{B} = \text{diag}\{B(k)\}_{k=0}^{\infty}$, $\boldsymbol{C} = \text{diag}\{C(k)\}_{k=0}^{\infty}$, and $\boldsymbol{D} = \text{diag}\{D(k)\}_{k=0}^{\infty}$ denote the operators for matrices. Notice that $\boldsymbol{Z}$ represents the forward shift operator and the operator $\text{diag}\{*(k)\}_{k=0}^{\infty}$ represents the block diagram matrix for the time varying matrix "*" from $k = 0$ to $k = \infty$, e.g.:

$$\text{diag}\{A(k)\}_{k=0}^{\infty} = \begin{bmatrix} \ddots & \vdots & \vdots \\ \cdots & A(1) & 0 \\ \cdots & 0 & A(0) \end{bmatrix} .$$

The bold symbols $\boldsymbol{x}$, $\boldsymbol{w}$, $\boldsymbol{u}$, $\boldsymbol{z}$ and $\boldsymbol{y}$ denote the stacked representation for the corresponding signal, e.g. $\boldsymbol{x} = \begin{bmatrix} \cdots & x^T(1) & x^T(0) \end{bmatrix}^T$.

The operator $\boldsymbol{A}$ is uniformly exponentially stable (UES) if there exist constants $c > 0$ and $\beta \in [0, 1)$ such that for all nonnegative integers l, $k \in Z^+$(the set of non-negative integers), we have

$$\|A(k+l-1)A(k+l-2)\cdots A(k)\| \leqslant c\beta^l .$$

The pair $(\boldsymbol{A}, \boldsymbol{B})$ is uniformly stabilizable, if there exists a bounded memoryless operator $\boldsymbol{F}$ such that $\boldsymbol{A} + \boldsymbol{B}\boldsymbol{F}$ is UES. Likewise, the pair $(\boldsymbol{C}, \boldsymbol{A})$ is uniformly detectable, if there exists a bounded memoryless operator $\boldsymbol{L}$ such that $\boldsymbol{A} + \boldsymbol{L}\boldsymbol{C}$ is UES.

In addition, the H_∞ norm of linear time-invariant systems is generalized as the ℓ_2 induced norm for discrete-time linear time-varying systems. For an LTV system H with input w and output z, its ℓ_2 induced norm is defined as

$$\|H\|_{2\leftarrow 2} = \left(\sup_{\boldsymbol{w}\in\mathcal{L}_2\setminus\{0\}} \frac{\sum_{k=0}^{\infty} z^T(k)z(k)}{\sum_{k=0}^{\infty} w^T(k)w(k)} \right)^{1/2} .$$

Moreover, the concept of entropy [41] is also required to be extended to linear time-varying systems. Suppose, the LTV system H (represented by the linear operator $\boldsymbol{H}$) has a matrix representation $(\boldsymbol{H})_{i,j} = H_{i,j}$. Here, the LTV system H is assumed to have the ℓ_2 induced norm less than γ, i.e. $\|H\|_{2\leftarrow 2} < \gamma$. Thus, the self-adjoint operator $\boldsymbol{I} - \gamma^{-2}\boldsymbol{H}^*\boldsymbol{H}$ has the following spectral factorization:

$$\boldsymbol{I} - \gamma^{-2}\boldsymbol{H}^*\boldsymbol{H} = \boldsymbol{M}^*\boldsymbol{M}$$

where $\boldsymbol{M}$ is a memoryless operator.

Then, the entropy of the LTV system H is defined as

$$\boldsymbol{E}(\boldsymbol{H},\gamma) := -\gamma^2 \mathrm{diag}\left\{ \ln\det(M_{k,k}^T M_{k,k}) \right\}_{k=0}^{\infty} . \tag{3.2}$$

Given the LPTV system defined in (3.1), the optimal H_∞ control objective is to find a minimum $\gamma > 0$ and an optimal linear time-varying compensator K with input $y(k)$ and output $u(k)$ so that the ℓ_2 induced norm of the closed-loop system $\mathcal{F}_\ell(G,K)$ that represents the system with the input $w(k)$ and the output $z(k)$ as depicted in Fig. 3.1, is less than γ, i.e.

$$\begin{aligned} \min_{K,\gamma} \quad & \gamma \\ \text{s.t.} \quad & \|\mathcal{F}_\ell(G,K)\|_{2\leftarrow 2} < \gamma . \end{aligned} \tag{3.3}$$

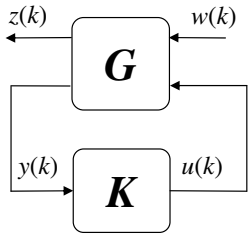

Figure 3.1: Block diagram of general LPTV control systems

In addition, we will use the following standard assumptions from [41], regarding the H_∞ control design of the time-varying system in (3.1):

A1. $D_{12}^T(k)D_{12}(k) \succ 0$ and $D_{21}(k)D_{21}^T(k) \succ 0$ for all k.

A2. the pair $(\boldsymbol{A}, \boldsymbol{B_2})$ is uniformly stabilizable and the pair $(\boldsymbol{C_2}, \boldsymbol{A})$ is uniformly detectable.

A3. the pair $\left(\boldsymbol{A - B_1 D_{21}^{\dagger} C_2},\ \boldsymbol{B_1}\left(\boldsymbol{I - D_{21}^{\dagger} D_{21}}\right)\right)$ is uniformly stabilizable with $\boldsymbol{D_{21}^{\dagger}} = \boldsymbol{D_{21}^{T}}\left(\boldsymbol{D_{21} D_{21}^{T}}\right)^{-1}$.

A4. the pair $\left(\left(\boldsymbol{I - D_{12} D_{12}^{\dagger}}\right)\boldsymbol{C_1},\ \boldsymbol{A - B_2 D_{12}^{\dagger} C_1}\right)$ is uniformly stabilizable with $\boldsymbol{D_{12}^{\dagger}} = \left(\boldsymbol{D_{12} D_{12}^{T}}\right)^{-1}\boldsymbol{D_{12}^{T}}$.

3.2 H_∞ Control Synthesis for Discrete-Time LPTV Systems

As mentioned in [41], there may exist many controllers that satisfy the inequality in (3.3) for a given γ. Similar to [36], we would like to obtain the minimum entropy controller [41] among all these controllers. The minimum entropy controller is intended to achieve the minimum entropy for the closed-loop time-varying system $\mathcal{F}_\ell(G, K)$. Note that the entropy for a time-varying system in (3.2) is defined as a memoryless operator. Unlike the minimum entropy for an LTI system, the minimum entropy for an LTV system means that its average entropy is minimum.

In order to synthesize the optimal H_∞ controller, we first need to obtain the unique minimum entropy controller satisfying the ℓ_2 induced norm constraint in (3.3) with a fixed γ, and then utilize a bi-section search method to find the minimum γ and the corresponding optimal controller. In the minimum entropy control synthesis methodology that follows, for simplicity and without loss of generality, we will assume that $\gamma = 1$.

3.2.1 Minimum Entropy Control for General Discrete-Time LTV Systems

In this section, we will temporarily ignore the periodicity of the LPTV system in (3.1) and utilize the similar techniques presented in [41] to develop the minimum entropy output-feedback control for general linear time-varying systems. In [41], the solution to the output feedback control problem can be obtained by transforming the output feedback control problem to an output estimation control problem, and then the solution to the output estimation control problem can be obtained as the dual of the disturbance feedforward control problem whose solution is obtained by solving the full information control problem. However, no explicit formulae are presented

in [41] for controllers synthesized using these steps. Alternatively, this dissertation synthesizes the output feedback minimum entropy control for general discrete-time LTV systems in the following three steps:

(I) the output feedback control problem is transformed to an output estimation control problem;

(II) the output estimation control problem is reduced to a full control problem;

(III) the solution to the full control problem is obtained as the dual of the full information control problem, whose solution is well known and provided in [41].

The details of the proposed techniques for the output feedback control problem reduction is discussed in Appendix A. Utilizing our proposed procedure yields the following unique stabilizing minimum entropy time-varying controller K which satisfies the constraint in (3.3) and is given by the following state space realization:

$$\begin{cases} \hat{x}(k+1) = \bar{A}(k)\hat{x}(k) + B_2(k)u(k) + F_t(k)\left(\bar{C}_2(k)\hat{x}(k) - y(k)\right) \\ u(k) = -T_{22}^{-1}(k)\bar{C}_{12}(k)\hat{x}(k) + L_t(k)\left(\bar{C}_2(k)\hat{x}(k) - y(k)\right) \end{cases} . \tag{3.4}$$

The parameters used to construct the controller in (3.4) are updated in the following steps:

1) Solve backwards in time the state feedback Riccati equation for all j:

$$\begin{aligned} X(j) = A^T(j)X(j+1)A(j) + C_1^T(j)C_1(j) - M(j) \times \\ \left(R(j) + B^T(j)X(j+1)B(j)\right)^{-1} M^T(j) \end{aligned} \tag{3.5}$$

where $M(j) = A^T(j)X(j)B(j) + C_1^T(j)D_{1\bullet}(j)$ and $R(j) = D_{1\bullet}^T(j)D_{1\bullet}(j) - \begin{bmatrix} I & 0 \\ 0 & 0 \end{bmatrix}$, so that the solution $X(j)(\succeq 0)$ is bounded for all j.

After obtaining the solution $X(j)$ for all $j = 0, 1, 2, \cdots$, we continue to calculate the other parameters.

2) Define $T(k) = \begin{bmatrix} T_{11}(k) & 0 \\ T_{21}(k) & T_{22}(k) \end{bmatrix}$ with $T_{11}(k) \succ 0$ and $T_{22}(k) \succ 0$, and then compute $T(k)$ using:

$$R(k) + B^T(k)X(k+1)B(k) = T^T(k)JT(k) \tag{3.6}$$

where $R(k) = D_{1\bullet}^T(k)D_{1\bullet}(k) - \begin{bmatrix} I & 0 \\ 0 & 0 \end{bmatrix}$, $J = \begin{bmatrix} -I & 0 \\ 0 & I \end{bmatrix}$.

3) Get $\begin{bmatrix} F_1(k) \\ F_2(k) \end{bmatrix} = \left(R(k) + B^T(k)X(k+1)B(k)\right)^{-1} M^T(k)$.

4) Calculate the following matrices for the filtering Riccati equation: $\bar{A}(k) = A(k) + B_1(k)F_1(k)$, $\bar{C}_2(k) = C_2(k) + D_{21}(k)F_1(k)$, and $\bar{C}_{12}(k) = -T_{22}(k)F_2(k)$. Let $D_\perp(k)$ be an orthogonal matrix to $D_{12}(k)$. In addition, define a matrix W such that $W^T(k)W(k) = I - T_{11}^T(k)T_{11}(k)$ and $W(k)$ has appropriate dimensions so that the following matrix multiplication is well defined:

$$\begin{bmatrix} \bar{D}_{111}(k) \\ \bar{D}_{112}(k) \end{bmatrix} = D_\perp(k)W(k) + D_{12}(k)T_{21}(k)$$

5) Update forwards in time the filtering Riccati equation solution with zero initial condition:

$$Y(k) = \bar{A}(k)Y(k-1)\bar{A}^T(k) + B_1(k)B_1^T(k) - \tilde{M}(k) \times \left(\tilde{R}(k) + \begin{bmatrix} \bar{C}_{12}(k) \\ \bar{C}_2(k) \end{bmatrix} Y(k-1) \begin{bmatrix} \bar{C}_{12}(k) \\ \bar{C}_2(k) \end{bmatrix}^T\right)^{-1} \tilde{M}^T(k) \quad (3.7)$$

where $Y(k) \succeq 0$ and

$$\begin{aligned} \tilde{M}(k) &= \bar{A}(k)Y(k-1) \begin{bmatrix} \bar{C}_{12}(k) \\ \bar{C}_2(k) \end{bmatrix}^T + B_1(k) \begin{bmatrix} \bar{D}_{112}(k) \\ D_{21}(k) \end{bmatrix}^T \\ \tilde{R}(k) &= \begin{bmatrix} \bar{D}_{112}(k) \\ D_{21}(k) \end{bmatrix} \begin{bmatrix} \bar{D}_{112}(k) \\ D_{21}(k) \end{bmatrix}^T - \begin{bmatrix} I & 0 \\ 0 & 0 \end{bmatrix} . \end{aligned}$$

6) Define $\tilde{T}(k) = \begin{bmatrix} \tilde{T}_{11}(k) & \tilde{T}_{12}(k) \\ 0 & \tilde{T}_{22}(k) \end{bmatrix}$, with $\tilde{T}_{11}(k) \succ 0$ and $\tilde{T}_{22}(k) \succ 0$, and compute $\tilde{T}(k)$ using

$$\tilde{R}(k) + \begin{bmatrix} \bar{C}_{12}(k) \\ \bar{C}_2(k) \end{bmatrix} Y(k-1) \begin{bmatrix} \bar{C}_{12}(k) \\ \bar{C}_2(k) \end{bmatrix}^T = \tilde{T}(k)\tilde{J}\tilde{T}^T(k) \quad (3.8)$$

where $\tilde{J} = \begin{bmatrix} -I & 0 \\ 0 & I \end{bmatrix}$.

7) Obtain

$$\begin{bmatrix} \tilde{F}_1(k) \\ \tilde{F}_2(k) \end{bmatrix} = \left(\tilde{R}(k) + \begin{bmatrix} \bar{C}_{12}(k) \\ \bar{C}_2(k) \end{bmatrix} Y(k-1) \begin{bmatrix} \bar{C}_{12}(k) \\ \bar{C}_2(k) \end{bmatrix}^T\right)^{-1} \tilde{M}^T(k) .$$

8) Calculate the filter gains:

$$L_t(k) = T_{22}^{-1}(k)\tilde{T}_{12}(k)\tilde{T}_{22}^{-1}(k) \text{ and } F_t(k) = \tilde{F}_1^T(k)\tilde{T}_{12}(k)\tilde{T}_{22}^{-1}(k) + \tilde{F}_2^T(k) .$$

3.2.2 The H_∞ Control Synthesis Applied to LPTV Systems

It should be noted that, because we are solving an infinite horizon problem and the state feedback Riccati equation given in Step 1) must be solved backwards in time, its exact solution does not currently exist [41]. Thus, the controller in (3.4) is not implementable for general time-varying systems. However, it is well known that the stabilizing solutions to the Riccati equations in Step 1) and Step 5) are unique [41]. Moreover, as shown in Lemma 1, these solutions for LPTV systems are also periodic. As a result, the solutions to two Riccati equations converge to the corresponding stabilizing solutions, which can be solved in a straightforward manner by iteration, starting respectively from zero final and initial conditions.

Lemma 1. *For LPTV systems with period N, the solutions to the Riccati equations in both Step 1) and Step 5) are periodic with period N. Furthermore, the H_∞ controller given by* (3.4) *is also periodic with period N.*

The proof of Lemma 1 is presented in Appendix B. The periodicity of H_∞ controllers for LPTV systems provides a significant advantage, since the Riccati equations in Step 1) and Step 5) for constructing the minimum entropy controller can be solved backward and forward respectively with zero initial conditions by iteration and their solutions will converge to the corresponding periodic solutions.

With Lemma 1, the optimal H_∞ control synthesis algorithm for LPTV systems is developed as follows.

Algorithm 1. *The following algorithm synthesizes optimal H_∞ control for general LPTV systems.*

S1. Choose a large initial interval and a large initial value γ.

S2. For a given value γ, calculate the minimum entropy controller:

- *Solve the state feedback Riccati equation* (3.5) *in Step 1) for constructing a minimum entropy controller with zero final conditions by iteration to obtain $X(j)$ $(j = 0, \ldots, N-1)$.*
- *If $X(j) \succeq 0$ and the factorization in* (3.6) *exists for $\forall j = 0, \ldots, N-1$, continue to solve the filtering Riccati equation in* (3.7) *with zero initial conditions by iteration to obtain $Y(k)$ $(k = 0, \ldots, N-1)$. Otherwise, stop.*
- *If $Y(k) \succeq 0$ and the factorization in* (3.8) *exists for $\forall k = 0, \ldots, N-1$, continue to calculate the control parameters for the minimum entropy controller. Otherwise, stop.*

S3. If the interval is small enough, stop. Otherwise, update the interval and γ and then go back to S2.

S4. Return the optimal H_∞ controller.

3.3 Design Examples for HDD Servo Systems

In HDDs, the dynamics from the VCM control to the head displacement have multiple structural resonance modes, which are subjected to unit-to-unit varying natural frequencies and damping ratios, due to manufacturing tolerances in mass production and changing operating conditions. Therefore, the control design of HDD servo systems must take performance robustness into account. As will be illustrated subsequently, optimal H_∞ control is quite suitable for HDD servo systems, since it is a convenient methodology for performing loop-shaping design and achieving a desired error rejection transfer function for a set of HDDs with plant variations.

In order to evaluate our proposed optimal H_∞ control design methodology in this chapter, the algorithm will be tested via a simulation study that utilizes a single-stage HDD benchmark model developed by the IEEJapan technical committee on Nano-Scale Servo (NSS) systems [49]. The nominal VCM model is indicated in Fig. 3.2. In the simulations, we will assume that the position error signal sampling frequency is $f_s = 26400$ Hz.

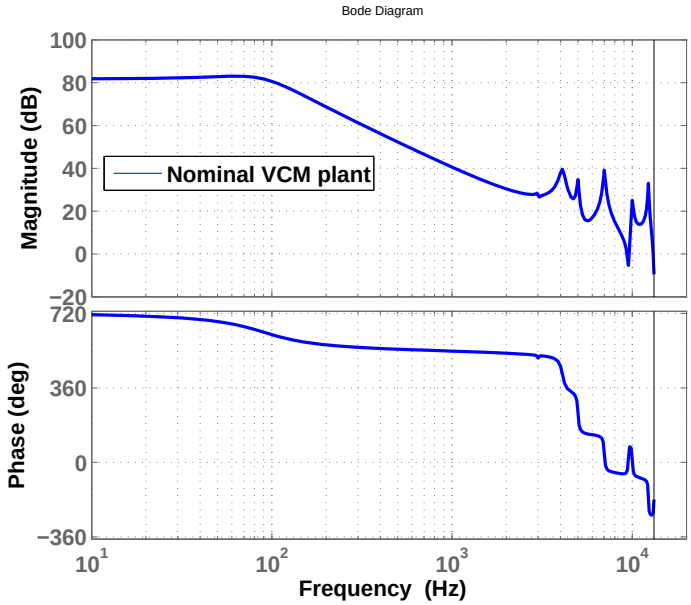

Figure 3.2: HDD benchmark VCM model

3.3.1 Optimal H_∞ Track-Following Control for Single-Rate HDD Servos

We consider the block diagram shown in Fig. 3.3 for the optimal H_∞ control design, where G_v^n, W_p, W_u, and $W_\triangle$ are respectively the nominal VCM plant, loop-shaping performance weighting function, control input weighting value, and plant uncertainty weighting function. In this example, we consider the case when the control actuation is performed at the same rate as the PES sampling rate. Thus, it is well known

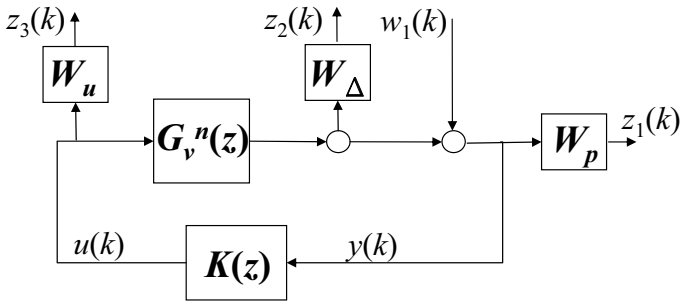

Figure 3.3: Control design formulation for single-rate HDDs

that the single-rate servo system is an LTI system that turns out to be an LPTV system with period $N = 1$. As a result, the corresponding control problem can be equivalently stated as:

$$\begin{array}{ll} \min_{K,\gamma} & \gamma \\ \text{s.t.} & \|T_{z\leftarrow w_1}\|_\infty < \gamma \ . \end{array} \tag{3.9}$$

$T_{z\leftarrow w_1}$ represents the transfer function matrix from w_1 to $z = \begin{bmatrix} z_1 & z_2 & z_3 \end{bmatrix}^T$ as shown in Fig. 3.3.

Notice that with $N = 1$, all of entries in the state-space realization of (3.1) are constant, and thus the Riccati equation solutions in (3.5) and (3.7) for constructing a minimum entropy controller converge to steady state solutions that can be computed via their corresponding discrete algebraic Riccati equations (DAREs). Consequentially, the synthesized optimal H_∞ controllers for LTI systems are also time-invariant.

In order to investigate the accuracy of the control synthesis algorithm presented in this chapter, we will compare a controller that is synthesized by our proposed methodology to the one that is synthesized by the Matlab function of "hinfsyn" in the Robust Control Toolbox using identical plant parameters and weighting functions. Notice that "hinfsyn" function in the Matlab version of R2007b performs H_∞ control synthesis for discrete-time systems by first mapping the discrete-time plant to a continuous-time plant using the bilinear transformation, performing H_∞ control synthesis in

continuous-time domain and then mapping the resulting H_∞ continuous-time control back to discrete-time domain using the bilinear transformation.

For the comparison, the weighting functions W_p and $W_\triangle$ and the weighting value W_u are selected so that the developed H_∞ control synthesis technique yields a solution to the minimization problem in (3.9) with $\gamma \leq 1$. Then, the magnitude Bode plot of the performance weighting function inverse for the single-rate design is illustrated in Fig. 3.4. With $\gamma \leq 1$, the designed servo is able to achieve the robust performance that the magnitude Bode plot of the designed error rejection transfer function will be below that of $|W_p(\omega)|^{-1}$ for all uncertainties characterized by the uncertainty weighting function $W_\triangle$. The magnitude Bode plot of $W_\triangle$ considered in this control design example is shown in Fig. 3.5, which indicates that the plant could have unstructured output uncertainty variation as high as $\pm 8\%$ at low frequency and $\pm 12\%$ at high frequency. In this chapter, $W_u = 2 \times 10^{-5}$ was selected so that the achieved γ is less than or equal to 1 and simultaneously the control actuation generated by the resulting controller is appropriate under the hardware constraints of real HDD servo systems.

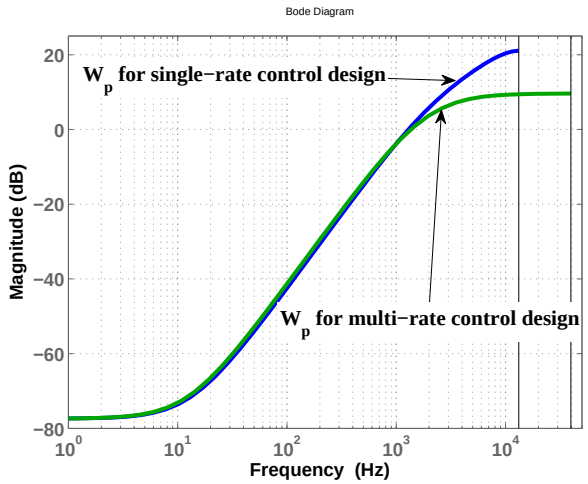

Figure 3.4: Magnitude Bode plots of performance weighting functions

The design results are illustrated in Fig. 3.6, which shows the magnitude Bode plot of the closed-loop error rejection transfer functions when the H_∞ controller is synthesized using the methodology proposed in this chapter and when it is synthesized using the Matlab function "hinfsyn". As shown in the figure, the Matlab function "hinfsyn" failed to synthesize a controller that could achieve the specified robust performance, while the synthesis technique proposed in this chapter produced an optimal H_∞ controller that satisfied all constraints with a minimum $\gamma^* = 0.99$. As stated in [24], the successive uses of the bilinear transformation (discrete time to continuous time and then back to discrete time) in the Matlab function "hinfsyn" may have introduced

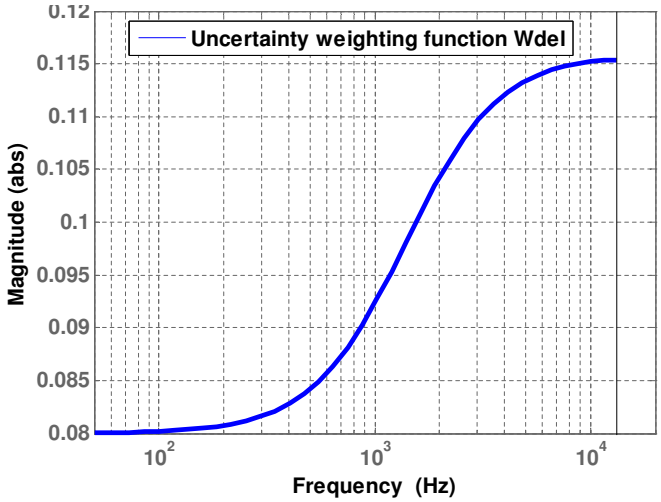

Figure 3.5: Magnitude Bode plots of the selected uncertainty weighting function

numeric accuracy problems, particularly when the systems are ill-conditioned. We have found in our simulation study that when the H_∞ constraints are relaxed, for example by selecting "less aggressive" performance weighting function W_p, the H_∞ controllers produced by the two synthesis techniques are almost identical.

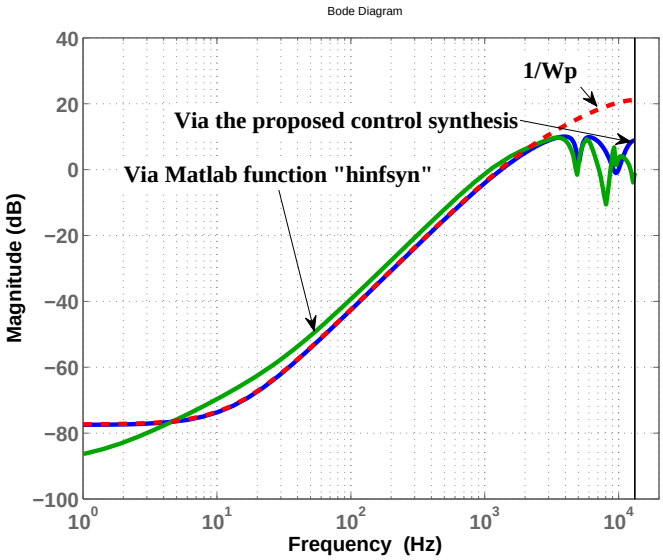

Figure 3.6: Sensitivity functions for the single-rate HDD servo

3.3.2 Optimal H_∞ Track-Following Control for Multi-Rate HDD Servos

In this section, the effectiveness of the developed control synthesis algorithm will be further evaluated by designing optimal H_∞ track-following controllers for multi-rate HDD servos. As discussed in [23], increasing the control actuation rate can improve both track-following control performance and robustness. In this subsection, we validate this idea by comparing the single-rate H_∞ controller that was designed in the previous section to a multi-rate H_∞ controller, where the actuation rate f_a is three times higher than the PES sampling rate f_s. In addition, since the higher rate actuation can be exploited to improve the control performance, a little more aggressive performance weighting function shown in Fig. 3.4 has been utilized for the multi-rate control design. Because of the higher actuation rate, it is necessary to discretize the plant model and the weighting functions indicated in the block diagram in Fig. 3.3 at the higher actuation rate f_a and to assume that PES measurements are only available at the instances $k \in \{0, N, 2N, \cdots\}$ where $N = 3$. Thus, HDD servo control systems with multi-rate sampling and actuation can be modeled by the block diagram shown in Fig. 3.7. Here, d is the overall contribution of all disturbances [37] including torque

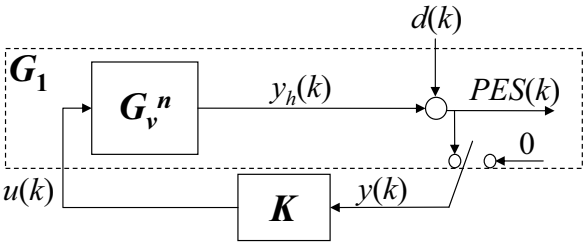

Figure 3.7: The HDD servo system with the nominal VCM plant

disturbance, windage, non-repeatable disk motions and measurement noise to PES. Then, the open loop plant for this servo system, indicated by the dashed box in Fig. 4.2, can be represented by following LPTV system with period $N = 3$:

$$G_1 \sim \begin{bmatrix} x(k+1) \\ y(k) \end{bmatrix} = \left[\begin{array}{c|cc} A^o & B_1^o & B_2^o \\ \hline C_2^o(k) & D_{21}^o(k) & 0 \end{array}\right] \begin{bmatrix} x(k) \\ d(k) \\ u(k) \end{bmatrix} . \tag{3.10}$$

Notice that all of matrices in (3.10) are constant except for $C_2^o(k)$ and $D_{21}^o(k)$, where

$$\begin{bmatrix} C_2^o(k) & D_{21}^o(k) \end{bmatrix} = \begin{cases} \begin{bmatrix} C_{2m}^o & D_{21m}^o \\ 0 & 0 \end{bmatrix} & k \in \{0, N, 2N, \cdots\} \\ \text{otherwise} \end{cases} .$$

From the standard assumption A1 listed in the preliminaries, the derived controller requires a condition $D_{21}(k)D_{21}^T(k) \succ 0$ for all k. Unfortunately, the typical approach

to enforce multi-rate sampling and actuation [34] will not work here because this would result in $D_{21}(k)D_{21}^T(k)$ being singular. In this chapter, we consider the block diagram shown in Fig. 3.8 for the multi-rate optimal H_∞ control synthesis. Here, we introduce a fictitious disturbance input w_2 which will be injected into the feedback signal y when the PES is not available so that the non-singularity assumption of $D_{21}(k)D_{21}^T(k)$ can be attained. Notice that if the gain of the resulting time varying controller K is zero when the PES measurement is unavailable at the time of k, then this fictitious noise will not affect the minimum closed-loop induced norm and the resulting optimal H_∞ controller. This expectation is achieved when the minimum entropy H_∞ control synthesis technique proposed in this paper is used, as will be discussed in detail later.

Unlike the standard H_∞ control problem formulation [47], here the performance weighting function is moved to the disturbance input side. By doing so, the feedback signal y is affected by a "colored" disturbance ($W_p w_1$) more directly when the sampling rate is lower than the actuation rate. In order to maintain the same H_∞ constraints as those that were used in Section 3.3.1, it is necessary to use the control synthesis architecture represented in Fig. 3.8 with the fictitious disturbance w_2, where the weighting functions W_p and $W_\triangle$ are the same as the weighting functions in Section 3.3.1.

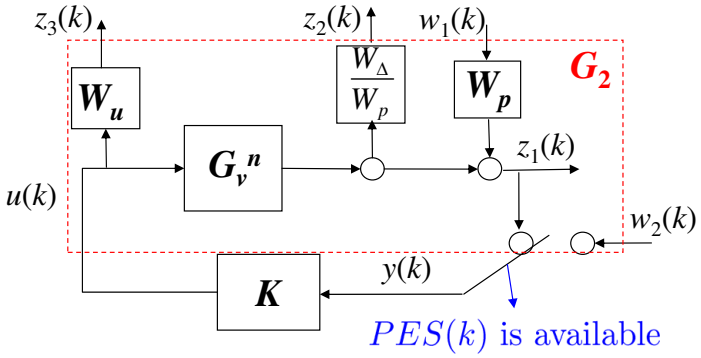

Figure 3.8: Control design formulation for HDDs with multi-rate sampling and actuation

As a result, we can formulate the optimal H_∞ control design problem as shown in (3.3) by replacing the system G by G_2, where G_2 is indicated by the dashed box in Fig. 3.8. Thus, G_2 is the open-loop map from $\begin{bmatrix} w_1 & w_2 & u \end{bmatrix}^T$ to $\begin{bmatrix} z_1 & z_2 & z_3 & y \end{bmatrix}^T$, which can be represented by the following LPTV system with period $N = 3$

$$G_2 \sim \begin{bmatrix} x(k+1) \\ z(k) \\ y(k) \end{bmatrix} = \left[\begin{array}{c|cc} A & B_1 & B_2 \\ \hline C_1 & D_{11} & D_{12} \\ C_2(k) & D_{21}(k) & 0 \end{array}\right] \begin{bmatrix} x(k) \\ w(k) \\ u(k) \end{bmatrix} \tag{3.11}$$

where

$$\begin{bmatrix} C_2(k) & D_{21}(k) \end{bmatrix} = \begin{cases} \begin{bmatrix} C_{2m} & \begin{bmatrix} D_{21m} & 0 \end{bmatrix} \end{bmatrix} & k \in \{k : PES(k) \text{ is available}\} \\ \begin{bmatrix} 0 & \begin{bmatrix} 0 & 1 \end{bmatrix} \end{bmatrix} & \text{otherwise} \end{cases} .$$

Notice that all the matrices (3.11) are constants except $C_2(k)$ and $D_{21}(k)$. Since all the matrices involved in the computation of the state feedback Riccati equation solution (3.5) in Step 1) are constant, the solution $X(k)$ will converge to a constant matrix which can be computed via its corresponding discrete algebraic Riccati equation (DARE). Moreover, the parameters X, T and F that are computed in Step 1-3) for constructing a minimum entropy controller are constant, which implies the parameters $\bar{A}(k)$ and $T_{22}^{-1}(k)\bar{C}_{12}(k)$ in the proposed controller (3.4) will also be constant. Additionally, the filtering Riccati equation solution $Y(k)$, which is computed forwards in time using (3.7) and a zero initial condition, will converge to a steady-state periodic solution with period N, as demonstrated by Lemma 1. It turns out that the filter gains $F_t(k)$ and $L_t(k)$ will also be periodic with period N. Furthermore, it is straightforward to show that both $\tilde{T}_{12}(k)$ and $\tilde{F}_2(k)$ are equal to zero at the instance k when the PES is not available, which is validated by Lemma 2 in Chapter 4. Thus, both $F_t(k)$ and $L_t(k)$ are also equal to zero at these instances, justifying the use of the fictitious disturbance w_2 in the control synthesis methodology. As a result, the minimum closed-loop ℓ_2 induced norm and the optimal H_∞ controller are unaffected by the use of the fictitious disturbance w_2 in the control synthesis methodology. With the zero gains of $F_t(k)$ and $L_t(k)$ at the instance when the PES is unavailable, the time varying control parameter $\bar{C}_2(k) = C_2(k) + D_{21}(k)F_1$ in (3.4) can be simply substituted by a constant parameter $\bar{C}_{2m} = C_{2m} + \begin{bmatrix} D_{21m} & 0 \end{bmatrix} F_1$ without affecting the controller effect. As a result, for the HDD servo systems with multi-rate sampling and actuation, all of the control parameters of the minimum entropy H_∞ controller shown in (3.4) except $F_t(k)$ and $L_t(k)$ are constant.

Performing a multi-rate optimal H_∞ control synthesis described above, produces a multi-rate H_∞ controller that returns the minimum ℓ_2 induced norm of $\gamma^* = 1.0$. As an illustration, the values of the computed periodically time-varying observer residual gain $L_t(k)$ of the controller given by (3.4) are shown in Fig. 3.9, indicating that $L_t(k) = 0$ in the instances when the PES is not available. Similar results were obtained for periodically time-varying vector $F_t(k)$.

With the more aggressive performance weighting function, the obtained optimal ℓ_2 induced norm of $\gamma^* = 1.0$ implies that the multi-rate strategy has the ability to improve the control performance. In order to further highlight the performance and robustness improvement that can be attained by introducing a higher actuation rate, a time domain simulation study was performed using both the single-rate optimal H_∞ control designed in Section 3.3.1 and the multi-rate optimal H_∞ control designed in this section. To evaluate the robust performance of the two control designs, each controller was tested on 50 different plants, which were randomly generated from

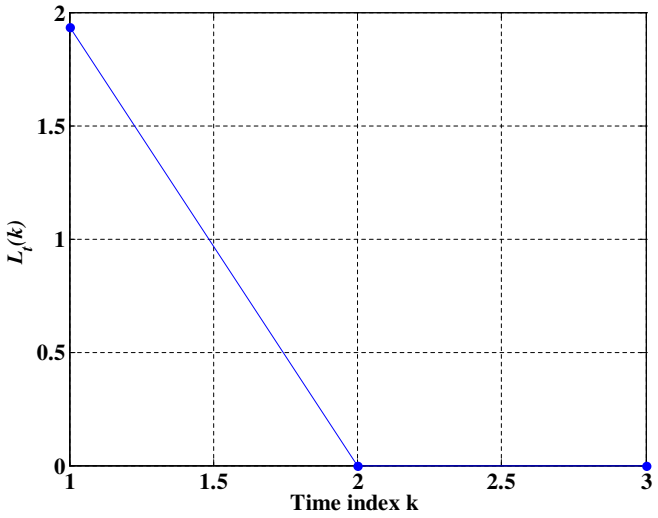

Figure 3.9: Designed periodic gain L_t for the multi-rate HDD servo

Table 3.1: Simulation results for HDD servos with single and multi rate sampling and actuation

	3σ PES (% of track)	
	Nominal	Worst
Single-rate control design	10.7	11.4
Multi-rate control design with $N = 3$	9.2	9.6

$G_v = G_v^n(1 + W_\triangle \triangle)$ ($\|\triangle\|_\infty < 1$) with the uncertainty weighting function indicated in Fig. 3.5 by using Matlab function "`usample`". Note that the disturbance models for our time domain simulation are provided in [49].

Table 3.1 contains the root mean square (RMS) 3σ values of the PES for the nominal plant and the worst-case results for each controller. These results indicate that a controller with a higher actuation rate is able to not only reduce the 3σ PES by 14.0% for the nominal plant, but also improve the servo performance for the worst-case situation by 15.8%.

3.4 Conclusion

The optimal H_∞ control synthesis via discrete Riccati equations for general discrete-time linear periodically time-varying systems was studied in this chapter. Using the results in [41], we first developed the optimal H_∞ control synthesis algorithm for general discrete-time linear time-varying systems. The control synthesis algorithm was subsequently applied to LPTV systems, and it was verified that the resulting con-

trollers are also periodically time-varying. The presented control synthesis technique was tested by designing both single-rate and multi-rate optimal H_∞ track-following controllers for HDD servo systems. In the case of single-rate control, the optimal H_∞ controller designed using the synthesis technique presented in this chapter was compared to the one designed using the Matlab function 'hinfsyn". Simulation results showed that the former synthesis technique is more numerically robust in calculating optimal discrete-time H_∞ controllers for discrete-time linear time-invariant systems than the latter. Moreover, the presented control synthesis algorithm is also applicable to HDD servos with multi-rate sampling and actuation, while the "hinfsyn" function in Matlab is only applicable for LTI plants. Simulation results demonstrated that multi-rate H_∞ controllers synthesized using the technique presented in this chapter consistently outperforms their single-rate counterparts and offers improved robust performance.

Chapter 4

Control Design and Implementation of Hard Disk Drives with Irregular Sampling Rates

Similar to the data packet dropout in networked control systems [30], the undesired inaccessibility of feedback signals may occur in hard disk drive servo systems. Consequently, sampling intervals for such hard disk drive servo systems may not remain equidistant. As discussed in Chapter 1, irregular sampling rates caused by missing PES samples also occur in HDD servos due to false PES demodulation that results from incorrect SAM detection or damaged servo patterns and in HDD self-servo track writing servos due to the collision of reading the PES with writing the final servo patterns. Thus, it is important to address the issue of designing servo systems for HDDs under missing PES samples.

Unlike the randomness of data packet dropout [57], the location of damaged servo sectors and the collision in the self-servo track writing process is consistent on each single servo track. In other words, the unavailability of position error signals for HDD servo systems takes place at some fixed locations for a given track. Furthermore, by considering that the natural periodicity of HDDs is related to the disk rotation, the servo systems can be represented as linear periodically time-varying systems with period equal to the number of servo sectors. In addition, by using a "lifting" procedure [35], an LPTV system can be transformed to the corresponding lifted LTI system [3]. However, the dimension of the resulting stacked LTI system turns out to be "huge" by considering the fact that modern hard disk drives have the order of 100 servo sectors [31]. Therefore, it is computationally intractable to design appropriate HDD servos using these stacked LTI systems whose order is significantly high. On the contrary,

the modeling of HDD servos with irregular sampling rates as LPTV systems will be utilized for their control design in this chapter.

Furthermore, since there tend to be large variations in HDD dynamics due to the variations in manufacturing and assembly, it is not sufficient to achieve adequate servo performance for a single plant. Therefore, the designed controllers must guarantee a pre-specified level of performance for a large set of HDDs. By utilizing classical loop-shaping ideas which are familiar to most practicing engineers, the H_∞ loop-shaping control design [47] is well-suited to deal with the robust performance of the desired loop shape. Using such control, a set of HDDs with plant variations and a regular sampling rate is able to yield a desired error rejection function for disturbance attenuation [21]. Thus, optimal H_∞ control is quite attractive for HDD servo systems. The purpose of this chapter is to extend these results to HDDs with missing PES samples.

In this chapter, we consider the optimal H_∞ track-following control design for single-stage HDD servo systems with missing PES samples. First, these servo systems with missing samples are modeled as LPTV systems, by considering that the natural periodicity is related to the disk rotation. Then, an optimal H_∞ track-following controller is synthesized using the control synthesis methodology for general LPTV systems developed in the Chapter 3. The resulting optimal H_∞ controller can be directly obtained by solving discrete Riccati equations. As a consequence, the designed HDD servos—even with missing PES samples—are still able to robustly achieve the error rejection function chosen in the loop-shaping design process for disturbance suppressions.

However, because the resulting controller is also periodically time-varying with period equal to the number of servo sectors, which is a large number for modern HDDs, a significant amount of memory is required to store all of the control parameters for the synthesized controller. Thus, in order to reduce the memory storage requirements, a simplified controller implementation is developed in this chapter, which utilizes a reduced number of periodic control parameters. In order to demonstrate the effectiveness of the developed control design algorithm, the resulting optimal H_∞ track-following control has been evaluated through both simulation and implementation study on a set of actual hard disk drives. The simulation study presented in this chapter validates the effectiveness of the proposed control and the feasibility of the control parameter simplification. Moreover, implementation results on the ten tested hard disk drives validate the obtained robust performance and furthermore illustrate that the proposed control is implementable in a set of real HDDs.

4.1 Modeling of HDD Servo Systems with Irregular Sampling Rates

As mentioned in Chapter 1, an irregular sampling rate can be caused by missing a sample when the PES is unavailable. Similar to [2], single-stage HDD servo control systems with missing PES samples can be modeled by the block diagram shown in Fig. 4.1. Here, we consider the output multiplicative uncertainty with the nominal plant of the voice coil motor G_v^n and the plant uncertainty weighting function $W_\triangle$ as

$$G_v = (1 + W_\triangle \triangle)\, G_v^n,\ \|\triangle\|_\infty \leq 1 \tag{4.1}$$

In Fig. 4.1, d is the overall contribution of all disturbances [37, 18] including torque disturbance, windage, non-repeatable disk motions and measurement noise to PES. In addition, K is the controller to be designed by using the feedback signal $y(k)$ in the case of irregular sample rates. Moreover, y is switched to PES when PES is available, while y is switched to 0 when PES is unavailable [34]. Then, the servo system with missing PES samples has the following state-space realization:

$$G_o \sim \begin{bmatrix} x(k+1) \\ y(k) \end{bmatrix} = \left[\begin{array}{c|cc} A^o & B_1^o & B_2^o \\ \hline C_2^o(k) & D_{21}^o(k) & 0 \end{array}\right] \begin{bmatrix} x(k) \\ d(k) \\ u(k) \end{bmatrix} . \tag{4.2}$$

Here, all of matrices except $C_2^o(k)$ and $D_{21}^o(k)$ in the above state-space realization are constant and

$$\begin{bmatrix} C_2^o(k) & D_{21}^o(k) \end{bmatrix} = \begin{cases} \begin{bmatrix} C_{2m}^o & D_{21m}^o \end{bmatrix} & k \in \{k : PES(k) \text{ is available}\} \\ \begin{bmatrix} 0 & 0 \end{bmatrix} & \text{otherwise} \end{cases} .$$

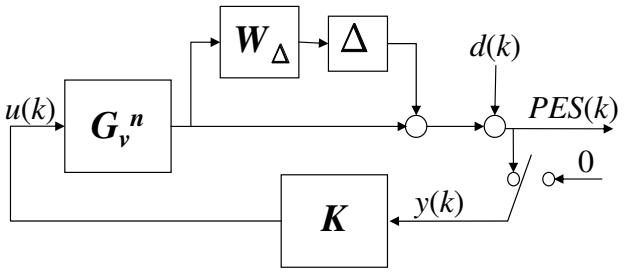

Figure 4.1: Modeling of HDD servo systems with missing PES sampling data

Since the location of damaged servo sectors and the collision in the self-servo track writing process is fixed for each servo track, the unavailability of PES for HDD servo systems takes place at some fixed and pre-determined locations [4] on the disk for each track. Throughout this chapter, the set of servo sectors for which the PES is unaccessible is defined as $M_{\text{miss}} = \{i : PES \text{ is unaccessible on servo sector } i\}$.

Furthermore, by considering that the natural periodicity of HDDs is related to the disk rotation, the servo systems can be represented by LPTV systems with the state-space realization in (4.2) whose elements are periodic, in particular, $\begin{bmatrix} C_2^o(k) & D_{21}^o(k) \end{bmatrix} = \begin{bmatrix} C_2^o(k+N) & D_{21}^o(k+N) \end{bmatrix}$. Here, N represents the number of servo sectors.

4.2 Optimal H_∞ Control for HDD Servo Systems with Irregular Sampling Rates

4.2.1 Optimal H_∞ Control Formulation

In order to deal with the HDD plant variations and missing PES samples, we will extend well-known error rejection loop-shaping design techniques for HDDs with regular sampling rates to HDDs with irregular sampling rates.

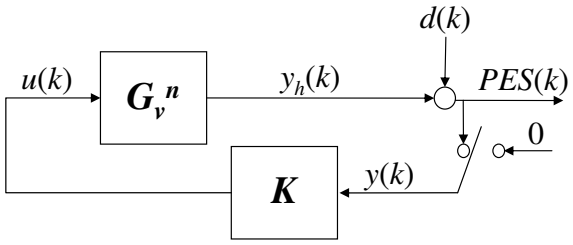

Figure 4.2: The HDD servo system with the nominal VCM plant

For the optimal H_∞ control of single-stage HDD servo systems illustrated by the block diagram in Fig. 4.1, we need to design a controller K satisfying the following conditions for the nominal VCM plant G_v^n:

$$\left\| \begin{bmatrix} T_s \cdot W_p & T_c \cdot W_\triangle \end{bmatrix} \right\|_{2\leftarrow 2} < 1 \tag{4.3}$$

where T_s is the sensitivity function (i.e. error rejection transfer function) from d to PES, as shown in Fig. 4.2, while T_c is the complementary sensitivity function from d to the plant output y_h. The W_p and $W_\triangle$ in (4.3) are the loop-shaping performance weighting function and the plant uncertainty weighting function respectively. It is known that Equation (4.3) guarantees the robust performance that the magnitude of the obtained error rejection function (for single-input-single-output (SISO) systems) is always smaller than $|W_p(e^{j\omega})|^{-1}$ for the uncertain plant characterized in (4.1).

Similar to the optimal H_∞ control of single-stage HDD servo systems with multi-rate sampling and actuation in Chapter 3, we consider the block diagram shown in Fig. 4.3

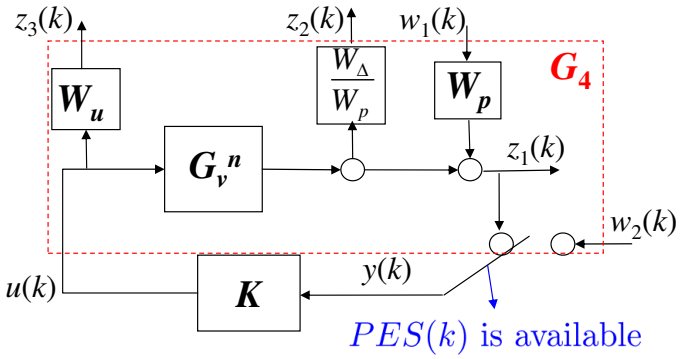

Figure 4.3: Control design formulation for HDDs with irregular sampling rates

for the control design of the servo systems with an irregular sampling rate. In the figure, W_u is the control input weighting value to be tuned so that the inequality in (4.3) holds. As illustrated in Chapter 3, this control design formulation is different from the standard H_∞ control problem formulation [47] due to the introduction of the fictitious disturbance w_2 and the fact that the performance weighting function was moved to the disturbance input side. As a result, the assumption in Chapter 3.1 that $D_{21}(k)D_{21}^T(k) \succ 0$ for all k is satisfied for this plant. In addition, it is known that the introduction of w_2 does not affect the optimal H_∞ controller and the optimal closed-loop ℓ_2 induced norm, which will also be shown later in this chapter. Moreover, by changing the position of the performance weighting function, the feedback signal y is affected by the "colored" disturbance $(W_p w_1)$ more directly when missing samples occur.

With these changes and utilizing the block diagram in Fig. 4.3, the optimal H_∞ control problem for HDD servos with an irregular sampling rate is to find an optimal linear time-varying controller K and a minimum γ with the closed loop ℓ_2 induced norm less than γ, i.e.

$$\begin{array}{ll} \min_{K,\gamma} & \gamma \\ \text{s.t.} & \|T_{z\leftarrow w}\|_{2\leftarrow 2} < \gamma \end{array} \tag{4.4}$$

where $T_{z\leftarrow w}$ represents the transfer function matrix from $w = \begin{bmatrix} w_1 & w_2 \end{bmatrix}^T$ to $z = \begin{bmatrix} z_1 & z_2 & z_3 \end{bmatrix}^T$. Suppose the LPTV system G_4 (with input $\begin{bmatrix} w_1 & w_2 & u \end{bmatrix}^T$ and output $\begin{bmatrix} z_1 & z_2 & z_3 & y \end{bmatrix}^T$) shown in Fig. 4.3 can be represented as the following state-space realization:

$$G_4 \sim \begin{bmatrix} x(k+1) \\ z(k) \\ y(k) \end{bmatrix} = \left[\begin{array}{c|cc} A & B_1 & B_2 \\ \hline C_1 & D_{11} & D_{12} \\ C_2(k) & D_{21}(k) & 0 \end{array}\right] \begin{bmatrix} x(k) \\ w(k) \\ u(k) \end{bmatrix} \tag{4.5}$$

with

$$\begin{bmatrix} C_2(k) & D_{21}(k) \end{bmatrix} = \begin{cases} \begin{bmatrix} C_{2m} & \begin{bmatrix} D_{21m} & 0 \end{bmatrix} \\ 0 & \begin{bmatrix} 0 & 1 \end{bmatrix} \end{bmatrix} & k \in \{k : PES \text{ is available}\} \\ \text{otherwise} \end{cases} . \quad (4.6)$$

In (4.5), all of the matrix entries are constant except $C_2(k)$ and $D_{21}(k)$ which are periodic with period N.

The corresponding matrices for the LPTV systems in (3.1) are $B = \begin{bmatrix} B_1 & B_2 \end{bmatrix}$, $D_{1\bullet} = \begin{bmatrix} D_{11} & D_{12} \end{bmatrix}$, $C(k) = \begin{bmatrix} C_1 \\ C_2(k) \end{bmatrix}$, and $D_{\bullet 1}(k) = \begin{bmatrix} D_{11} \\ D_{21}(k) \end{bmatrix}$.

4.2.2 Optimal H_∞ Track-Following Control

The optimal H_∞ control synthesis algorithm developed in Chapter 3 will be applied to synthesize the optimal H_∞ track-following control for single-stage HDD servos with an irregular sampling rate. In the algorithm, we first need to obtain the unique minimum entropy controller satisfying the ℓ_2 induced norm constraint in (4.4) with a fixed γ, and then utilize a bi-section search method to find the minimum γ and the corresponding optimal controller.

Utilizing the control design methodology presented in the Chapter 3, we obtain the following unique stabilizing minimum entropy time-varying controller K, which satisfies the constraint in (4.4) and is given by the following state space realization:

$$\begin{cases} \hat{x}(k+1) = \bar{A}\hat{x}(k) + B_2 u(k) + F_t(k)\left(\bar{C}_{2m}\hat{x}(k) - y(k)\right) \\ u(k) = -T_{22}^{-1}\bar{C}_{12}\hat{x}(k) + L_t(k)\left(\bar{C}_{2m}\hat{x}(k) - y(k)\right) \end{cases} . \quad (4.7)$$

Notice that for the irregular-sampling-rate HDD servo system shown in (4.5), all matrix entries in the state-space realization (4.5) are constant except $C_2(k)$ and $D_{21}(k)$. Consequentially, the algorithm for constructing a minimum entropy controller in Chapter 3 can be further simplified as follows.

1. Solve the state feedback algebraic Riccati equation:

$$X = A^T X A + C_1^T C_1 - M\left(R + B^T X B\right)^{-1} M^T \quad (4.8)$$

   where $M = A^T X B + C_1^T D_{1\bullet}$.

2. Define $T = \begin{bmatrix} T_{11} & 0 \\ T_{21} & T_{22} \end{bmatrix}$ with $T_{11} \succ 0$ and $T_{22} \succ 0$, and compute T using:

$$R + B^T X B = T^T J T \quad (4.9)$$

   where $R = D_{1\bullet}^T D_{1\bullet} - \begin{bmatrix} I & 0 \\ 0 & 0 \end{bmatrix}$, $J = \begin{bmatrix} -I & 0 \\ 0 & I \end{bmatrix}$.

3. Get $\begin{bmatrix} F_1 \\ F_2 \end{bmatrix} = \left(R + B^T X B\right)^{-1} M^T$.

4. Calculate the following matrices for the filtering Riccati equation: $\bar{A} = A + B_1 F_1$, $\bar{C}_2(k) = C_2(k) + D_{21}(k) F_1$, and $\bar{C}_{12} = -T_{22} F_2$. Let $D_\perp$ be an orthogonal matrix to D_{12}. In addition, define a matrix W such that $W^T W = I - T_{11}^T T_{11}$ and W has appropriate dimensions so that the following matrix multiplication is well defined:
$$\begin{bmatrix} \bar{D}_{111} \\ \bar{D}_{112} \end{bmatrix} = D_\perp W + D_{12} T_{21} \ .$$

5. Update forwards in time the filtering Riccati equation solution with zero initial condition:
$$Y(k) = \bar{A} Y(k-1) \bar{A}^T + B_1 B_1^T - \tilde{M}(k) \times \left(\tilde{R}(k) + \begin{bmatrix} \bar{C}_{12} \\ \bar{C}_2(k) \end{bmatrix} Y(k-1) \begin{bmatrix} \bar{C}_{12} \\ \bar{C}_2(k) \end{bmatrix}^T \right)^{-1} \tilde{M}^T(k) \quad (4.10)$$
where $Y(k) \succeq 0$ and
$$\begin{aligned} \tilde{M}(k) &= \bar{A} Y(k-1) \begin{bmatrix} \bar{C}_{12} \\ \bar{C}_2(k) \end{bmatrix}^T + B_1 \begin{bmatrix} \bar{D}_{112} \\ D_{21}(k) \end{bmatrix}^T \\ \tilde{R}(k) &= \begin{bmatrix} \bar{D}_{112} \\ D_{21}(k) \end{bmatrix} \begin{bmatrix} \bar{D}_{112} \\ D_{21}(k) \end{bmatrix}^T - \begin{bmatrix} I & 0 \\ 0 & 0 \end{bmatrix} \ . \end{aligned}$$

6. Define $\tilde{T}(k) = \begin{bmatrix} \tilde{T}_{11}(k) & \tilde{T}_{12}(k) \\ 0 & \tilde{T}_{22}(k) \end{bmatrix}$, with $\tilde{T}_{11} \succ 0$ and $\tilde{T}_{22} \succ 0$, and compute $\tilde{T}(k)$ using
$$\tilde{R}(k) + \begin{bmatrix} \bar{C}_{12} \\ \bar{C}_2(k) \end{bmatrix} Y(k-1) \begin{bmatrix} \bar{C}_{12} \\ \bar{C}_2(k) \end{bmatrix}^T = \tilde{T}(k) \tilde{J} \tilde{T}^T(k) \quad (4.11)$$
where $\tilde{J} = \begin{bmatrix} -I & 0 \\ 0 & I \end{bmatrix}$.

7. Obtain
$$\begin{bmatrix} \tilde{F}_1(k) \\ \tilde{F}_2(k) \end{bmatrix} = \left(\tilde{R}(k) + \begin{bmatrix} \bar{C}_{12} \\ \bar{C}_2(k) \end{bmatrix} Y(k-1) \begin{bmatrix} \bar{C}_{12} \\ \bar{C}_2(k) \end{bmatrix}^T \right)^{-1} \tilde{M}^T(k) \ . \quad (4.12)$$

8. Calculate the filter gains
$$L_t(k) = T_{22}^{-1} \tilde{T}_{12}(k) \tilde{T}_{22}^{-1}(k) \text{ and } F_t(k) = \tilde{F}_1^T(k) \tilde{T}_{12}(k) \tilde{T}_{22}^{-1}(k) + \tilde{F}_2^T(k) \ .$$

Since, as proved in Appendix B, the Riccati equation solution $Y(k)$ in (4.10) of constructing a minimum entropy control is unique and periodic, $Y(k)$ computed "forwards" in time with a zero initial condition converges to a steady-state periodic solution with period N. It turns out that the filter gains $F_t(k)$ and $L_t(k)$ are also periodic with period N. As illustrated in Lemma 2, both $\tilde{T}_{12}(k)$ and $\tilde{F}_2(k)$ are equal to zero at the instance k when the PES is unavailable.

Lemma 2. *Both $\tilde{T}_{12}(k)$ and $\tilde{F}_2(k)$ in the above algorithm are equal to zero at the instance k when $PES(k)$ is unavailable.*

The proof of Lemma 2 is provided in Appendix C. Thus, both $F_t(k)$ and $L_t(k)$ are also equal to zero at whenever $PES(k)$ is unavailable, which verifies the claim that the fictitious disturbance w_2 does not affect the optimal H_∞ controller. With the zero gains of $F_t(k)$ and $L_t(k)$ at the instance when a missing PES sample occurs, the time varying control parameter $\bar{C}_2(k) = C_2(k) + D_{21}(k)F_1$ in (4.7) can be simply substituted by a constant parameter $\bar{C}_{2m} = C_{2m} + \begin{bmatrix} D_{21m} & 0 \end{bmatrix} F_1$ without affecting the controller effect. As a result, for the HDD servo systems with missing PES samples, all of the control parameters of the minimum entropy H_∞ controller shown in (4.7) except $F_t(k)$ and $L_t(k)$ are constant.

4.3 Control Synthesis Evaluation on Real HDDs

In this section, we apply our developed optimal H_∞ control design methodology to the track-following control of multiple hard disk drives with missing PES samples. The algorithm was evaluated through both simulation study and experimental study. The ten single-stage hard disk drives considered here were provided by Western Digital Technologies. For these 2.5" disk drives, the number of servo sectors is $N = 274$ and the spindle rotation speed is 9000 RPM. For one of these disk drives, servo patterns on some servo sectors at the inside diameter (ID) have been damaged and thus the PES on these servo sectors is not available for the servo system. Specifically, we found that for this particular drive, the PES is unaccessible on the following 57 servo sectors:

$$\begin{aligned} M_{\text{miss}} = \quad & \{2, 6, 10, 14, 18, 27, 31, 35, 39, 43, 47, 52, 56, 60, 64, 68, 72, 81, 85, 89, 93, 97, \\ & 101, 110, 114, 118, 122, 126, 135, 139, 143, 147, 151, 155, 164, 168, 172, 176, \\ & 180, 184, 193, 197, 201, 205, 209, 218, 222, 226, 230, 234, 238, 247, 251, 255, \\ & 259, 263, 272\}. \end{aligned}$$

Such a missing sample sequence will be utilized to synthesize the optimal H_∞ track-following controller in this section. For the other nine disk drives, there are no damaged servo sectors. However, in order to test the synthesized controller's ability

of achieving robust performance and handling missing PES samples, the feedback PES has also been dropped at the specific servo sectors described by M_{miss} for the nine undamaged disk drives.

4.3.1 Nominal Plant Identification and Weighting Function Selection

For convenience in the control synthesis step, notch filters [45] are incorporated into the VCM plant G_v. In order to obtain the nominal VCM plant, the actual VCM plant frequency response for one single drive was measured in the disk area where there are no missing PES samples. Then, the nominal VCM model $G_v^n(s)$ was identified to match the experiment frequency response, as described in [37]. Note that in order to reduce the controller order, the nominal VCM plant is just identified as a 7th order model.

The uncertainty weighting function $W_\triangle$ considered in the control design is shown in Fig. 4.4. The selected uncertainty weighting function demonstrates that the real plant could have an unstructured uncertainty of a $\pm 26\%$ gain variation at low frequency and a $\pm 112\%$ gain variation at high frequency from the nominal plant G_v^n.

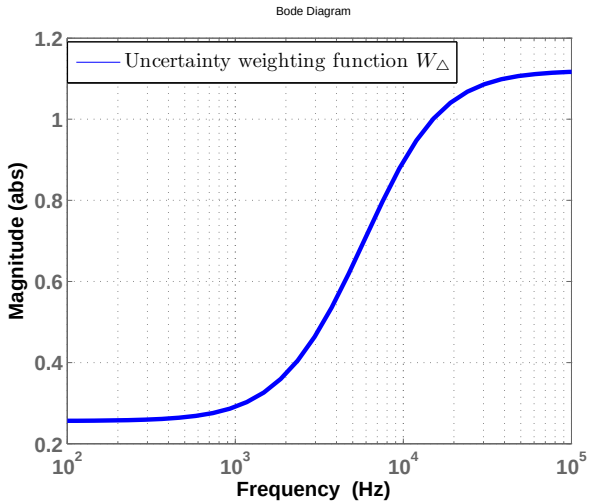

Figure 4.4: Plant uncertainty weighting function $W_\triangle$

In order to attenuate disturbances, the performance weighting function W_p is designed as a low-pass filter and thus W_p^{-1} is a high-pass filter. The inverse of the frequency response for the designed performance weighting function is shown in Fig. 4.5. Then, with the proposed control synthesis technique, all of the disk drives are expected to

possess better disturbance attenuation than the one described by the inverse of the performance weighting function.

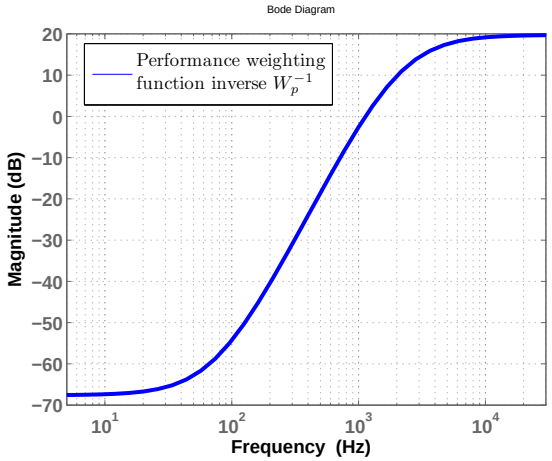

Figure 4.5: The frequency response of the performance weighting function inverse

4.3.2 Control Design and Simplification

It is well know that if the optimal H_∞ controller yields a minimum $\gamma^* \leq 1$, then the controller is able to achieve the robust performance by satisfying the corresponding conditions illustrated in (4.3). In other words, the designed controller achieves better disturbance attenuation than the inverse of performance weighting function shown in Fig. 4.5 for all the plant variations with the multiplicative plant uncertainty weighting function in Fig. 4.4. With the determined performance weighting function and plant uncertainty weighting function, the weighting value W_u is to be tuned so that the achieved γ is less than or equal to 1 and simultaneously the control actuation generated by the resulting controller K is appropriate under the hardware constraints of real HDD servo systems.

For the real hard disk drives described in the previous section, a weighting value of $W_u = 40$ was selected and thus the resulting optimal H_∞ control is able to achieve the optimal ℓ_2 induced norm $\gamma^* = 0.88$. Moreover, the resulting gains $F_t(k)$ and $L_t(k)$ in (4.7) are zero when the feedback PES is unavailable at the instance k, which verifies our prediction about the time-varying control parameters in Section 4.2. The designed gain $L_t(k)$ for one HDD revolution is shown in Fig. 4.6.

Since the control parameters $F_t(k)$ and $L_t(k)$ are time-varying, we have to save all 217 $(= 274 - 57)$ sets of non-zero time-varying control parameters, requiring a significant amount of memory. Unfortunately, it is almost impossible to reserve so much memory for storing these control parameters in real HDDs. Fortunately, we found that the

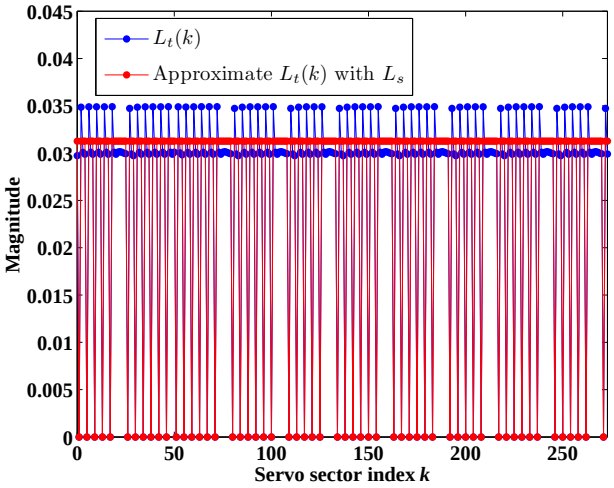

Figure 4.6: The designed $L_t(k)$ for the HDD servo with an irregular sampling rate

non-zero time-varying parameters $F_t(k)$ and $L_t(k)$ have very small variations, which motivates us to treat all non-zero time-varying control parameter values as constants. Specifically, the constant values F_s and L_s for $F_t(k)$ and $L_t(k)$ are obtained by taking the average of all non-zero $F_t(k)$ and $L_t(k)$ respectively. Then, the approximate control parameters F_s and L_s will be applied when the PES is available. Consequentially, just one set of control parameters F_s and L_s has to be stored in memory. The approximate values for $L_t(k)$ with L_s are also shown in Fig. 4.6. The simulation study, which will be presented in next section, shows that such control parameter approximation has a tolerable negative affect on the control performance.

4.3.3 Simulation Study

In order to evaluate the robust performance of the designed controller, a total of 50 different VCM plants were collected. These various VCM plants were randomly generated based on the VCM plant model in (4.1) with the identified nominal plant G_v^n and the uncertainty weighting function $W_\triangle$ shown in Fig. 4.4 by using Matlab function "`usample`".

The simulation results of the Root Mean Square (RMS) 3σ values of PES for the nominal plant and the worst-case plant are illustrated in Table 4.1. Based on these time-domain simulation results, we are confident that the proposed optimal H_∞ control indeed attains its predicted robust performance. Moreover, Table 4.1 also shows the simulation results by using the approximate control parameters. The results imply that the performance degradation caused by the control parameter approximation is so small that the control simplification presented in the previous section is viable.

Table 4.1: Time-domain simulation results for the control parameter approximation

	3σ PES (% track)	
	Nominal	Worst
With the original control parameters $F_t(k)$ and $L_t(k)$	4.24	5.50
With the approximate control parameters using F_s and L_s	4.30	5.58

4.3.4 Experimental Study

The simulation results presented in the previous section illustrate that the optimal H_∞ controller synthesized using the developed control algorithm in Chapter 3 is able to handle an irregular sampling rate and achieve robust performance. In this section, we discuss its implementation on a set of actual single-stage hard disk drives with missing PES samples. The designed controller was coded on the disk drives' own processor by changing their firmware code. For the disk drive with damaged servo sectors, the designed H_∞ control was tested and evaluated in the disk area where the missing samples occur with the missing sample sequence of M_{miss} as defined in the previous section. As a result, for the servo sectors $i \in M_{\text{miss}}$, the PES is unavailable. For the other nine undamaged disk drives, the feedback PES was also manually dropped on the servo sectors described by M_{miss} during the experimental study, so as to evaluate the designed controller.

Unlike linear time-invariant systems, a linear time-varying system with irregular sampling rates has no well-defined error rejection transfer function. However, in order to evaluate the implemented controller for the considered disk drives, we define the following disturbance-PES relationship called approximate error rejection transfer function. A sweep sinusoid excitation is injected into the position of the disturbance d shown in Fig. 4.1, which is the same as the way that the excitation is injected for measuring the error rejection transfer function for disk drives with a regular sampling rate. Then, the PES response caused by the excitation is collected. Since the PES is unaccessible at the time when missing samples are encountered, we approximately treat the previous available PES as the current unavailable PES. Afterwards, the discrete Fourier transform (DFT) is computed for the collected PES data and then the DFT component at the frequency of the sinusoid excitation is identified. As a result, the approximate frequency response from the disturbance d to PES is calculated by dividing the identified PES DFT component by the corresponding excitation DFT component. Finally, the approximate error rejection transfer functions were measured on the ten considered disk drives and are shown as the black lines in Fig. 4.7.

Figure 4.7 also shows the inverse of the performance weighting function, which is indicated by the red line. The experiment results in Fig. 4.7 illustrate that all of the

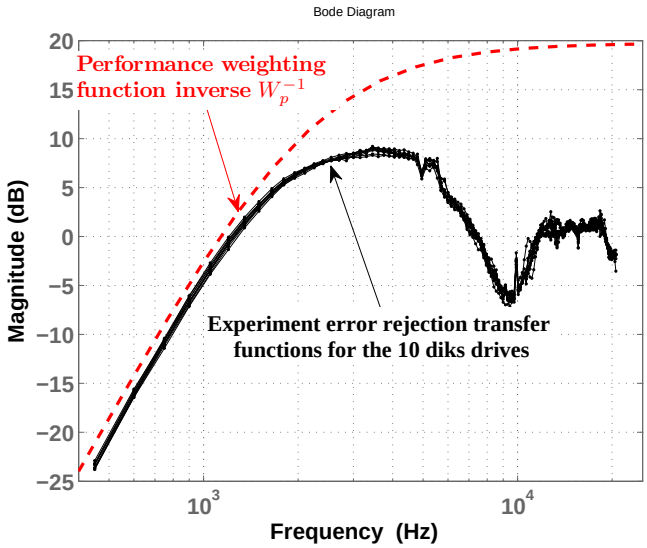

Figure 4.7: Experiment result for approximate error rejection functions

measured approximate error rejection transfer functions are below the inverse of the performance weighting function at every frequency. Thus, the obtained experiment results on multiple real disk drives demonstrate that the optimal H_∞ track-following control synthesized by our proposed control algorithm achieves the robust performance of the desired disturbance attenuation.

Figure 4.8 shows the 3σ values for the closed-loop NRRO PES with the implemented controller on the tested disk drives. Note that these experiment results for the closed-loop PES are similar to the simulation results listed in Table 4.1. Moreover, the controller designed using our proposed optimal H_∞ control synthesis algorithm improves 3σ PES by around 20% in the experimental study, compared to an intuitionistic methodology in which an unavailable PES is substituted by the previous available one when a missing sample occurs.

4.4 Conclusion

In hard disk drive servo systems, sometimes an irregular sampling rate is unavoidable, for example, when false PES demodulation is caused by damaged servo sectors and when the unavailability of feedback signals is due to the collision in the self-servo track writing process. By considering the positions of the unavailable feedback signal to be fixed and taking into account the natural periodicity of HDDs due to the disk rotation, the servo systems with missing PES samples were represented as linear periodically time-varying systems. In addition, since there tend to be large variations

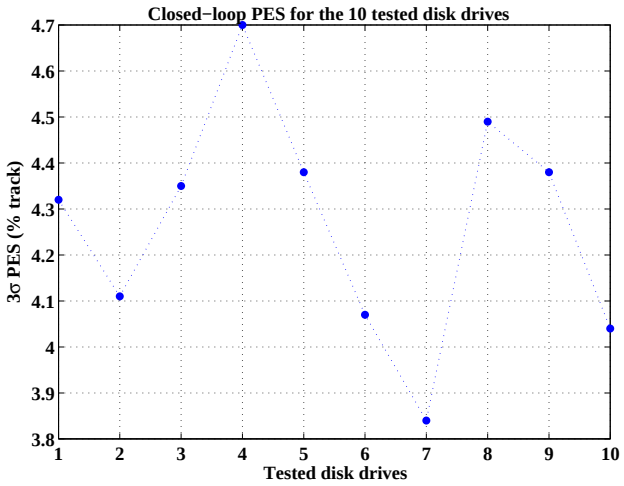

Figure 4.8: 3σ values of the closed-loop PES for the ten tested hard disk drives

in HDD dynamics due to variations in manufacturing and assembly, the designed controllers must guarantee a pre-specified level of performance for a large set of hard disk drives. Based on the optimal H_∞ control synthesis methodologies presented in Chapter 3 for general LPTV systems, an optimal H_∞ track-following controller was synthesized in this chapter for HDD servos with missing PES samples. The simulation and implementation study on multiple hard disk drives demonstrates the synthesized controller's effectiveness in handling irregular sampling rates and achieving the robust control performance of a desired error rejection transfer function for disturbance attenuation. Moreover, the simulation results were validated by the implementation results on the ten actual 2.5" single-stage hard disk drives. In the experimental study, around 20% improvement of the 3σ PES was obtained by the proposed control algorithm over the intuitionistic methodology for the ten tested disk drives.

Chapter 5

Control Design of Concentric Self-servo Track Writing

In modern hard disk drive servo systems, the feedback PES is decoded from servo patterns in so-called servo sectors. These servo patterns must be pre-recorded onto the disk surfaces by using servo track writing process before HDD servo systems can be used to position read/write magnetic heads. In addition, as mentioned in Chapter 1, any track errors introduced in servo track-writing process will later appear as written-in repeatable runout which degrades servo control performance. Therefore, the accuracy and precision of the servo track writing process plays a crucial role in dictating the ultimate track density and areal storage density of HDDs. In order to reduce track misregistration [9] and increase track density [60], it is necessary to improve the quality of the servo pattern writing process.

Conventionally, servo patterns are written by costly dedicated servowriting equipment [31] external to disk drives. Self-servo track writing (SSTW) [5, 26] is an alternative method of writing servo patterns using HDDs' own read and write heads and servo systems, in order to save the process cost and improve the servowriting quality. During SSTW, the timing and radial information are obtained from the previously-written track using the read head, while timing and radial positioning servo patterns for the current track are being written using the write head. As a consequence, the external equipment is no longer needed in the servo-pattern writing and thus the servo track writing does not have to be carried out in any clean room environment. As mentioned in Chapter 1, there are two popular SSTW methodologies, spiral-based SSTW and concentric-based SSTW. In this chapter, we just focus on the compensation scheme for concentric self-servo track writing. Specifically, the process of the concentric self-servo track writing is depicted in Fig. 5.1 and it generally involves the following steps [59]:

1. Write one or more concentric servo sector tracks using conventional servowriting methodologies. These tracks are used as the initial seed tracks, from which reference timing and radial position information is measured to write the next (adjacent) track in a bootstrap manner, and can be pre-written on the disks before the disks are assembled in the HDD.

2. Assume that the read-head to write-head position offset is equal to one track width [14]. Using the read head, collect timing and radial information from the previously written seed track and use this information to generate the position error signals to track follow the seed track, while the write head writes actual servo patterns for the current track.

3. Use the track written in Step 2 as the new seed track and go back to Step 2 until all concentric tracks are written.

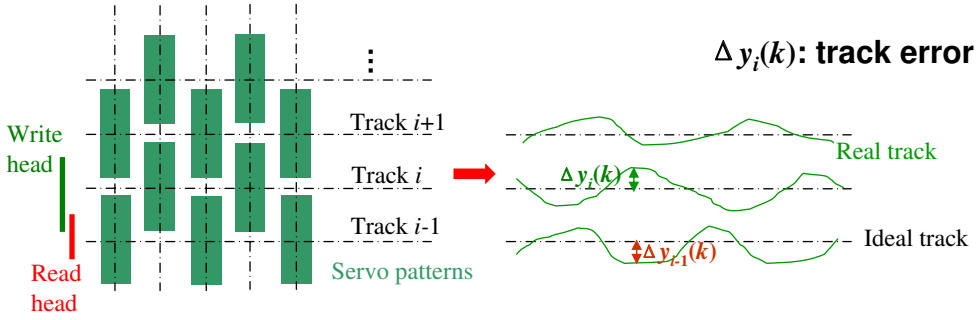

Figure 5.1: Modeling of concentric SSTW servo systems

However, several challenges arise with the SSTW process such as the fact that radial position errors from the previous track can propagate into the currently-written track. This radial positioning error propagation will result in instability unless it is contained by guaranteeing that the magnitude for the error propagation term is sufficiently attenuated. In order to contain the error propagation, iterative learning control (ILC) and 2-Dimensional H_2 control have been studied in [56] and [16] respectively. In [56], a feedforward based iterative learning control is designed in the lifted domain assuming zero initial conditions at the beginning of each track writing stage and the existence of finite impulse-response (FIR) representations for the servo's sensitivity and complimentary sensitivity functions. However, we note that these assumptions are not strictly true for real HDDs. In [16], a novel 2-Dimensional H_2 control synthesis technique for SSTW is formulated to satisfy a sufficient rather than a necessary condition by making some matrices be block diagonal in order to transfer the optimization to the form of linear matrix inequalities (LMI).

In this chapter, we present two novel control synthesis methodologies for performing concentric self-servo track writing in hard disk drives using a feedforward control structure [56]. In the first methodology, a non-causal feedforward controller, which

utilizes the stored error signal [56] from writing the previous track, is designed given a pre-defined causal track-following controller. Standard H_∞ control synthesis techniques are used to avoid the propagation of track errors from the previous tracks, while achieving sufficient disturbance attenuation. In the second methodology, an analytic expression for the power spectrum density of track errors is derived and approximated. The approximate expression is subsequently used to formulate the simultaneous design of both feedback and feedforward controllers, using a mixed H_2/H_∞ control scheme, which ensures the containment of the error propagation and the achievement of good disturbance attenuation and is solved via the solution of a set of LMIs with a controller parameterization. Neither of these techniques utilizes the simplifying assumptions in [56]. Simulation results using the single-stage HDD benchmark problem developed in [49] show that the controllers synthesized by the proposed schemes outperform the controllers synthesized by the techniques in [56], and offer levels of performance that are comparable to the 2-Dimensional H_2 control technique in [16] while having a much simpler control structure.

5.1 Non-Causal Feedforward Control Design via H_∞ Control

5.1.1 Feedforward-Control Structure Based SSTW System

Figure 5.2 illustrates the block diagram of the self-servo track writing system with a feedforward control structure [16]. The system includes a feedforward controller $F(z)$ and a standard track-following servo loop with the VCM plant $P(z)$ and the feedback controller $C(z)$. In Fig. 5.2, i and k denote the track index and servo sector index respectively, while $\triangle y_i(k)$, $w_i(k)$, $r_i(k)$ and $n_i(k)$ denote the track error, windage, track runout due to disk vibrations, and measurement noise, respectively, at the position of track i and servo sector k. Moreover, since the feedforward controller $F(z)$ utilizes the error signal $e_{i-1}(k)$, which can be stored when writing the previous track, and hence the entire $e_{i-1}(k)$ sequence in (k) is available when writing the current track. Thus, a non-causal feedforward controller $F(z)$ is feasible for the control structure in Fig. 5.2. Here, windage and measurement noise are modeled as white noises with the variance σ_w^2 and σ_n^2 respectively, while the track runout caused by disk vibrations is modeled as a color noise generated by feeding a white noise d_r input to the filter $G_r(z)$.

Based on the block diagram in Fig. 5.2, we can get the following recursive expression for track errors:

$$\triangle y_i(k) = G_1(q)\triangle y_{i-1}(k) + T(q)n_i(k) + S(q)d_i(k) - S(q)F(q)d_{i-1}(k) \qquad (5.1)$$

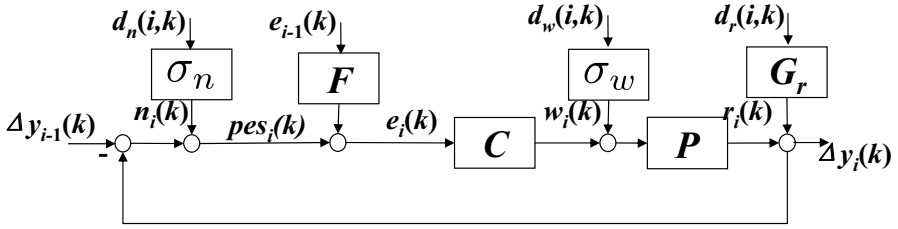

Figure 5.2: Feedforward control structure based SSTW system

where $T(z) = \frac{C(z)P(z)}{1+C(z)P(z)}$, $S(z) = \frac{1}{1+C(z)P(z)}$, $d_i(k) = P(z)w_i(k) + r_i(k)$, and $G_1(z) = \frac{C(z)P(z)+F(z)}{1+C(z)P(z)}$.

Notice that $G_1(z)$ becomes the key transfer function relating the previous and the current track errors.

5.1.2 Non-causal Feedforward Control Design

Like the iterative learning control in [56, 32], a feedback controller $C(z)$ for track following is first designed to achieve good disturbance attenuation. Here, $C(z)$ is designed as an optimal H_2 controller [37]. In order to contain the error propagation, the designed controllers must satisfy $\|G_1(e^{j\omega})\|_\infty < 1$. Furthermore, in order to make the error propagation converge as quickly as possible, we want $\|G_1(e^{j\omega})\|_\infty$ to be sufficiently small. From (5.1), we learn that the current track error is also affected by the disturbances from the previous track. In order not to degrade the disturbance attenuation performance of the track-following controller $C(z)$, the magnitude of the filter $F(z)$ also needs to be sufficiently small. In all, the feedforward control $F(z)$ must be designed to achieve the following target:

$$\begin{cases} \|G_1(z)\|_\infty : \text{sufficiently small and less than 1} \\ \|F(z)\|_\infty : \text{sufficiently small} \end{cases} . \tag{5.2}$$

As a consequence, we consider the following optimization:

$$\min_{F(z)} \quad \left\| \begin{bmatrix} G_1(z) & w_{t1}F(z) \end{bmatrix} \right\|_\infty \tag{5.3}$$

where w_{t1} is a weighting value to be tuned to achieve the target in (5.2). The optimization in (5.3) is a standard H_∞ control problem, which can be easily solved, as shown later in this section. However, the solution to (5.3) can only produce a causal compensator $F(z)$ [15]. Obviously, a smaller objective value may be achieved if $F(z)$ is allowed to be non-causal. In order to design a non-causal filter $F(z)$, we consider

the following facts:

$$\begin{aligned} \left\| \begin{bmatrix} G_1(z) & w_{t1}F(z) \end{bmatrix} \right\|_\infty &= \left\| \begin{bmatrix} z^{-n_d}G_1(z) & w_{t1}z^{-n_d}F(z) \end{bmatrix} \right\|_\infty \\ &= \left\| \begin{bmatrix} \frac{z^{-n_d}P(z)C(z)+\tilde{F}(z)}{1+P(z)C(z)} & w_{t1}\tilde{F}(z) \end{bmatrix} \right\|_\infty \end{aligned} \tag{5.4}$$

where $F(z) = z^{n_d}\tilde{F}(z)$ and n_d is a positive integer. Thus, the optimization in (5.3) can be transformed into the following optimization:

$$\min_{\tilde{F}(z)} \left\| \begin{bmatrix} \frac{z^{-n_d}P(z)C(z)+\tilde{F}(z)}{1+P(z)C(z)} & w_{t1}\tilde{F}(z) \end{bmatrix} \right\|_\infty . \tag{5.5}$$

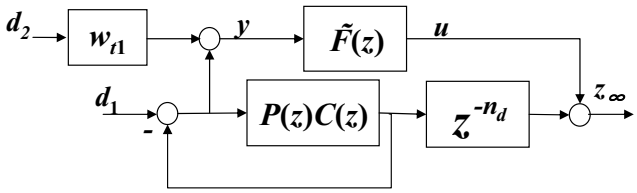

Figure 5.3: Block diagram for the non-causal feedfoward control design using H_∞ control

By considering the block diagram in Fig. 5.3, we have

$$T_{z_\infty \leftarrow d_\infty} = \begin{bmatrix} \frac{z^{-n_d}P(z)C(z)+\tilde{F}(z)}{1+P(z)C(z)} & w_{t1}\tilde{F}(z) \end{bmatrix}$$

where $d_\infty = \begin{bmatrix} d_1 & d_2 \end{bmatrix}^T$. Note that the symbol $T_{A \leftarrow B}$ represents the transfer function from signal B to signal A. Thus, the optimization in (5.5) can be interpreted as the H_∞ control problem for the linear fractional transformation (LFT) in Fig. 5.4 to minimize $\|T_{z_\infty \leftarrow d_\infty}\|_\infty$. Here, $G(z)$ is the transfer function matrix from $\begin{bmatrix} d_\infty^T & u \end{bmatrix}^T$ to $\begin{bmatrix} z_\infty^T & y \end{bmatrix}^T$ as shown in Fig. 5.3.

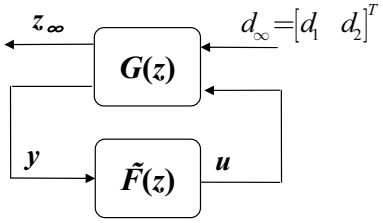

Figure 5.4: LFT representation for the non-causal feedfoward control design using H_∞ control

Then, the standard H_∞ control synthesis technique can be applied to the control problem as shown in Fig. 5.4 to generate the controller $\tilde{F}(z)$. Once a causal $\tilde{F}(z)$ is designed, a non-causal feedforward controller can be constructed with $F(z) = z^{n_d}\tilde{F}(z)$.

5.2 Track Error Analysis for the Feedforward Control Based SSTW

5.2.1 Power Spectrum Density of Track Errors

In order to investigate the relationship between the current track error and disturbances from the previously-written tracks, we assume that the servo patterns on each track are written after the system reaches its steady state. Then, based on the recursive form of track errors in (5.1), we have the complete expression for track errors described as:

$$\begin{aligned}
\triangle y_i(k) &= G_1^i \triangle y_0(k) + \sum_{l=1}^{i} G_1^{i-l} T n_l(k) + \sum_{l=1}^{i} G_1^{i-l} S d_l(k) - \sum_{l=1}^{i-1} G_1^{i-1-l} SF d_l(k) \\
&= \sum_{l=1}^{i-1} G_1^{i-1-l} T\left[(T+SF)n_l(k) - S(1-F)d_l(k)\right] + G_1^i \triangle y_0(k) \\
&\qquad\qquad + T n_i(k) + S d_i(k) \\
&= \sum_{l=1}^{i-1} G_1^{i-1-l} T\left[G_1 n_l(k) - S(1-F)d_l(k)\right] + G_1^i \triangle y_0(k) + T n_i(k) + S d_i(k)\ .
\end{aligned} \tag{5.6}$$

Furthermore, we assume that the seed track error $\triangle y_0$, measurement noises and disturbances are uncorrelated with each other and the track error on the seed track has a power spectrum density $\Phi_{\triangle y_0 \triangle y_0}$. Moreover, measurement noises on different tracks are uncorrelated and have the same variance σ_n^2, while disturbances on different tracks are also uncorrelated and have the same power spectrum density $\Phi_{dd}(e^{j\omega})$. With these assumptions, we can get the following power spectrum density for the track error on track i:

$$\begin{aligned}
\Phi_{\triangle y_i \triangle y_i}(e^{j\omega}) &= \sum_{l=1}^{i-1} |G_1|^{2(i-l-1)} |T|^2 \left(|G_1|^2 \sigma_n^2 + |S|^2 |1-F|^2 \times \right. \\
&\qquad \left. \Phi_{dd}\right) + |G_1|^{2i} \Phi_{\triangle y_0 \triangle y_0} + |T|^2 \sigma_n^2 + |S|^2 \Phi_{dd}\ .
\end{aligned} \tag{5.7}$$

When the track index i is quite large, $|G_1(e^{j\omega})|^{2i}$ will be closed to zero, since $|G_1(e^{j\omega})| < 1$. Then, for the large track index i, we have:

$$\Phi_{\triangle y_i \triangle y_i}(e^{j\omega}) = \frac{|T|^2}{1-|G_1|^2}\left[\sigma_n^2 + |\hat{F}|^2 \Phi_{dd}(e^{j\omega})\right] + |S|^2 \Phi_{dd}(e^{j\omega})\ . \tag{5.8}$$

In order to conveniently make use of the mixed H_2/H_∞ scheme, which will be discussed in Section 5.3, we utilize the parameterization $G_1(z) = 1 + \hat{F}(z)$ and $\hat{F}(z) = S(z)\,(F(z) - 1)$.

5.2.2 Discussion

From (5.8), we note that, in order to reduce track errors, not only a good track-following feedback controller is necessary, but also both $|G_1(e^{j\omega})|$ and $\left|\hat{F}(e^{j\omega})\right|$ should be sufficiently small. However, $|G_1(e^{j\omega})|$ and $\left|\hat{F}(e^{j\omega})\right|$ can not be small simultaneously, since $G_1(z) = 1 + \hat{F}(z)$. Intuitively, in order to accomplish a good tracking performance, the H_2 norm of the transfer functions from disturbances to track errors must be minimized and simultaneously an appropriately small $\|G_1(z)\|_\infty$ must be guaranteed. This idea turns out to be a mixed H_2/H_∞ control problem, which will be discussed in next section.

5.3 The Design of Feedback and Feedforward Control by Using Mixed H_2/H_∞ Synthesis

5.3.1 Problem Formulation

As discussed in Section 5.2, (5.8) educes the idea of a mixed H_2/H_∞ control design in order to achieve a good tracking performance. Let's rewrite (5.8) as:

$$\Phi_{\triangle y_i \triangle y_i}(e^{j\omega}) = |T|^2 \left(\frac{\sigma_n^2}{1-|G_1|^2}\right) + |\hat{F}|^2 \left(\frac{|T|^2}{1-|G_1|^2}\Phi_{dd}(e^{j\omega})\right) + |S|^2\Phi_{dd}(e^{j\omega}) \ . \quad (5.9)$$

Clearly, (5.9) shows that the track error can be considered as the output of the system $\bar{G}_2(z) = \begin{bmatrix} T(z) & \hat{F}(z) & S(z) \end{bmatrix}$ with the input of $\left[\frac{n_i}{(1-|G_1|^2)^{1/2}} \quad \frac{T}{(1-|G_1|^2)^{1/2}}\tilde{d}_i \quad d_i\right]^T$. Here, $\tilde{d}_i$'s are artificial disturbances, which are uncorrelated with n_i and d_i and have the same power spectrum density as d_i. Since the weighting functions $\frac{1}{(1-|G_1|^2)^{1/2}}$ and $\frac{T}{(1-|G_1|^2)^{1/2}}$ for n_i and $\tilde{d}_i$ are not affine in $G_1(z)$ and $T(z)$, the two weighting functions are replaced by two weighting values w_{t2} and w_{t3} respectively, in order to conveniently construct a linear system to represent the transfer function matrix from the input $\begin{bmatrix} n_i & \tilde{d}_i & d_i \end{bmatrix}^T$ to $\triangle y_i$. Such substitution is further validated by the fact that the magnitude frequency responses of both G_1 and T are expected to be flat at low and middle frequencies [56].

By considering the system denoted in Fig. 5.5 where d_w, d_r, d_n, $\tilde{d}_w$, and $\tilde{d}_r$ are assumed to be uncorrelated white noises, we obtain the following expression for the power spectrum density of z_2:

$$\Phi_{z_2 z_2}(e^{j\omega}) = |T|^2 w_{t2}^2 \sigma_n^2 + |\hat{F}|^2 w_{t3}^2 \Phi_{dd}(e^{j\omega}) + |S|^2\Phi_{dd}(e^{j\omega}) \ . \quad (5.10)$$

Obviously, the power spectrum density of z_2 is similar to that of $\triangle y_i$ except the replacement of the weighting functions in (5.9) with the corresponding weighting values in (5.10). Thus, with appropriate weighting values w_{t2} and w_{t3}, $\Phi_{\triangle y_i \triangle y_i}(e^{j\omega})$ can be approximated by $\Phi_{z_2 z_2}(e^{j\omega})$. Let $G_2(z) = \left[T_{z_2 \leftarrow \begin{bmatrix} d_w & d_r & d_n \end{bmatrix}^T} \quad w_{t3}\hat{F} * T_{\tilde{d} \leftarrow \begin{bmatrix} \tilde{d}_w & \tilde{d}_r \end{bmatrix}^T} \right]$ denote the transfer function matrix from $\begin{bmatrix} d_w & d_r & d_n & \tilde{d}_w & \tilde{d}_r \end{bmatrix}^T$ to z_2, as shown in Fig. 5.5. Therefore, in order to accomplish good tracking error performance, we

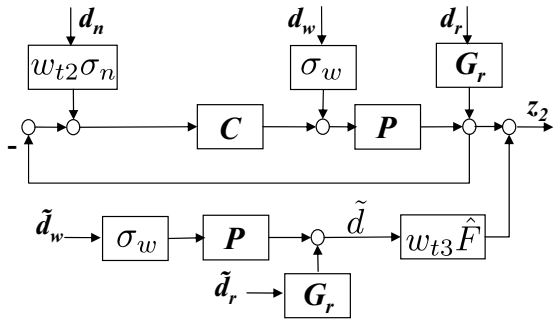

Figure 5.5: Block diagram for the interpretation of $G_2(z)$ by using mixed H_2/H_∞ control

consider the mixed H_2/H_∞ optimization problem

$$\begin{array}{cc} \min_{C(z),F(z)} & \|G_2(z)\|_2 \\ \text{s.t.} & \|G_1(z)\|_\infty < \gamma_0 < 1 \end{array} \tag{5.11}$$

to design $C(z)$ and $F(z)$ simultaneously. Here, γ_0 is a given constant to guarantee good convergence for the track error propagation and a good attenuation for the disturbances from the previously-written tracks.

5.3.2 Mixed H_2/H_∞ Synthesis via LMIs

A number of techniques [7] have been developed to formulate the mixed H_2/H_∞ control problems such as (5.11), and the problems are frequently solved as solutions of linear matrix inequalities. However, in order to recover the convexity of the optimization, the solution approach through LMIs has to impose a constraint which brings significant conservatism to the control synthesis, as discussed in Chapter 2. Moreover, the mixed H_2/H_∞ optimization in (5.11) is quite difficult to be solved, because both $G_1(z)$ and $G_2(z)$ not only include the feedback controller $C(z)$ but also the feedforward controller $F(z)$. In order to simplify the synthesis and reduce the conservatism, we utilize the parameterization of $G_1(z) = 1 + \hat{F}(z)$. Then, with

$\hat{F}(z) = S(z)\,(F(z) - 1)$, the optimization in (5.11) can be reformulated as:

$$\begin{aligned} \min_{C(z),\hat{F}(z)} \quad & \|G_2(z)\|_2 \\ \text{s.t.} \quad & \|1 + \hat{F}(z)\|_\infty < \gamma_0 < 1 \,. \end{aligned} \tag{5.12}$$

The advantage of the formulation in (5.12) over the formulation in (5.11) is that the H_∞ norm constraint is independent of the feedback controller $C(z)$. Moreover, the mixed H_2/H_∞ control synthesis is free from the conservative constraint in (2.8), which will be seen from the subsequent control formulation using LMIs.

Obviously, $G_2(z)$ can be rewritten as

$$G_2(z) = \begin{bmatrix} T_{z_2 \leftarrow \begin{bmatrix} d_w & d_r & d_n \end{bmatrix}^T} & 0 & 0 \end{bmatrix} + \hat{F} \times \begin{bmatrix} 0 & 0 & 0 & T_{\tilde{d} \leftarrow \begin{bmatrix} \tilde{d}_w & \tilde{d}_r \end{bmatrix}^T} \end{bmatrix} \,.$$

Suppose we have the following state space realizations:

$$C(z) \sim \left[\begin{array}{c|c} A_c & B_c \\ \hline C_c & D_c \end{array}\right] \tag{5.13}$$

$$\begin{bmatrix} T_{z_2 \leftarrow \begin{bmatrix} d_w & d_r & d_n \end{bmatrix}^T} & 0 & 0 \end{bmatrix} \sim \left[\begin{array}{c|c} A_{cl2} & B_{cl2} \\ \hline C_{cl2} & D_{cl2} \end{array}\right] \tag{5.14}$$

$$\begin{bmatrix} 0 & 0 & 0 & T_{\tilde{d} \leftarrow \begin{bmatrix} \tilde{d}_w & \tilde{d}_r \end{bmatrix}^T} \end{bmatrix} \sim \left[\begin{array}{c|c} A_d & B_d \\ \hline C_d & D_d \end{array}\right] \tag{5.15}$$

$$\hat{F} \sim \left[\begin{array}{c|c} A_{\hat{F}} & B_{\hat{F}} \\ \hline C_{\hat{F}} & D_{\hat{F}} \end{array}\right], G_1 = 1 + \hat{F} \sim \left[\begin{array}{c|c} A_{\hat{F}} & B_{\hat{F}} \\ \hline C_{\hat{F}} & 1 + D_{\hat{F}} \end{array}\right] \tag{5.16}$$

$$\hat{F} \begin{bmatrix} 0 & 0 & 0 & T_{z_2 \leftarrow \begin{bmatrix} \tilde{d}_w & \tilde{d}_r \end{bmatrix}^T} \end{bmatrix} \sim \left[\begin{array}{c|c} \bar{A}_f & \bar{B}_f \\ \hline \bar{C}_f & \bar{D}_f \end{array}\right] = \left[\begin{array}{cc|c} \bar{A}_d & 0 & B_d \\ B_{\hat{F}} C_d & A_{\hat{F}} & B_{\hat{F}} D_d \\ \hline D_{\hat{F}} C_d & C_{\hat{F}} & D_{\hat{F}} D_d \end{array}\right] \tag{5.17}$$

$$G_2 \sim \left[\begin{array}{c|c} \bar{A}_{cl2} & \bar{B}_{cl2} \\ \hline C_{cl2} & D_{cl2} \end{array}\right] = \left[\begin{array}{cc|c} \bar{A}_{cl2} & 0 & B_{cl2} \\ 0 & \bar{A}_f & \bar{B}_f \\ \hline C_{cl2} & \bar{C}_f & D_{cl2} + \bar{D}_f \end{array}\right] \tag{5.18}$$

Then the optimization in (5.12) can be synthesized as the following optimization [7]:

$$\begin{aligned}
\min \quad & \underset{A_c,B_c,C_c,D_c,C_{\hat{F}},D_{\hat{F}}}{} \operatorname{trace}(W) \\
\text{s.t.} \quad & \begin{bmatrix} W & \bar{C}_{cl2} & \bar{D}_{cl2} \\ * & X_2 & 0 \\ * & * & I \end{bmatrix} \succ 0 && (5.19) \\
& \begin{bmatrix} X_2 & X_2\bar{A}_{cl2} & P_2\bar{B}_{cl2} \\ * & X_2 & 0 \\ * & * & I \end{bmatrix} \succ 0 && (5.20) \\
& \begin{bmatrix} X_1 & X_1A_{\hat{F}} & X_1B_{\hat{F}} & 0 \\ * & X_1 & 0 & C_{\hat{F}}^T \\ * & * & I & 1+D_{\hat{F}}^T \\ * & * & * & \gamma_0^2 I \end{bmatrix} \succ 0 && (5.21)
\end{aligned}$$

where the symbol "$*$" denotes the transpose of the corresponding element at its transposed position. Since both X_1 and X_2 are coupled with $A_{\hat{F}}$ and $B_{\hat{F}}$ in (5.21) and (5.20) respectively, the filter $\hat{F}(z)$ is chosen as an FIR filter, which means that $A_{\hat{F}}$ and $B_{\hat{F}}$ are known and thus (5.21) becomes an LMI. Moreover, in order to recover the convexity of (5.19) and (5.20) by a suitable nonlinear transformation [40], the matrix X_2 is chosen as $X_2 = \operatorname{diag}\{X_{22}, X_{ff}\}$. As a result, the optimization involving (5.19), (5.20) and (5.21) is a convex optimization, which can be easily solved. After synthesizing $\hat{F}(z)$, we can reconstruct the feedforward control by

$$F(z) = 1 + S^{-1}(z)\hat{F}(z) = 1 + (1 + P(z)C(z))\hat{F}(z) \ .$$

5.4 Simulation Study

In order to evaluate the concentric SSTW design methodologies presented in this chapter, they will be tested via a simulation study that utilizes the benchmark model developed by the IEEJapan technical committee on Nano-Scale Servo (NSS) system [49] for single-stage HDDs. This model was also utilized to test the concentric SSTW design scheme presented in [56]. This benchmark model was originally developed to test track-following servos and must be modified to test servo systems for self-servo track writing control. For the simulated hard disk drive, the servo sector number N is equal to 220 and the disk speed is 7200 RPM. Thus, the sampling frequency for this drive is $f_s = 220 \times 7200/60 = 26400$ Hz.

5.4.1 Weighting Value Determination

Before using the presented two control synthesis methodologies, we have to determine the corresponding weighting values w_{t1}, w_{t2}, and w_{t3}. For the technique presented in Section 5.1, since the track error propagation term G_1 may result in instability (if $\|G_1(z)\|_\infty > 1$), it is reasonable to choose a relatively small w_{t1}. Intuitively, the selection of $w_{t1} < 1$ is desirable to emphasize G_1.

For the technique presented in Section 5.3, γ_0 must be less than 1 and is required to be closed to 1 so that the obtained H_2 norm cost for track errors in (5.11) is not too conservative according to the H_∞ norm constraint. In addition, w_{t2} and w_{t3} are utilized to approximate $\frac{1}{(1-|G_1|^2)^{1/2}}$ and $\frac{T}{(1-|G_1|^2)^{1/2}}$ respectively. As mentioned in Section 5.3, the magnitude of T and G_1 are flat at the low and middle frequencies and thus it is desirable to determine w_{t2} and w_{t3} using the DC gains of T and G_1. It is well known that in order to attenuate low-frequency disturbances, $T = \frac{PC}{1+PC}$ is usually designed to have a unit DC gain. Thus, w_{t2} and w_{t3} can be roughly selected by

$$w_{t2} = w_{t3} = \frac{1}{\left(1 - (\text{Expected DC Gain of } G_1)^2\right)^{1/2}} .$$

5.4.2 Control Design Results

An optimal H_2 track following compensator $C(z)$ was first synthesized and then a non-causal feedforward compensator $F(z)$ was designed using the H_∞ control design methodology presented in Section 5.1, with the weighting value $w_{t1} = 0.16$ and $n_d = 7$. The designed control system achieves $\|G_1(z)\|_\infty = 0.9781 < 1$ and $\|F(z)\|_\infty = 1.3633$. The corresponding frequency response plots for the designed $F(z)$, $\frac{P(z)C(z)+F(z)}{1+P(z)C(z)}$, $\frac{1}{1+P(z)C(z)}$, and $\frac{F(z)}{1+P(z)C(z)}$ are shown in Fig. 5.6.

Subsequently, a feedforward compensator $F(z)$ constructed from the FIR filter $\hat{F}(z)$ and a feedback compensator $C(z)$ were simultaneously designed using the mixed H_2/H_∞ control synthesis methodology in Section 5.3. The designed control system achieves $\|G_1(z)\|_\infty = 0.9737$ with the tuning parameters $w_{t2} = 4$, $w_{t3} = 4$ and $\gamma_0 = 0.98$. The frequency response plots for the resulting controllers are shown in Fig. 5.7.

5.4.3 Time-Domain Simulation Results

For the benchmark problem in [49], the modeled sensor noise has a sigma value of 1.5% of track pitch; that of the track runout due to disk vibrations is 1.7% of track

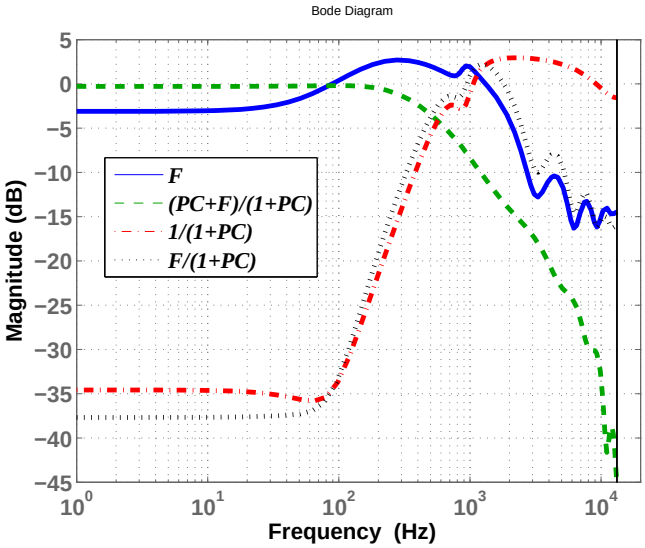

Figure 5.6: Frequency responses for the non-causal feedforward control design via H_∞ control

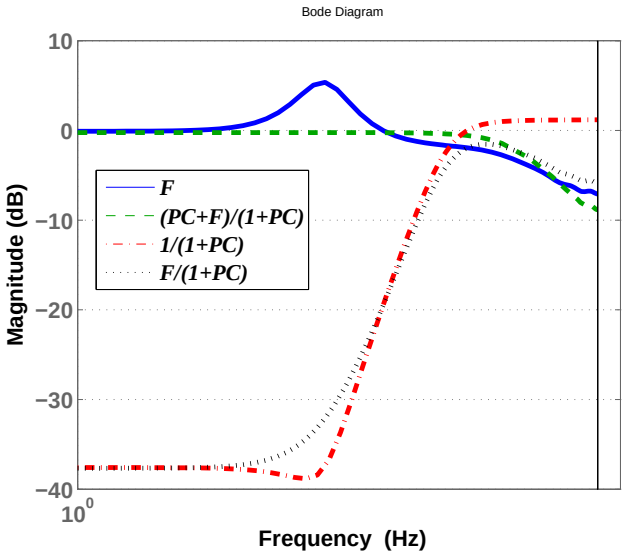

Figure 5.7: Frequency responses for the feedback and feedforward control designs using the mixed H_2/H_∞ synthesis methodology

pitch; the contribution of the windage to PES has a sigma value of 12.2% track width. The track error for the seed track is assumed to be a sigma value of 14% track width. In the simulation, a total of 5000 servo tracks data was collected. In order to interpret the simulated results better, we also provide the time-domain simulation results for the 2-Dimensional H_2 SSTW synthesis technique presented in [16]. The sigma values of the first 5000 self-servo written tracks for the proposed two methods in this chapter and for the 2-D H_2 system are depicted in Fig. 5.8. Obviously, the track error propagation is well contained for the three design methodologies.

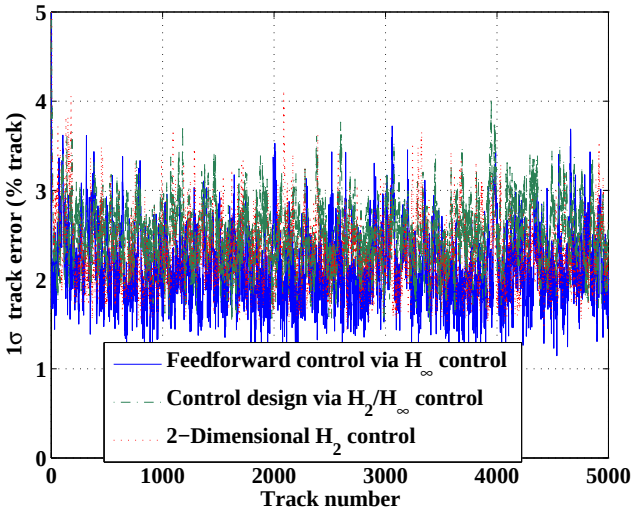

Figure 5.8: Time domain simulation results for track errors. Since the performance of the control design via H_2/H_∞ is closed to that of 2-D H_2 control, the green dashed line is almost covered by the red dotted line.

Meanwhile, by considering the relatively large variance of the seed track, we are also interested in checking how fast the transition response caused by the seed track converges. The zoomed in figure for the transition response is illustrated in Fig. 5.9. The results demonstrate that the effect of the bad seed track on the subsequently written tracks by the proposed controllers disappears very quickly. Specifically, the simulation results show that the transition responses disappear after about 15 tracks.

We now consider another common performance index called AC squeeze in order to quantify the quality of written tracks. The AC squeeze for track i is defined as:

$$\text{ACsqueeze}_i = \min_{k\in[0,N-1]} \{1 + \triangle y_i(k) - \triangle y_{i-1}(k)\} \tag{5.22}$$

where track errors $\triangle y_i(k)$ and $\triangle y_{i-1}(k)$ are normalized by the track width. When the AC squeeze is too small, two adjacent tracks with narrow track spacing may interfere with each other and cause data corruption. The ideal value of AC squeeze is 1 track

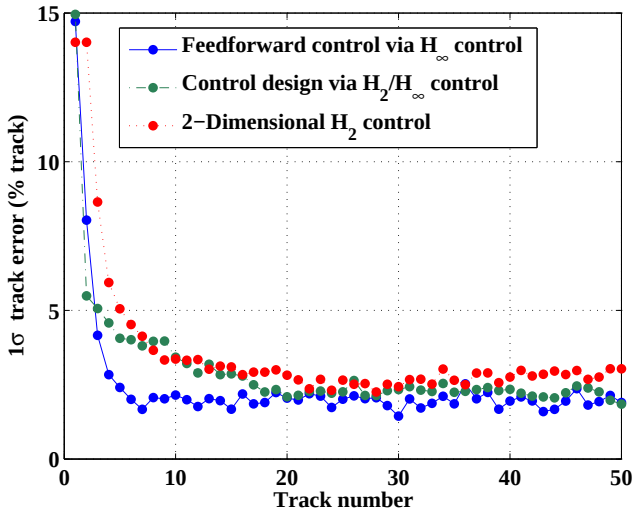

Figure 5.9: Zoomed in Fig. 5.8 to check the transition response caused by the seed track.

width, which means the adjacent tracks are perfectly parallel to each other. The AC squeeze values for the simulated self-servo written tracks are shown in Fig. 5.10. Moreover, the resulting average values of $\sigma\left(\triangle y_{i-1}(k)\right)$ and ACsqueeze_i are presented in Table 5.1. Note that the non-causal feedforward control design through standard H_∞ control achieves the best performance for track errors, while the feedback and feedforward control designs by using the mixed H_2/H_∞ control accomplish the best AC squeeze.

In order to provide the better comparison for our proposed control synthesis techniques, the simulation results reported in [56] by using the iterative learning control in lifted domain are also listed in Table 5.1. Obviously, the two proposed control design methodologies are able to improve both track errors and AC squeeze compared to the ILC technique. Meanwhile, the two proposed control design techniques offer the comparable performances to the 2-Dimensional H_2 control technique in [16] while having a much simpler control structure.

5.5 Conclusion

This chapter discussed two novel controller synthesis methodologies using a feedforward control structure for performing concentric self-servo track writing in disk drives. In the first methodology, it is assumed that a conventional causal track-following controller has been designed and then a non-causal feedforward controller—which utilizes the stored error signal from writing the previous track—is designed based on standard

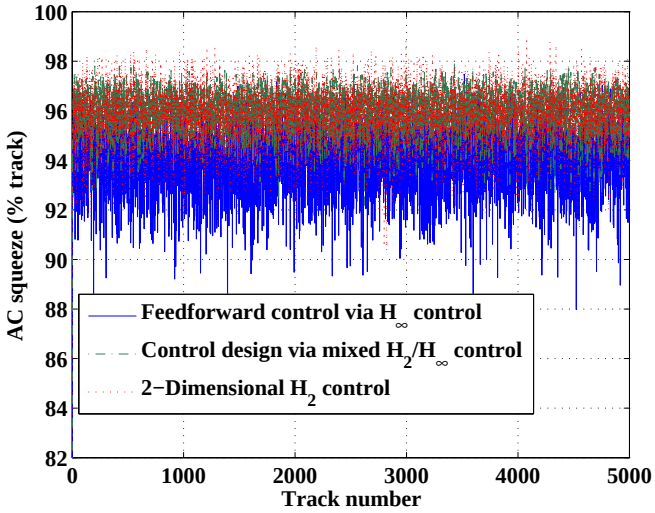

Figure 5.10: Time domain simulation results for AC Squeeze. Since the performance of the control design via H_2/H_∞ is closed to that of 2-D H_2 control, the green dashed line is almost covered by the red dotted line.

Table 5.1: Time-domain simulation results for SSTW controllers

	Non-causal feedforward control using H_∞ control	Control designs using mixed H_2/H_∞ control	2-D H_2 control	ILC in lifted domain [21]
Average of 1σ track error (% track)	2.11	2.50	2.27	2.88
Average of AC squeeze (% track)	94.0	96.0	95.8	88

H_∞ control synthesis techniques. The designed controllers were used to prevent the track errors from propagating and to achieve good disturbance attenuation. In the second methodology, an analytic expression for the power spectrum density of track errors was derived. The expression was subsequently used to formulate the simultaneous design of both feedback and feedforward controllers, using a mixed H_2/H_∞ control scheme, which ensures the containment of the error propagation and the achievement of good disturbance attenuation. In addition, a controller parameterization was employed so as to reduce the conservatism which is caused by the constraint imposed to recover the convexity. Then, the mixed H_2/H_∞ control was solved via the solution of a set of LMIs. Neither of these techniques utilizes the simplifying assumptions in [56]. Simulation results using the HDD benchmark problem developed in [49] showed that the controllers synthesized using the proposed schemes outperform the controllers synthesized by the techniques in [56], and offer levels of performances that are comparable with the 2-Dimensional H_2 control technique in [16] while having a simpler structure. Moreover, the track error propagation converged after about 15 tracks despite the seed track having a large track error.

Chapter 6

Conclusions

6.1 Conclusions

In order to sustain the continuing increase of HDD data storage density, dual-stage actuator servo systems have been developed to increase their servo bandwidth and thus improve the precision of read/write head positioning control. Unfortunately, the sampling intervals in HDDs are not always equidistant and even sometime an irregular sampling rate due to missing PES sampling data is unavoidable, for example, the unavailability of the feedback signals in HDD servos with false PES demodulation (due to incorrect servo address mark detection or damaged servo patterns). In addition, such an irregular sampling rate also often occurs in self-servo track writing process with the "collision" of reading the PES with writing the final servo patterns. Therefore, it is important to address the issue of designing HDD servo systems under irregular sampling rates. In addition, since servo patterns are used to generate the feedback PES, the quality of servo track writing also plays an important role in increasing HDD data storage density. In this dissertation, dual-stage control design methodologies, optimal H_∞ control algorithm for the servos with irregular sampling rates, and control design techniques for concentric self-servo track writing were developed for HDD servo systems.

In the control design of dual-stage track-following servos, the modeling of these dual-stage servo systems was first established. Subsequently, the disturbance observer with the base line control of the sensitivity-decoupling control and the control synthesis using the idea of a mixed H_2/H_∞ control scheme were developed. Because of the conservatism of mixed H_2/H_∞ control synthesis using LMIs, a controller was alternatively designed using nominal H_2 control synthesis in which the control input weighting value was tuned to achieve robust stability. Consequently, the designed nominal H_2 control can achieve not only a good servo performance but also the

robust stability. The designs were experimentally validated using a dual-stage servo system with a PZT-actuated suspension. The sensitivity-function crossover frequency of the disturbance observer design is 2.08 KHz and that of the nominal H_2 control design is 3.67 KHz. The 3σ NRRO PES for the disturbance observer design is 13.1 nm, while the 3σ NRRO PES for the nominal H_2 control design is 9.4 nm.

For the control design of HDD servo systems with irregular sampling rates caused by missing PES sampling data, these servo systems were modeled as linear periodically time-varying systems with period equal to the number of servo sectors. An optimal H_∞ control synthesis algorithm based on the solution of discrete Riccati equations was developed to for LPTV systems achieve the robust performance for large variations in HDD dynamics due to variations in manufacturing and assembly. First, the developed control synthesis technique was tested by designing both single-rate and multi-rate H_∞ track-following controllers for single-stage HDD servo systems. Compared to the control synthesis methodology in the Matlab function of "hinfsyn", our proposed synthesis technique is more numerically robust in calculating optimal discrete-time H_∞ controllers for discrete-time linear time-invariant systems. Moreover, the presented control synthesis algorithm is also applicable to multi-rate sampling and actuation, while the "hinfsyn" function in Matlab is only applicable for LTI plants. Simulation results demonstrate that multi-rate H_∞ controllers synthesized using the technique presented in this dissertation consistently outperform their single-rate counterparts and offer the improved robust performance.

The developed optimal H_∞ control algorithm was then applied to HDD servo systems with irregular sampling rates. In order to make the resulting periodic controllers more practical for implementation in real hard disk drives, a control parameter simplification was established. The simulation and experimental studies on multiple hard disk drives validate the synthesized controller's effectiveness in handling irregular sampling rates and achieving the robust performance of a desired error rejection transfer function for disturbance attenuation. The simulation results were verified by the implementation results on ten actual 2.5" single-stage hard disk drives. Moreover, compared to the currently-used methodology for missing PES samples, our proposed optimal H_∞ control algorithm has improved the 3σ PES by around 20% for the tested hard disk drives in the experimental study.

In order to improve the quality of servo track writing and reduce its cost, two novel controller synthesis methodologies using a feedforward control structure were proposed for performing concentric self-servo track writing in single-stage hard disk drives. In the first methodology, it is assumed that a conventional causal track-following controller has been designed and a non-causal feedforward controller, which utilizes the stored error signal from writing the previous track, is designed using standard H_∞ control synthesis techniques. In the second methodology, an analytic expression for the power spectrum density of track errors was derived. The expres-

sion was subsequently used to formulate the simultaneous design of both feedback and feedforward controllers, using a mixed H_2/H_∞ control scheme. By imposing a constraint to recover the convexity, the mixed H_2/H_∞ control problem was solved via the solution of a set of LMIs. In addition, a controller parameterization was employed so as to reduce the conservatism caused by the constraint. Simulation results show that the controllers synthesized using the proposed schemes outperform the controllers synthesized by the iterative learning control techniques in [56] and offer levels of performances that are comparable with the 2-dimensional H_2 control technique in [16] while having a simpler structure. Moreover, the track error propagation converges very quickly despite the seed track having a large track error.

6.2 Future Work

Related to the work presented in this dissertation, several interesting future research topics are described as follows.

The HDD dual-stage track-following control design methodologies presented in Chapter 2 just considered the stability robustness for the hard disk drive with dynamic uncertainties. In reality, it is more interesting that all of many several hard disk drives could achieve as better servo performance as possible by using one single controller. In other words, we have to synthesize a controller to achieve the best performance for the worst case of these HDDs with defined uncertainties. Since disk drives are stochastic systems and their performance is represented by the statistical distribution of the PES, the HDD servo performance can be characterized by the H_2 norm of the close-loop system. Thus, synthesizing controllers that minimize the H_2 norm of the worst case of the closed-loop systems under the uncertainties is an interesting research topic and this topic turns out to be a robust H_2 control problem. For convenience in its control synthesis, H_2 guaranteed cost control problem [13] has been recently studied as a conservative approximation of a robust H_2 control problem.

By considering that HDD servos with irregular sampling rates can be represented as linear periodically time-varying systems, another interesting research topic is to extend H_2 guaranteed cost control synthesis techniques to discrete-time LPTV systems. As a result, the H_2 guaranteed cost control design methodology could then be applied to disk drives with missing PES sampling data.

In this dissertation, the servo control designs of self-servo track writing were based on the single-stage HDD configuration. In the future, the dual-stage HDD configuration may be utilized in self-servo track writing process. Then, the servo design of dual-stage self-servo track writing is a quite attractive research topic by considering that we can improve the accuracy of positioning write heads using dual-stage actuation.

On the other hand, the precision of read/write head positioning in HDD servos can also be improved by amending HDD hardware. For example, instead of using actuated-suspension assembly, we can utilize actuated-head assembly [33, 53] for dual-stage actuation. In the actuated-head approach, a micro-actuator is integrated into the slider structure and moves the read/write head only. Consequentially, the actuated-head type micro-actuator has a much higher bandwidth than the actuated-suspension type. Currently, one member in our research group is working on the fabrication of such micro-actuator prototype. In addition, the technique of using additional sensing [19, 20] has also been employed to improve the HDD servo control. In our research group, high resolution thin film strain sensors have been successfully integrated into instrumented suspension prototypes and some basic experimental studies have been carried out on these instrumented suspensions in order to evaluate the effectiveness of the sensors. In the future, more complicated system models by integrating the additional sensor signal into dual-stage HDDs need to be established for synthesizing track-following controllers. It is interesting to investigate the advantages of introducing additional sensing by applying our currently-developed robust control synthesis algorithms to HDDs with an instrumented suspension.

Bibliography

[1] D. Abramovitch and G. Franklin. A brief history of disk drive control. *IEEE Control Systems Magazine*, 22(3):28–42, 2002.

[2] D. Abramovitch, T. Hurst, and D. Henze. An overview of the pes pareto method for decomposing baseline noise sources in hard disk position error signals. *IEEE Trans. on Magnetics*, 34(1):17–23, 1998.

[3] S. Bittanti and P. Colaneri. Invariant representations of discrete-time periodic systems. *Automatica*, 36(12):1777–1793, 2000.

[4] D. Brunnett, Y. Sun, and L. Guo. Method and apparatus for performing a self-servo write operation in a disk drive using spiral servo information. U.S. Patent 7230789B1, 2007.

[5] T. Chainer, M. D. Schultz, B. C. Webb, and E. D. Yarmchuk. Self servowriting system with dynamic error propagation reduction. U.S. Patent 5793554, 1998.

[6] B. Chen, T. Lee, and V. Venkataramanan. *Hard Disk Drive Servo Systems*. Adavances in Industrial Control Series. Springer, New York, 2006.

[7] X. Chen and K. Zhou. Multiobjective h_2/h_∞ control design. *SIAM J. Control Optim.*, 40(2):628–660, 2001.

[8] R. Conway. Multi-objective control design for discrete time periodic systems via convex optimization. Technical report, Mechanical Engineering Department, University of California, Berkeley, California, April 2007.

[9] R. Conway, J. Choi, R. Nagamune, and R. Horowitz. Robust track-following controller design in hard disk drives based on parameter dependent lyapunov functions. *IEEE Trans. Magnetics*, 46(4):1060–1068, 2010.

[10] R. Conway and R. Horowitz. A quasi-newton algorithm for lqg controller design with variance constraints. In *Proc. of Amer. Control Conf.*, 2008.

[11] R. Conway and R. Horowitz. Analysis of h_2 guaranteed cost performance. In *Proc. of the 2009 Dynamic Systems and Control Conference*, 2009.

[12] R. Conway and R. Horowitz. Guaranteed cost control for linear periodically time-varying systems with structured uncertainty and a generalized h_2 objective. *Mechatronics*, 20(1):12–19, 2010.

[13] Richard Conway and Roberto Horowitz. Optimal full information h_2 guaranteed cost control of discrete-time systems. In *Proc. of 2010 ASME Dynamic Systems and Control Conference*, Cambridge, Massachusetts, USA, 2010.

[14] D. Cribbs, M. Ellenberger, and J. Hassler. Self-servo writing disk drive and method. U.S. Patent 5448429, 1995.

[15] J. Doyle, K. Glover, P. Khargonekar, and B. Francis. State-space solutions to standard h_2 and h_∞ control problems. *IEEE Trans. Automatic Control*, 34(8):831–847, 1989.

[16] C. Du, L. Xie, J. N. Teoh, and G. Guo. h_2 control for head positioning in axial and radial dimensions for self-servo track writing. *IEEE Trans. on Control Systems Technology*, 16(1):177–181, 2008.

[17] R. Ehrlich. Methods for improving servo-demodulation robustness. U.S. Patent 6943981B2, 2005.

[18] R. Ehrlich and D. Curran. Major hdd tmr sources and projected scaling with tpi. *IEEE Trans. on Magnetics*, 35(2):885–891, 1999.

[19] S. Felix, J. Nie, and R. Horowitz. Strain sensing with piezoelectric zinc oxide thin films for vibration suppression in hard disk drives. In *Proc. of the 2008 ASME Dyanmic Systems and Control Conference*, 2008.

[20] S. Felix, J. Nie, and R. Horowitz. Enhanced vibration suppression in hard disk drives using instrumented suspensions. *IEEE Trans. Magnetics*, 45(11):5188–5122, 2010.

[21] M. Hirata, T. Mita K. Liu, and T. Yamaquchi. Head positioning of a hard disk drive using h_∞ theory. In *Proc. of the 31st IEEE Conference on Control and Decision*, pages 2460–2461, 1992.

[22] X. Huang. *Robust Track-Following Control Design for Dual-Stage Servo Systems with a MEMS Microactuator and an Instrumented Suspension.* PhD thesis, Berkeley, California, 2008.

[23] X. Huang, R. Nagamune, and R. Horowitz. A comparison of multirate robust track-following control synthesis techniques for dual-stage and multi-sensing

servo system in hard disk drives. *IEEE Transactions On Magnetics*, 42(7):1896–1904, 2006.

[24] P. Iglesias and K. Glover. State-space approach to discrete-time control. *International Journal of Control*, 54(5):1031–1073, 1991.

[25] F. Jorgenson. *Complete Handbook of Magnetic Recording*. McGraw-Hill, 1995.

[26] H.J. Kang, C.W. Lee, C.C. Chung, and H.S. Lee. Control design for self-servo track writing using a state-space disturbance observer. *IEEE Trans. Magnetics*, 45(11):5148–5151, 2009.

[27] H. Lee and M. Tomizuka. Robust digital tracking controllers for high-accuracy positioning systems. *IEEE Transactions on Industrial Electronics*, 43(1):48–55, 1996.

[28] Y. Li. *Dual-Stage Servo Control and Active Vibration Compensation in Magnetic Hard Disk Drives*. PhD thesis, Berkeley, California, 2003.

[29] Y. Li and R. Horowitz. Mechatronics of electrostatic microactuators for computer disk drive dual-stage servo systems. *IEEE/ASME Transactions on Mechatronics*, 6(2):111–121, 2001.

[30] H. Lin, G. Zhai, and P. Antsaklis. Robust stability and disturbance attenuation analysis of a class of networked control systems. In *Proc. of the 42nd IEEE Conference on Decision and Control*, 2003.

[31] A. Mamun, G. Guo, and C. Bi. *Hard disk drive: Mechatronics and Control*. Boca Raton, FL: CRC, 2006.

[32] H. Melkote and R. J. McNab. Modeling and control for self-servowriting in hard disk drives: A repetitive process approach. In *Proc. of the the 2006 American Control Conference*, pages 2005–2010, 2006.

[33] M. Mita, H. Toshiyoshi, and H. Fujita. Electrostatic piggyback microactuators for head element positioning. In *Proc. of ASME/IEEE Asia Pacific Magnetic Recording Conference*, 2002.

[34] R. Nagamune, X. Huang, and R. Horowitz. Multi-rate track-following control with robust stability for a dual-stage multi-sensing servo systems in hdds. In *Proc. of the Joint 44th IEEE Conference on Decision and Control and European Control Conference*, pages 3886–3891, 2005.

[35] R. Nagamune, X. Huang, and R. Horowitz. Robust control synthesis techniques for multirate and multisensing track-following servo systems in hard disk drives.

Journal of Dynamic Systems, Measurement and Control, Transactions of the ASME, 132(2):1–10, 2010.

[36] J. Nie, R. Conway, and R. Horowitz. Optimal h_∞ control for linear periodically time-varying systems in hard disk drives. In *Proc. of the 2010 Dynamic Systems and Control Conference*, 2010.

[37] J. Nie and R. Horowitz. Design and implementation of dual-stage track-following control for hard disk drives. In *Proc. of the 2009 Dynamic Systems and Control Conference*, 2009.

[38] J. Nie and R. Horowitz. Control design of concentric self-servo track writing systems for hard disk drives. In *Proc. of the 2010 American Control Conference*, pages 2631–2640, 2010.

[39] J. Nie, E. Sheh, and R. Horowitz. Track-following control design and implementation for hard disk drives with missing samples. In *to appear in Proc. of the 18th World Congress,International Federation of Automatic Control*, 2011.

[40] M. C. De Oliveira, J. C. Geromel, and J. Bernussou. Extended h_2/h_∞ norm characterization and controller parametrizations for discrete-time systems. *IEEE Trans. on Control Systems Technology*, 75(9):666–679, 2002.

[41] M. A. Peters and P. A. Iglesias. *Minimum Entropy Control for Time-Varying Systems. Systems & Control: Foundations & Applications*. Birkhäuser, Boston, MA, 1997.

[42] A. Sacks, M. Bodson, and W. Messener. Adaptive methods for repeatable runout compensation. *IEEE Transactions On Magnetics*, 31(2):1031–1036, 1995.

[43] S. Schroeck, W. Messner, and R. McNab. On compensator design for linear time-invariant dual-input single-output systems. *IEEE/ASME Transactions on Mechatronics*, 6(1):50–57, 2001.

[44] S. Semba, T. Hirano, J. Hong, and L. Fan. Dual-stage servo controller for hdd using mems actuator. *IEEE Transactions on Mechatronics*, 35(5):2271–2273, 1999.

[45] T. Semba, N. Kagami, and A. Tokizono. Method and apparatus for suppressing mechanical reasonance in a disk drive storage device using a notch filter. U.S. Patent 6219196, 2001.

[46] D. Shim, H. Lee, and L. Guo. Mixed-objective optimization of track-following controllers using linear matrix inequalities. In *Proc. of the the 2003 American Control Conference*, pages 4323–4328, 2003.

[47] S. Skogestad and I. Postlethwaite. *Multivariable feedback control: analysis and design*. John Wiley, Hoboken, NJ, 2005.

[48] T. Suzuki, T. Usui, M. Sasaki, F. Fujisawa, T. Yoshida, and H. Hirai. Mr-48 comparison of robust track-following control systems for a dual stage hard disk drive. In *International Conf. on Micromechatronics for Info. and Precision Equipment*, 1997.

[49] IEEJapan technical committee on Nano-Scale Servo (NSS) system. Url http://mizugaki.iis.u-tokyo.ac.jp/nss/. NSS homepage, 2006.

[50] J. Teoh, C. Du, G. Guo, and L. Xie. R/w gap delay estimation for self-servo track writing. In *Proc. of 9th IEEE International Workshop on Advanced Motion Control*, volume 2006, pages 149–152, 2006.

[51] M. Tomizuka. Class notes for advanced control systems ii: Part i. Department of Mechanical Engineering, University of California, Berkeley, 2007.

[52] Y. Tomoyoshi, F. Masanori, S. Hiroyuki, and T. Kazuhiko. Servo writing technology. *Fujitsu Scientific and Technical Journal*, 42(1):93–102, 2006.

[53] H. Toshiyoshi. Electrostatic piggyback microactuators for head element positioning. http://toshi.fujita3.iis.u-tokyo.ac.jp, 2002.

[54] Y. Uematsu, M. Fukushi, and K. Taniguchi. Development of the pushpin free stw. *IEEE Trans. Magnetics*, 37(2):964–968, 2001.

[55] T. Umeno and Y. Hori. Robust speed control of dc servomotors using modern two degrees-of-freedom controller design. *IEEE Transactions on Industrial Electronics*, 38(5):363–368, 1991.

[56] S. Wu and M. Tomizuka. An iterative learning control design for self-servowriting in hard disk drives. In *Proc. of the 17th World Congress, International Fedration of Automatic Control*, volume 17, 2008.

[57] J. Xiong and J. Lam. Stabilization of linear systems over networks with bounded packet loss. *Automatica*, 43(1):80–87, 2007.

[58] T. Yamaguchi. Modelling and control of a disk file head-positioning system. *Proceedings of the Institution of Mechanical Engineers. Part I: Journal of Systems and Control Engineering*, 215(6):549–568, 2001.

[59] H. Ye, V. Sng, C. Du, J. Zhang, and G. Guo. Radial error propagation issues in self servo track writing technology. *IEEE Trans. Magnetics*, 38(5):2180–2182, 2002.

[60] Z. Yuan, B. Liu, T. Zhou, C. Goh, C. Ong, C. Cheong, and L. Wang. Perspetives of magnetic recording system at 10 tb/in^2. *IEEE Trans. Magnetics*, 45(11):5038–5043, 2009.

[61] G. Zames. Feedback and optimal sensitivity: Model reference transformations multiplicative seminorms, and approximate inverses. *IEEE Trans. Automatic Control*, 26(2):301–320, 1981.

[62] J. Zhang, R. Chen, G. Guo, and T.S. Low. Modified adaptive feedforward runout compensation for dual-stage servo system. *IEEE Transactions On Magnetics*, 36(5l):3581–3584, 2000.

[63] S. Zhang and E. Wai. Evaluation of servo patterns for perpendicular recording. In *Digest of Asia-Pacific Magnetic Recording Conference 2006*, 2006.

Appendix A

Minimum Entropy Output Feedback Control Reduction

In this appendix, we will reduce the output feedback control problem for the linear time-varying system $G_{OF} := G$ in (3.1) to a full control problem. With the assumption of $D_{12}^T(k)D_{12}(k) \succ 0, \forall k$ in Chapter 3, we can assume without loss of generality that $D_{12}(k) = \begin{bmatrix} 0 & I \end{bmatrix}^T$. Throughout this appendix, we say a controller K is admissible for a system $\bar{G}$ if and only if $\|\mathcal{F}_\ell(\bar{G}, K)\|_{2\leftarrow 2} < 1$.

A.1 Reduction to Output Estimation Problem

We now consider a full information system with the state-space realization

$$G_{FI} \sim \left[\begin{array}{c|cc} A(k) & B_1(k) & B_2(k) \\ \hline C_1(k) & D_{11}(k) & D_{12}(k) \\ \begin{bmatrix} I \\ 0 \end{bmatrix} & \begin{bmatrix} 0 \\ I \end{bmatrix} & 0 \end{array}\right] . \tag{A.1}$$

Obviously, if there exists an admissible controller K_{OF} for G_{OF} in (3.1), then the controller $K_{OF}\begin{bmatrix} C_2 & D_{21} \end{bmatrix}$ is admissible for G_{FI} since

$$\mathcal{F}_\ell(G_{OF}, K_{OF}) = \mathcal{F}_\ell(G_{FI}, K_{OF}\begin{bmatrix} C_2 & D_{21} \end{bmatrix}) .$$

Based on the results in [41], we know if there exists an admissible controller K_{OF} for G_{OF}, then there must exist $X(k)$ and $T(k)$ such that

- $X(k) \succeq 0$, $T(k) = \begin{bmatrix} T_{11}(k) & 0 \\ T_{21}(k) & T_{22}(k) \end{bmatrix}$, $T_{11}(k) \succ 0$, and $T_{22}(k) \succ 0$;

- $R(k)+B^T(k)X(k+1)B(k) = T^T(k)JT(k)$ where $R(k) = D_{1\bullet}^T(k)D_{1\bullet}(k) - \begin{bmatrix} I & 0 \\ 0 & 0 \end{bmatrix}$, $J = \begin{bmatrix} -I & 0 \\ 0 & I \end{bmatrix}$;
- $$X(k) = A^T(k)X(k+1)A(k) + C_1^T(k)C_1(k) - M(k) \times \left(R(k) + B^T(k)X(k+1)B(k)\right)^{-1} M^T(k)$$
  where $M(k) = A^T(k)X(k)B(k) + C_1^T(k)D_{1\bullet}(k)$;
- $A_{cl}(k) = A(k) + B(k)F(k)$ is UES with
$$\begin{bmatrix} F_1(k) \\ F_2(k) \end{bmatrix} = \left(R(k) + B^T(k)X(k+1)B(k)\right)^{-1} M^T(k) \, .$$

Let $D_\perp(k) = \begin{bmatrix} I & 0 \end{bmatrix}^T$ be an orthogonal matrix to $D_{12}(k)$ and define a matrix $W(k)$ such that $W^T(k)W(k) = I - T_{11}^T(k)T_{11}(k)$ and $W(k)$ has appropriate dimensions so that the following matrix multiplication is well defined:

$$\bar{D}_{11}(k) = D_\perp(k)W(k) + D_{12}(k)T_{21}(k) \, .$$

In addition, we define the following LTV system G_{tmp} with the state-space realization

$$\begin{aligned} G_{tmp} &\sim \left[\begin{array}{c|cc} \bar{A}(k) & B_1(k) & B_2(k)T_{22}^{-1}(k) \\ \hline \bar{C}_1(k) & \bar{D}_{11}(k) & D_{12}(k) \\ \bar{C}_2(k) & D_{21}(k) & 0 \end{array}\right] \\ &:= \left[\begin{array}{c|cc} A(k) + B_1(k)F_1(k) & B_1(k) & B_2(k)T_{22}^{-1}(k) \\ \hline -D_{12}(k)T_{22}(k)F_2(k) & \bar{D}_{11}(k) & D_{12}(k) \\ C_2(k) + D_{21}(k)F_1(k) & D_{21}(k) & 0 \end{array}\right] . \end{aligned} \tag{A.2}$$

Then, we have the following lemma:

Lemma 3. *The controller K_{OE} is admissible for G_{tmp} if and only if the controller given by $T_{22}^{-1}(k)K_{OE}$ is admissible for G_{OF}.*

Proof. Suppose the controller K_{OE} admits the state-space realization

$$K_{OE} \sim \left[\begin{array}{c|c} A_c(k) & B_c(k) \\ \hline C_c(k) & D_c(k) \end{array}\right]$$

and consider the LTV system

$$G_{vyru} \sim \left[\begin{array}{c|cc} A(k) + B_1(k)F_1(k) & B_1(k)T_{11}^{-1}(k) & B_2(k) \\ \hline -T_{22}(k)F_2(k) & T_{21}(k)T_{11}^{-1}(k) & T_{22}(k) \\ C_2(k) + D_{21}(k)F_1(k) & D_{21}(k)T_{11}^{-1}(k) & 0 \end{array}\right] .$$

Then, we have

$$
\begin{aligned}
&\begin{bmatrix} D_\perp(k) & D_{12}(k) \end{bmatrix} \begin{bmatrix} W(k) \\ \mathcal{F}_\ell\left(G_{uvru}, T_{22}^{-1}(k)K_{OE}(k)\right) T_{11}(k) \end{bmatrix} \\
=&\left[\begin{array}{cc|c} A + B_1F_1 + B_2T_{22}^{-1}D_c\left(C_2 + D_{21}F_1\right) & B_2T_{22}^{-1}C_c & B_1 + B_2T_{22}^{-1}D_cD_{21} \\ B_c\left(C_2 + D_{21}F_1\right) & A_c & B_cD_{21} \\ \hline -D_{12}T_{22}F_2 + D_{12}D_c\left(C_2 + D_{21}F_1\right) & D_{12}C_c & D_\perp W + D_{12}T_{21} + D_{12}C_cD_{21} \end{array}\right] \\
=&\mathcal{F}_\ell(G_{tmp}(k), K_{OE}(k))
\end{aligned}
$$

where the time index k is skipped for the last equality. By considering $D_\perp(k)^T D_\perp(k) = I$ and $D_\perp(k)^T D_{12}(k) = 0$, we have

$$
\begin{aligned}
&I - \mathcal{F}_\ell(G_{tmp}(k), K_{OE})^T \mathcal{F}_\ell(G_{tmp}(k), K_{OE}) \\
=&I - W^T(k)W(k) - T_{11}^T(k)\mathcal{F}_\ell\left(G_{uvru}, T_{22}^{-1}(k)K_{OE}\right)^T \mathcal{F}_\ell\left(G_{uvru}, T_{22}^{-1}(k)K_{OE}\right) T_{11}(k) \\
=&T_{11}^T(k)\left[I - \mathcal{F}_\ell\left(G_{uvru}, T_{22}^{-1}(k)K_{OE}\right)^T \mathcal{F}_\ell\left(G_{uvru}, T_{22}^{-1}(k)K_{OE}\right)\right] T_{11}(k) \\
\Rightarrow\quad &\left\|\mathcal{F}_\ell(G_{tmp}, K_{OE})\right\|_{2\leftarrow 2} < 1 \Leftrightarrow \left\|\mathcal{F}_\ell(G_{vyru}, T_{22}^{-1}K_{OE})\right\|_{2\leftarrow 2} < 1\,.
\end{aligned}
$$

From [41], we learn that

$$
\left\|\mathcal{F}_\ell(G_{OF}, T_{22}^{-1}K_{OE})\right\|_{2\leftarrow 2} < 1 \Leftrightarrow \left\|\mathcal{F}_\ell(G_{vyru}, T_{22}^{-1}K_{OE})\right\|_{2\leftarrow 2} < 1\,.
$$

Thus, we conclude that

$$
\left\|\mathcal{F}_\ell(G_{tmp}, K_{OE})\right\|_{2\leftarrow 2} < 1 \Leftrightarrow \left\|\mathcal{F}_\ell(G_{vyru}, T_{22}^{-1}K_{OE})\right\|_{2\leftarrow 2} < 1\,.
$$

□

With Lemma 3, the output feedback control problem is reduced to an output estimation problem associated with G_{tmp}.

A.2 Reduction to Full Control Problem

With $D_{12}(k) = \begin{bmatrix} 0 & I \end{bmatrix}^T$, we have

$$
\bar{C}_1(k) = \begin{bmatrix} 0 \\ -T_{22}(k)F_2(k) \end{bmatrix},\ \bar{D}_{11}(k) = \begin{bmatrix} \bar{D}_{111}(k) \\ \bar{D}_{112}(k) \end{bmatrix},\ \bar{B}_2(k) = B_2(k)T_{22}^{-1}(k)\,.
$$

Then, G_{tmp} in (A.2) can be represented by

$$
G_{tmp} \sim \left[\begin{array}{c|cc} \bar{A}(k) & B_1(k) & \bar{B}_2(k) \\ \hline \begin{bmatrix} 0 \\ \bar{C}_{12}(k) \end{bmatrix} & \begin{bmatrix} \bar{D}_{111}(k) \\ \bar{D}_{112}(k) \end{bmatrix} & \begin{bmatrix} 0 \\ I \end{bmatrix} \\ \bar{C}_2(k) & D_{21}(k) & 0 \end{array}\right]\,.
$$

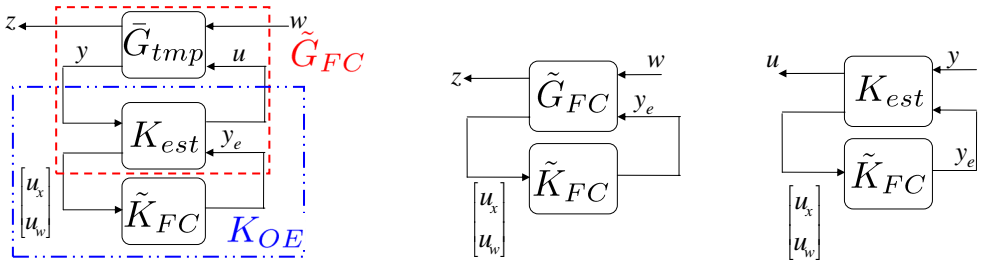

Figure A.1: Fixed control structure for the output estimation control problem

Since the first part of both C and D matrix is zero, the minimum entropy H_∞ control design for G_{tmp} is equivalent to the one for the following LTV system $\bar{G}_{tmp}$

$$\bar{G}_{tmp} \sim \left[\begin{array}{c|cc} \bar{A}(k) & B_1(k) & \bar{B}_2(k) \\ \hline \bar{C}_{12}(k) & \bar{D}_{112}(k) & I \\ \bar{C}_2(k) & D_{21}(k) & 0 \end{array}\right]. \tag{A.3}$$

In order to construct an admissible controllable for G_{OF}, we consider fixing the control structure of K_{OE} for $\bar{G}_{tmp}$ as shown in Fig. A.1a. Choose K_{est} with the following state-space realization:

$$K_{est} \sim \begin{bmatrix} x_e(k+1) \\ u(k) \\ y_e(k) \end{bmatrix} = \left[\begin{array}{c|cc} \bar{A}(k) - \bar{B}_2(k)\bar{C}_{12}(k) & 0 & \begin{bmatrix} 0 & -\bar{B}_2(k) \end{bmatrix} \\ \hline \bar{C}_{12}(k) & 0 & \begin{bmatrix} 0 & I \end{bmatrix} \\ \bar{C}_2(k) & I & \begin{bmatrix} 0 & 0 \end{bmatrix} \end{array}\right] \begin{bmatrix} x_e(k) \\ y(k) \\ \begin{bmatrix} u_x(k) \\ u_w(k) \end{bmatrix} \end{bmatrix} \tag{A.4}$$

Let $\tilde{G}_{FC}$ denote the interconnection of $\bar{G}_{tmp}$ and K_{est}, and it can be written as

$$\tilde{G}_{FC} \sim \left[\begin{array}{cc|c|c} \bar{A}(k) & \bar{B}_2(k)\bar{C}_{12}(k) & B_1(k) & \begin{bmatrix} 0 & \bar{B}_2(k) \end{bmatrix} \\ 0 & \bar{A}(k) - \bar{B}_2(k)\bar{C}_{12}(k) & 0 & \begin{bmatrix} I & -\bar{B}_2(k) \end{bmatrix} \\ \hline \bar{C}_{12}(k) & \bar{C}_{12}(k) & \bar{D}_{112}(k) & \begin{bmatrix} 0 & I \end{bmatrix} \\ \bar{C}_2(k) & \bar{C}_2(k) & D_{21}(k) & \begin{bmatrix} 0 & 0 \end{bmatrix} \end{array}\right].$$

Then, after applying the state transformation matrix $T_{st} = T_{st}^{-1} = \begin{bmatrix} -I & 0 \\ I & I \end{bmatrix}$ to the above state-space realization for all k, we get

$$\tilde{G}_{FC} \sim \left[\begin{array}{cc|c|c} \bar{A}(k) - \bar{B}_2(k)\bar{C}_{12}(k) & -\bar{B}_2(k)\bar{C}_{12}(k) & -B_1(k) & \begin{bmatrix} 0 & -\bar{B}_2(k) \end{bmatrix} \\ 0 & \bar{A}(k) & B_1(k) & \begin{bmatrix} I & 0 \end{bmatrix} \\ \hline 0 & \bar{C}_{12}(k) & \bar{D}_{112}(k) & \begin{bmatrix} 0 & I \end{bmatrix} \\ 0 & \bar{C}_2(k) & D_{21}(k) & \begin{bmatrix} 0 & 0 \end{bmatrix} \end{array}\right] \tag{A.5}$$

Obviously, the first part of the state in (A.5) is unobservable but stable by considering that $\bar{A}(k) - \bar{B}_2(k)\bar{C}_{12}(k) = A(k) + B_1(k)F_1(k) + B_2(k)F_2(k) = A(k) + B(k)F(k)$ is

UES which is guaranteed in Lemma 3. As a result, $\tilde{G}_{FC}$ can be simplified as

$$\tilde{G}_{FC} \sim \left[\begin{array}{c|c|cc} \bar{A}(k) & B_1(k) & I & 0 \\ \hline \bar{C}_{12}(k) & \bar{D}_{112}(k) & 0 & I \\ \bar{C}_2(k) & D_{21}(k) & 0 & 0 \end{array}\right] . \tag{A.6}$$

Obviously, $\tilde{G}_{FC}$ with the state-space realization in (A.3) is a full control system. Then, we consider the following lemma to reduce an output estimation problem to a full control problem.

Lemma 4. *There exists an admissible controller $K_{OE}(k)$ for $\bar{G}_{tmp}$ if and only if there exists an admissible controller $\tilde{K}_{FC}$ for $\tilde{G}_{FC}$.*

Proof. In this proof, we prove sufficiency and necessity separately.

- Sufficiency can be obtained with the control structure shown in Fig. A.1c and state transformation $T_{st} = \begin{bmatrix} -I & 0 \\ I & I \end{bmatrix}$. Suppose that $\tilde{K}_{FC}$ is admissible for $\tilde{G}_{FC}$, then the controller given by $K_{OE} = \mathcal{F}_\ell(K_{est}, \tilde{K}_{FC})$ is admissible for $\bar{G}_{tmp}$ where K_{est} is defined in (A.4).
- Necessity is trivial. If K_{OE} is admissible for $\bar{G}_{tmp}$, then the controller

  $$\tilde{K}_{FC} = \begin{bmatrix} B_2(k) \\ I \end{bmatrix} K_{est}$$

  is admissible for $\tilde{G}_{FC}$, since Fig. A.1 demonstrates that

  $$\mathcal{F}_\ell(\tilde{G}_{FC}, \tilde{K}_{FC}) = \mathcal{F}_\ell(\bar{G}_{tmp}, K_{OE})$$

□

At this point, we are able to reduce an output feedback control problem to a full control problem and thus we can reconstruct the output feedback controller K_{OF} from the controller $\tilde{K}_{FC}$ solved in the corresponding full control problem by using

$$K_{OF} = T_{22}^{-1}(k) K_{OE} = T_{22}^{-1}(k) \mathcal{F}_\ell(K_{est}, \tilde{K}_{FC}) .$$

Notice that the minimum entropy controller for the full control problem is provided in [41].

Appendix B

Proof of Lemma 1

First, we will show the periodicity of the solution to the discrete Riccati equation (3.5) in Step 1). Suppose $(\cdots, X(j), X(j+1), \cdots)$ is a solution to the discrete Riccati equation in (3.5), which means that

$$X(j) = A^T(j)X(j+1)A(j) + C_1^T(j)C_1^T(j) - \eta_j\left(X(j+1)\right)$$

where

$$\eta_j(X(j+1)) \;=\; M_j(X(j+1))\left(R(j) + B^T(j)X(j+1)B(j)\right)^{-1} M_j^T(X(j+1))$$

with $M_j(X(j+1)) = A^T(j)X(j+1)B(j) + C_1^T(j)D_{1\bullet}(j)$. At the time of $j+N$,

$$\begin{aligned} X(j+N) \;=\; & A^T(j+N)X(j+N+1)A(j+N) + \\ & C_1^T(j+N)C_1(j+N) - \eta_{j+N}\left(X(j+N+1)\right)\ . \end{aligned}$$

By considering that the plant G in (3.1) is periodic with period N (i.e. $A(j+N) = A(j)$, $B(j+N) = B(j)$, $C_1(j+N) = C_1(j)$, and $D_{1\bullet}(j+N) = D_{1\bullet}(j)$), we have:

$$X(j+N) = A^T(j)X(j+N+1)A(j) + C_1^T(j)C_1(j) - \eta_j\left(X(j+N+1)\right) \qquad \text{(B.1)}$$

where

$$\begin{aligned} \eta_j(X(j+N+1)) \;=\; & M_j(X(j+N+1))\left(R(j) \quad + \right. \\ & \left. B^T(j)X(j+N+1)B(j)\right)^{-1} M_j^T(X(j+N+1))\ . \end{aligned}$$

Thus, the equation in (B.1) implies that $(\cdots, X(j+N), X(j+N+1), \cdots)$ is another solution to the discrete Riccati equation in (3.5). From [41], we know that the bounded stabilizing solution to the discrete Riccati equation in (3.5) is unique, which implies $X(j) = X(j+N)$.

As a result, all matrices $\bar{A}(k)$, $\begin{bmatrix} \bar{C}_{12}(k) \\ \bar{C}_2(k) \end{bmatrix}$, and $\begin{bmatrix} \bar{D}_{112}(k) \\ D_{21}(k) \end{bmatrix}$ for (3.7) are periodic with period N.

Moreover, the periodicity of the solution to the discrete Riccati equation (3.7) in Step 5) for constructing a minimum entropy controller, i.e. $Y(k) = Y(k+N)$, can be shown in a similar manner. Consequentially, the periodicity of $X(k)$ and $Y(k)$ implies that all of the parameters to construct the H_∞ controller in (3.4) are periodic with period N. Therefore, the optimal H_∞ controller for the linear periodically time-varying system G is also periodic with period N.

Appendix C

Proof of Lemma 2

Since $L_t(k) = T_{22}^{-1}(k)\tilde{T}_{12}(k)\tilde{T}_{22}^{-1}(k)$ and $F_t(k) = \tilde{F}_1^T(k)\tilde{T}_{12}(k)\tilde{T}_{22}^{-1}(k)+\tilde{F}_2^T(k)$, the proof is done if we can show $\tilde{T}_{12}(k) = 0$ and $\tilde{F}_2^T(k) = 0_{n\times 1}$ when $PES(k)$ is unavailable. Here n is the order of the system G_4 in (4.5). During the following proof, we just consider the instance k when $PES(k)$ is unavailable.

C.1 Proof of $\tilde{T}_{12}(k) = 0$

With the equation in (4.11), we have

$$\begin{bmatrix} -\tilde{T}_{11}(k)\tilde{T}_{11}^T(k) + \tilde{T}_{12}(k)\tilde{T}_{12}^T(k) & \tilde{T}_{12}(k)\tilde{T}_{22}^T(k) \\ \tilde{T}_{22}(k)\tilde{T}_{12}^T(k) & \tilde{T}_{22}(k)\tilde{T}_{22}^T(k) \end{bmatrix} = \begin{bmatrix} \bar{D}_{112} \\ D_{21}(k) \end{bmatrix} \begin{bmatrix} \bar{D}_{112} \\ D_{21}(k) \end{bmatrix}^T - \begin{bmatrix} I & 0 \\ 0 & 0 \end{bmatrix} + \begin{bmatrix} \bar{C}_{12} \\ \bar{C}_2(k) \end{bmatrix} Y(k-1) \begin{bmatrix} \bar{C}_{12} \\ \bar{C}_2(k) \end{bmatrix}^T$$

$$\Rightarrow \tilde{T}_{22}(k)\tilde{T}_{22}^T(k) = D_{21}(k)\bar{D}_{112}^T + \bar{C}_2(k)Y(k-1)\bar{C}_{12} \ .$$

With $C_2(k) = 0_{1\times n}$ and $D_{21}(k) = \begin{bmatrix} 0 & 1 \end{bmatrix}$ from (4.6), we know

$$\tilde{T}_{22}(k)\tilde{T}_{12}^T(k) = \begin{bmatrix} 0 & 1 \end{bmatrix} \bar{D}_{112}^T \ .$$

Obviously, if $\bar{D}_{112}$ has the form of $\bar{D}_{112} = \left[\ * \ \vdots\ 0\ \right]$, then $\tilde{T}_{12}(k) = 0$. Here, we utilize "*" to represent unspecified elements in a matrix. Since $\begin{bmatrix} \bar{D}_{111} \\ \bar{D}_{112} \end{bmatrix} = D_\perp W + D_{12}T_{21}$, we just need to show that W and T_{21} have the following representation

$$W = \left[\ * \ \vdots\ 0\ \right] \text{ and } T_{21} = \left[\ * \ \vdots\ 0\ \right] \ .$$

With the equation in (4.9), we have

$$\left[\begin{array}{c|c} -T_{11}^T T_{11} + T_{21}^T T_{21} & T_{21}^T T_{22} \\ \hline T_{22}^T T_{21} & T_{22}^T T_{22} \end{array}\right] = \left[\begin{array}{c} \bar{D}_{11}^T \\ \hline \bar{D}_{12}^T \end{array}\right] \left[\begin{array}{c|c} D_{11} & D_{12} \end{array}\right] - \left[\begin{array}{c|c} I & 0 \\ \hline 0 & 0 \end{array}\right] + \left[\begin{array}{c} B_1^T \\ \hline B_2^T \end{array}\right] X \left[\begin{array}{c|c} B_1 & B_2 \end{array}\right]$$

$$\Rightarrow \left\{\begin{array}{l} D_{11}^T D_{11} + B_1^T X B_1 - I = T_{21}^T T_{21} - T_{11}^T T_{11} \\ D_{12}^T D_{11} + B_2^T X B_1 = T_{22}^T T_{21} \end{array}\right. .$$

Since the fictitious disturbance w_2 directly goes into the feedback signal $y(k)$ when $PES(k)$ is unavailable, the elements in D_{11} and B_1 associated with w_2 are zero. As a result, we have:

$$\begin{aligned} D_{11} &= \left[\begin{array}{c|c} * & 0_{n_z \times 1} \end{array}\right] \text{ and } B_1 = \left[\begin{array}{c|c} * & 0_{n \times 1} \end{array}\right] \\ \Rightarrow T_{21} &= T_{22}^{-T} \left\{ D_{12}^T D_{11} + B_2^T X B_1 \right\} = T_{22}^{-T} \left[\begin{array}{c|c} * & 0 \end{array}\right] = \left[\begin{array}{c|c} * & 0 \end{array}\right] \end{aligned}$$

where n_z is the dimension of the "performance monitoring" output z. In addition, for W, we have

$$\begin{aligned} W^T W &= I - T_{11}^T T_{11} = D_{11}^T D_{11} + B_1^T X B_1 - T_{21}^T T_{21} \\ &= \left[\begin{array}{c|c} * & 0 \\ \hline 0 & 0 \end{array}\right] + \left[\begin{array}{c|c} * & 0 \\ \hline 0 & 0 \end{array}\right] + \left[\begin{array}{c|c} * & 0 \\ \hline 0 & 0 \end{array}\right] = \left[\begin{array}{c|c} * & 0 \\ \hline 0 & 0 \end{array}\right] . \end{aligned}$$

Obviously, we can take the factorization of $W = \left[\begin{array}{c|c} * & 0 \end{array}\right]$. Therefore, $W = \left[\begin{array}{c|c} * & 0 \end{array}\right]$ and $T_{21} = \left[\begin{array}{c|c} * & 0 \end{array}\right]$ implies $\bar{D}_{112} = \left[\begin{array}{c|c} * & 0 \end{array}\right]$, which results in

$$\tilde{T}_{12}^T(k) = \tilde{T}_{22}^{-1}(k) D_{12} \bar{D}_{112}^T = \tilde{T}_{22}^{-1}(k) \left[\begin{array}{c|c} 0 & 1 \end{array}\right] \left[\begin{array}{c} * \\ \hline 0 \end{array}\right] = 0 .$$

C.2 Proof of $\tilde{F}_2^T(k) = 0_{n \times 1}$

From the previous section, we learn that $C_2(k) = 0_{1 \times n}$, $D_{21}(k) = \begin{bmatrix} 0 & 1 \end{bmatrix}$, and $B_1 = \left[\begin{array}{c|c} * & 0_{n \times 1} \end{array}\right]$. Thus, we calculate

$$\begin{aligned} \tilde{M}^T(k) &= \left[\begin{array}{c} \bar{C}_{12} \\ \hline \bar{C}_2(k) \end{array}\right] Y(k-1) \bar{A}^T + \left[\begin{array}{c} \bar{D}_{112} \\ \hline \bar{D}_{21}(k) \end{array}\right] B_1^T \\ &= \left[\begin{array}{c} \bar{C}_{12} Y(k-1) \bar{A}^T \\ \hline 0_{1 \times n} \cdot Y(k-1) \bar{A}^T \end{array}\right] + \left[\begin{array}{c} \bar{D}_{112} B_1^T \\ \hline \bar{D}_{21}(k) B_1^T \end{array}\right] \\ &= \left[\begin{array}{c} * \\ \hline 0_{1 \times n} \end{array}\right] + \left[\begin{array}{c} * \\ \hline 0_{1 \times n} \end{array}\right] = \left[\begin{array}{c} * \\ \hline 0_{1 \times n} \end{array}\right] . \end{aligned}$$

The result $\tilde{T}_{12}(k) = 0$ from the previous section implies

$$\begin{aligned}
\tilde{T}(k)\tilde{J}\tilde{T}^T(k) &= \begin{bmatrix} -\tilde{T}_{11}(k)\tilde{T}_{11}^T(k) + \tilde{T}_{12}(k)\tilde{T}_{12}^T(k) & \tilde{T}_{12}(k)\tilde{T}_{22}^T(k) \\ \tilde{T}_{22}(k)\tilde{T}_{12}^T(k) & \tilde{T}_{22}(k)\tilde{T}_{22}^T(k) \end{bmatrix} \\
&= \begin{bmatrix} -\tilde{T}_{11}(k)\tilde{T}_{11}^T(k) & 0 \\ 0 & \tilde{T}_{22}(k)\tilde{T}_{22}^T(k) \end{bmatrix} .
\end{aligned}$$

Substitute the right side of (4.11) into the right side of the equation (4.12):

$$\begin{aligned}
\begin{bmatrix} \tilde{F}_1(k) \\ \hline \tilde{F}_2(k) \end{bmatrix} &= \left(\tilde{T}(k)\tilde{J}\tilde{T}^T(k)\right)^{-1} \tilde{M}^T(k) \\
&= \left[\begin{array}{c|c} -\left(\tilde{T}_{11}(k)\tilde{T}_{11}^T(k)\right)^{-1} & 0 \\ \hline 0 & \left(\tilde{T}_{22}(k)\tilde{T}_{22}^T(k)\right)^{-1} \end{array}\right] \left[\begin{array}{c} * \\ \hline 0_{1\times n} \end{array}\right] \\
&= \left[\begin{array}{c} * \\ \hline 0_{1\times n} \end{array}\right] \\
\Rightarrow \tilde{F}_2(k) &= 0_{1\times n} .
\end{aligned}$$

With the above proof, we conclude that

$$\tilde{T}_{12}(k) = 0 \text{ and } \tilde{F}_2^T(k) = 0_{n\times 1}$$

at the instance k when $PES(k)$ is unavailable.